

**HYDRODYNAMIC OPTIMIZATION OF THE
SUBMARINE WITH A FULLY PARAMETRIC CAD
MODEL**

**BİR DENİZALTININ TAM PARAMETRİK CAD
MODELİYLE HİDRODİNAMİK OPTİMİZASYONU**

OSMAN GARGI

ASSOC. PROF. DR. ÖZGÜR EKİCİ

Supervisor

DR. ERTAN KARAIŞMAİL

Co-Supervisor

Submitted to

Graduate School of Science and Engineering of Hacettepe University

as a Partial Fulfillment to the Requirements

for the Award of the Degree of Master of Science

in Mechanical Engineering.

February 2023

To my father

ABSTRACT

HYDRODYNAMIC OPTIMIZATION OF THE SUBMARINE WITH A FULLY PARAMETRIC CAD MODEL

Osman GARGI

Master of Science, Mechanical Engineering

Supervisor: Assoc. Prof. Dr. Özgür EKİCİ

Co-Supervisor: Dr.Ertan KARAİSMAİL

January 2023, 121 Pages

This study was conducted to compare the performance of four different optimization studies that can be done to reduce the drag force that a submarine is exposed to in fully submerged conditions. The submarine used in the study is DARPA SUBOFF AFF-1, which aims to improve this design's hydrodynamic performance with drag reduction in fully submerged condition

First of all, to obtain close results with the hydrodynamic experiment of this submarine design in the literature, a mesh independence study was carried out, and the most suitable mesh structure was found. Afterwards, the most used design variables and constraints were investigated by examining the submarine optimization studies in the literature, divided into four different optimization studies. After that, the design was fully parametrically modelled in the CAESES environment. During this modelling, changes were made in the parametric model according to each optimization study's design limits and design constraints. In all optimization studies, the buoyancy centres of the new designs derived using the Lackenby method were ensured to remain the same as the DARPA SUBOFF AFF-1. In this way, only the derived designs' hydrodynamic characteristics were changed, keeping the manoeuvrability constant. Optimization studies

were carried out in two steps. Design of Experiment Methodology was used in the first step, and Tangent Search Algorithm was used in the second step. In these steps, a total of 1044, 532, 347 and 532 different designs were derived by CAESES, respectively. For these designs, solutions were obtained with the CFD simulation model verified by experiment in ANSYS Fluent environment and the results were evaluated over the drag force.

After the study, approximately 13%, 8%, 9% and 10% lower drag forces were obtained, respectively, compared to DARPA SUBOFF AFF-1 in the optimum designs obtained in each optimization study.

In addition, the optimization study that will reduce the drag force the most according to the design limits that should be considered when optimizing any submarine design and the relationship of the optimum design obtained as a result of this study with the initial design was learned.

On the other hand, if there is no design limit before the optimization, an optimization study that will reduce the drag force at the maximum level without changing the manoeuvrability of the existing design has also been learned.

Keywords: Computational Fluid Dynamics, Hydrodynamic Optimization, Design of Experiment Method, Tangent Search Algorithm, DARPA

ÖZET

BİR DENİZALTININ TAM PARAMETRİK CAD MODELİYLE HİDRODİNAMİK OPTİMİZASYONU

Osman GARGI

Yüksek Lisans, Makina Mühendisliği

Danışman: Doç. Dr. Özgür EKİCİ

Eş Danışman: Dr.Ertan KARAİSMAIL

Ocak 2023, 121 Sayfa

Bu çalışma; bir denizaltının tam batma durumunda maruz kaldığı sürüklenme kuvvetini azaltmak için yapılan dört farklı optimizasyon çalışmasının verimliliklerini kıyaslamak amacıyla yapılmıştır. Çalışmada kullanılan denizaltı DARPA SUBOFF AFF-1 olup, bu tasarımın tam batma durumundaki hidrodinamik performansını artırmak hedeflenmiştir.

İlk olarak bu denizaltı tasarımının literatürde yer alan hidrodinamik deneyi ile yakın sonuçlar alınması hedefiyle ağdan bağımsızlık çalışması gerçekleştirilmiş ve en uygun çözüm ağı bulunmuştur. Devamında literatürde yer alan denizaltı optimizasyon çalışmaları incelenerek en çok kullanılan tasarım değişkenleri ve tasarım kısıtları araştırılmış ve bunlar dört farklı optimizasyon çalışmasına bölünmüştür. Sonrasında, tasarım CAESES ortamında tam parametrik modellenmiş olup bu modelleme esnasında, her bir optimizasyon çalışmasının tasarım limitleri ve tasarım kısıtlarına göre parametrik modelde değişiklikler yapılmıştır. Tüm optimizasyon çalışmalarında Lackenby yöntemi kullanılarak türetilen yeni tasarımların sephiye merkezlerinin DARPA SUBOFF AFF-1 ile aynı kalması sağlanmıştır. Bu sayede türetilen tüm tasarımların manevra kabiliyetleri sabit tutularak sadece hidrodinamik karakteristikleri değiştirilmiştir. Optimizasyon çalışmaları iki adımda gerçekleştirilmiştir. İlk adımda Deney Tasarımı, ikinci adımda ise

Tanjant Arama Algoritması kullanılmıştır. Bu adımlarda, CAESES tarafından sırasıyla toplam 1044, 532, 347 ve 532 farklı tasarım türetilmiştir. Bu tasarımlar için, ANSYS Fluent ortamında, deney ile doğrulanan CFD simülasyon modeli ile çözüm alınıp sonuçlar direnç kuvveti üzerinden değerlendirilmiştir.

Çalışma sonrasında, her bir optimizasyon çalışmasında elde edilen optimum tasarımlarda DARPA SUBOFF AFF-1'e kıyasla sırasıyla yaklaşık %13, %8, %9 ve %10 daha düşük direnç kuvvetleri elde edilmiştir.

Buna ek olarak, herhangi bir denizaltı tasarımının maruz kaldığı sürüklenme kuvveti azaltılmak istendiğinde göz önüne alınması gereken tasarım limitlerine göre sürüklenme kuvvetini en fazla azaltan optimizasyon çalışması ve bu çalışma sonrası elde edilen optimum tasarımın ilk tasarımla olan ilişkisi öğrenilmiştir.

Diğer taraftan, optimizasyon öncesi herhangi bir tasarım limiti bulunmaması halinde, mevcut tasarımın manevra kabiliyetini değiştirmeden sürüklenme kuvvetini azaltmanın en verimli yöntemi de öğrenilmiştir.

Anahtar Kelimeler: Hesaplamalı Akışkanlar Dinamiği, Hidrodinamik Optimizasyon, Deney Tasarımı, Tanjant Arama Algoritması, DARPA

ACKNOWLEDGEMENTS

I want to express my endless thanks to my thesis advisor, Assoc. Prof. Dr. Özgür Ekici, who always supported me throughout my thesis work, shared his excitement and knowledge with me at every step of the work we did and who is an exemplary researcher with his meticulous and perfectionist attitude in every subject.

I would also like to thank Prof. Dr. M. Metin Yavuz, Prof. Dr. Murat Köksal, Assoc. Prof. Dr. Bilsay Sümer and Assist. Prof. Dr. Özgür Uğraş Baran, who participated in my thesis defence and shared their valuable opinions with me and helped me move my work to a better point.

I would like to thank my esteemed manager and thesis co-supervisor Dr. Ertan Karaismail, whose patience and tolerance I always felt throughout the study.

I want to thank my dear elders Ahmet Yusuf Gürkan and Buğra Uğur Yazıcı, who shared their opinions and suggestions with me at every step of my work.

I would like to express my gratitude to my mother Dilek Gargı and my uncle Kurtuluş Gargı, who supported me not only throughout my thesis work but in every moment of my life.

I would also like to thank my dear brother and colleague Yasin Gargı, who has provided me with both human and professional guidance throughout my life.

Finally, I would like to thank Seray İçöz for her endless support and patience throughout the study.

TABLE OF CONTENTS

ABSTRACT	i
ÖZET	iii
ACKNOWLEDGEMENTS	v
TABLE OF CONTENTS	vi
LIST OF FIGURES	ix
LIST OF TABLES	xii
SYMBOLS AND ABBREVIATIONS	xiv
1. INTRODUCTION	16
1.1.Literature	18
1.2. Motivation	23
1.3. Purpose of the Thesis	24
1.4. Outline of the Thesis	26
2.THEORY AND MODELLING	27
2.1. Navier-Stokes Equations	27
2.2. Turbulence Modelling	28
2.2.1. Reynolds Averaged Navier-Stokes Equations	29
2.2.2. SST k- ω Turbulence Model	29
3. OPTIMIZATION METHODOLOGY	32
3.1. Theory of Optimization Methodology	33
3.2. Design of Experiment Methodology (DoE)	34
3.2.1. Terminology in Design of Experiments	34
3.2.2. Sobol Sequence Algorithm in Design of Experiments.....	35
3.3. Metaheuristics Optimization Methodologies	35
3.4. Tangent Search Algorithm	36
4.SIMULATION MODEL	38
4.1. Geometrical Model.....	38

4.2. Simulation Domain and Boundary Conditions	39
4.3. Simulation Parameters and Solver Settings	42
4.4. Mesh Generation.....	46
4.5. Mesh Independence Study	51
5. HYDRODYNAMIC OPTIMIZATION PROCESS OF THE SUBMARINE.....	55
5.1. Geometrical Modelling	56
5.2. Parametrical Modelling.....	57
5.2.1. Parametrical Modelling of the Nose Cone.....	57
5.2.2. Parametrical Modeling of the Stern	59
5.2.3. Lackenby Methodology	59
5.3. Constraints of the Optimization Process	70
5.4. Running the Optimization Process	71
5.5. Review the Optimization Process	74
6. RESULTS	76
6.1. Optimization Process-1	76
6.1.1. DoE-1 Results	77
6.1.2. T-Search-1 Results.....	81
6.1.3. Specifying Optimum Design-1	85
6.2. Optimization Process-2.....	87
6.2.1. DoE-2 Results	88
6.2.2. T-Search-2 Results.....	91
6.2.3. Specifying Optimum Design-2	94
6.3. Optimization Process-3.....	96
6.3.1. DoE-3 Results	102
6.3.2. T-Search-3 Results.....	106
6.3.3. Specifying Optimum Design-3	107
6.4. Optimization Process-4.....	109
6.4.1. DoE-4 Results	111
6.4.2. T-Search-4 Results.....	115
6.4.3. Specifying Optimum Design-4	117
6.5. Review of the Optimization Processes	119
6.5.1. Review of Hydrostatic and Geometrical Properties	120

6.5.2. Review of Hydrodynamic Properties	122
7. CONCLUSION	129
7.1. Conclusion and Discussion	129
7.2. Future Works.....	131
8.REFERENCES.....	132
APPENDIX 1 - THESIS ORIGINALITY REPORT ..	Error! Bookmark not defined.
RESUME.....	Error! Bookmark not defined.

LIST OF FIGURES

Figure 1.1. HMS Holland-1 Submarine [1]	16
Figure 1.2. The Sample UUV Design [11]	18
Figure 1.3. Hydrodynamic Test Geometries of DARPA SUBOFF Experimental Program [12]	19
Figure 1.4. a) Initial b) Hydrodynamically Optimal Submarine Forms of Paz and Munoz's Study [15]	20
Figure 1.5. a) The test Models b) The Optimized Model's of Gao et. al's Study [16] ..	21
Figure 1.6. An Optimum Form of Divsalar's Study [17]	22
Figure 1.7. Supercavitation with a) Blunt Type b) Cone Type Nose Cavitator [21]	23
Figure 3.1. Optimization Process Steps Followed in the Thesis	32
Figure 3.2. Classification of Optimization Methods	33
Figure 3.3. Steps of the Tangent Search Algorithm	37
Figure 4.1. The Symbols of the Main Geometric Details	38
Figure 4.2. Dimensions of the Computational Domain	40
Figure 4.3. Boundary Conditions	41
Figure 4.4. Locations of Convergence Control Points a) Side View b) Top View	44
Figure 4.5. Convergence Control Graphs a) Residuals b) Drag Force c) Velocity at Control Points	45
Figure 4.6. Mesh Generation Steps	46
Figure 4.7. Different Types of Mesh Elements [65]	47
Figure 4.8. Volume Mesh of JSM-WBNP a) Hexcore b) Poly-Hexcore [66]	48
Figure 4.9. Refinement Regions to Control Mesh Density	49
Figure 4.10. Boundary Layer Mesh Around at Different Locations a) the hull b) the nose c) the stern	50
Figure 4.11. Comparison of Seven Different Mesh Structures	53
Figure 4.12. Mesh Structure to be Used in the Validated Simulation Model a) Overview b) Boundary Layer Transition on the Nose	54
Figure 5.1. Steps of the Optimization Process	55
Figure 5.2. Geometric Sections of the DARPA SUBOFF AFF-1 Model	56
Figure 5.3. Sections in the Nose Cone (CAESSES)	58
Figure 5.4. First Sectional Area Curve Derived by Lackenby [75]	61

Figure 5.5. LPP of the DARPA SUBOFF AFF-1	61
Figure 5.6. Parameters of Prismatic Coefficient [81].....	62
Figure 5.7. Gravity and buoyancy forces acting on a submarine a) Side view b) Front view [82]	63
Figure 5.8. Parameters of the Longitudinal Centre of Buoyancy [83]	64
Figure 5.9. Steps of the Parametrization	65
Figure 5.10. The first Sectional Area Curve	66
Figure 5.11. The Last SAC Form and the Working Area of the Lackenby Method.....	68
Figure 5.12. SoftwareConnector Interface on CAESES	72
Figure 5.13. Pareto frontiers for the multiobjective optimizations a) convex b) nonconvex	74
Figure 6.1. Workfields of Optimization Process-1	76
Figure 6.2. Pareto Analyses of DoE-1 a) S-1 b) S-2 c) S-3 d) S-4	79
Figure 6.3. Optimum Design-1 a) Section View b) Isometric View.....	86
Figure 6.4. Workfields of Optimization Process-2	87
Figure 6.5. Pareto Analyses of DoE-2 a) S-1 b) S-2 c) S-3 d) S-4	90
Figure 6.6. Optimum Design-2 a) Section View b) Isometric View.....	96
Figure 6.7. The Forms Derived in Optimization Process-3	97
Figure 6.8. Workfields of Optimization Process-3	97
Figure 6.9. Sample Form-2	99
Figure 6.10. A Cylinder Created for Dimension Calculation for Form-3.....	100
Figure 6.11. Sample Form-3	101
Figure 6.12. Sample Form-4	102
Figure 6.13. Pareto Analyses of DoE-3 a) S-1 b) S-2 c) S-3 d) S-4 e) DV5.....	104
Figure 6.14: Optimum Design-3 a) Section View b) Isometric View.....	109
Figure 6.15. Workfields of Optimization Process-4	110
Figure 6.16. Pareto Analyses of DoE-4 a) S-1 b) S-2 c) S-3 d) S-4 e) DV5.....	113
Figure 6.17. Optimum Design-4 a) Section View b) Isometric View.....	119
Figure 6.18. Review of all Designs a) DARPA SUBOFF AFF-1 b) Optimum Design-1 c) Optimum Design-2 d) Optimum Design-3 d) Optimum Design-4	121
Figure 6.19. Velocity Contours (m/s) for a) DARPA SUBOFF AFF-1 b) Optimum Design-1 c) Optimum Design-2 d) Optimum Design-3 e) Optimum Design-4	125

Figure 6.20. Static Pressure Contours (Pa) for a) DARPA SUBOFF AFF-1 b) Optimum Design-1 c) Optimum Design-2 d) Optimum Design-3 e) Optimum Design-4 128

LIST OF TABLES

Table 4.1. The Main Particulars of DARPA SUBOFF AFF-1	39
Table 4.2. Boundary Conditions Details	42
Table 4.3. Methods and Discretization Schemes Used	43
Table 4.4. Coordinates of Convergence Control Points	44
Table 4.5. Details of the Boundary Layer Mesh	50
Table 4.6. Details of Mesh Structures (All sizes are in mm)	51
Table 4.7. Drag Force Values for Calculated Each Mesh Structure	52
Table 5.1. Sample Designs Taken for Different Coefficients	58
Table 5.2. Change of the SAC Form According to The Displacement Difference Between Form-1 And Form-2.....	67
Table 5.3. Centers of Buoyancy Positions without the Lackenby Method	69
Table 5.4. LCB and Displacement Differences of Derived Designs.....	70
Table 5.5. Design Constraints of the Optimization Processes	71
Table 6.1. Design Variables of Optimization Process-1	76
Table 6.2. Design Constraints of Optimization Process-1	77
Table 6.3. Top 20 Designs of DoE-1	78
Table 6.4. Top 5 Designs of DoE-1	80
Table 6.5. Results of T-Search-1	82
Table 6.6. Top 5 Designs of T-Search-1	84
Table 6.7. Comparison between DARPA SUBOFF AFF-1 and the Optimum Design-1	85
Table 6.8. Comparison of Hydrostatic and Hydrodynamic Parameters between Optimum Design and Initial Design	86
Table 6.9. Design Variables of Optimization Process-2	88
Table 6.10. Design Constraints of Optimization Process-2	88
Table 6.11. Top 20 Designs of DoE-2	89
Table 6.12. Top 5 Designs of DoE-2	91
Table 6.13. Results of T-Search-2.....	92
Table 6.14. Top 5 Designs of T-Search-2	94

Table 6.15. Comparison between DARPA SUBOFF AFF-1 and the Optimum Design-2	95
Table 6.16. Comparison of Hydrostatic and Hydrodynamic Parameters between DARPA SUBOFF AFF-1 and the Optimum Design-2	95
Table 6.17. Design Variables of Optimization Process-3.....	98
Table 6.18. Design Constraints of Optimization Process-3.....	98
Table 6.19. Design Variables of Sample Form-2	99
Table 6.20. The parameters of Form-2	101
Table 6.21. Comparison of Hydrostatic Properties of Sample Forms	102
Table 6.22. Top 20 Designs of DoE-3	103
Table 6.23. Top 5 Designs of DoE-3	105
Table 6.24. Top 10 Designs of T-Search-3.....	106
Table 6.25. Top 5 Designs of T-Search-3.....	107
Table 6.26. Comparison between DARPA SUBOFF AFF-1 and the Optimum Design-3	108
Table 6.27. Comparison of Hydrostatic and Hydrodynamic Parameters between Optimum Design-3 and DARPA SUBOFF AFF-1	108
Table 6.28. Design Variables of Optimization Process-3.....	110
Table 6.29. Design Constraints of Optimization Process-4.....	110
Table 6.30. Top 20 Designs of DoE-4	112
Table 6.31. Top 5 Designs of DoE-4	114
Table 6.32. Results of T-Search-4	115
Table 6.33. Top 5 Designs of T-Search-4.....	117
Table 6.34. Comparison between DARPA SUBOFF AFF-1 and the Optimum Design-4	118
Table 6.35. Comparison of Hydrostatic and Hydrodynamic Parameters between DARPA SUBOFF AFF-1 and the Optimum Design-4	118
Table 6.36. Design Constraints and Objective Functions.....	120
Table 6.37. Rate of Change of LCB and Displacement Compared to DARPA SUBOFF AFF-1	120
Table 6.38. The Hydrostatic and Geometric Properties of All Designs	121
Table 6.39. The Drag Forces and Coefficients of All Designs.....	122

SYMBOLS AND ABBREVIATIONS

Symbols

C_d	Drag Coefficient
F_d	Drag Force
ρ	Density of the fluid
u	Velocity of the fluid
$\frac{\partial}{\partial t}$	Material derivative
μ	Viscosity of the fluid
g	Gravity
p	Pressure
t	Time
\bar{u}	Time averaged velocity
\bar{p}	Time averaged pressure
δ_{ij}	Kronecker delta
y	The distance from the wall in the normal direction
k	Turbulent kinetic energy
w	Specific dissipations
y^+	Dimensionless wall thickness

Abbreviations

UUV	Unmanned Underwater Vehicle
DARPA	Defense Advanced Research Projects Agency
DNS	Direct Numerical Solution
RANS	Reynolds Averaged Navier-Stokes Equations
LES	Large Eddy Simulation
DoE	Design of Experiment

T-Search	Tangent Search
GSB	Gradient Search Based
GFS	Gradient-Free Search
LCB	Longitudinal Centre of Buoyancy
SAC	Sectional Area Curve
CP	Prismatic Coefficient
ITTC	The International Towing Tank Conference

1. INTRODUCTION

The appearance of submarines on the stage of history dates back to ancient times. Many successful and unsuccessful attempts have been made to develop today's modern submarine design technologies. Since the general design principles are similar, the early and modern submarines look alike Figure 1.1 shared below belongs to the first submarine designed by John Holland in 1897, which laid the foundations of today's modern submarine technology [1].

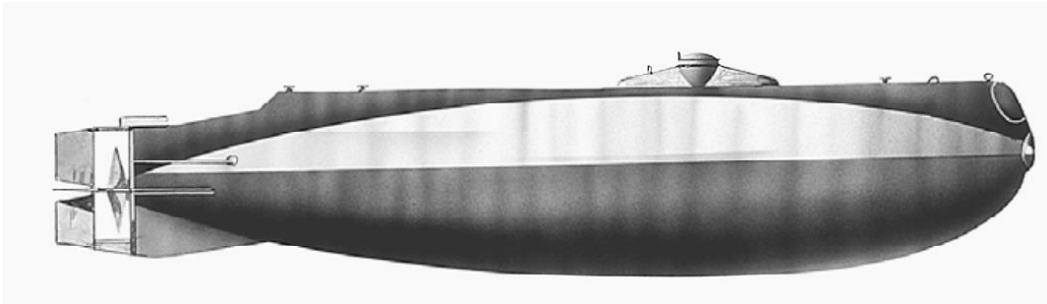


Figure 1.1. HMS Holland-1 Submarine [1]

A submarine is generally divided into four different sections [2].

i. Hull Surfaces

It is the most exciting part of the design of the submarine. Usually, submarines have two different hulls nested inside each other. The outer body is entirely waterproof, while the inner body is resistant to water pressure and has a stronger structure [2].

ii. Appendages

Submarines use attachments positioned in different parts of their outer hulls. These appendages control the submarine's movement in the water by creating lift and drag forces [2].

iii. Ballast Tanks

It was mentioned in the hull surfaces that submarines have two different hulls. The spaces between the two hulls are called ballast tanks. These tanks control the sinking or surfacing movements of submarines [2]. These movements are carried out thanks to the Archimedes principle. When ballast tanks are filled with air, since the force due to the weight of the air is less than the force due to the weight of the submarine, the submarine has positive buoyancy and rises to the water's surface. However, when the tanks are filled with water, the weight of the water inside can be greater than the weight of the submarine. This causes negative buoyancy, and the submarine begins to sink.

Ballast tanks consist of several sections so that the sinking and rising movements do not occur suddenly, and water intake or discharge starts from the tanks in the front. For this reason, submarines start to sink and exit from the front first [3].

iv. Propulsion Systems

The most researched subject in the development process of submarines, is propulsion systems. Air-fed diesel engines powered the first designed submarines. However, this caused these submarines to constantly need air supply over the water with the help of snorkels. Since this situation restricts the mobility of submarines and causes them to be easily noticed from the outside, air-independent propulsion systems such as closed cycle steam turbines and nuclear batteries have been developed and used [4].

Today, the use of submarines has become quite common. Although the first designs were made for military use, Unmanned underwater vehicles (UUV) are widespread in tourism and civil activities, and new technologies continue to be developed in this area [5].

UUV designs with different equipment are made especially for search and rescue, target determination, underwater sampling or underwater observation studies that may pose a danger to human health [6-8].

On the other hand, UUVs can also be used for communication and logistic support between all naval systems on the water. While the designs used for communication purposes are smaller and lighter, the designs used for logistics support are designed large according to the helpful load capacity they will carry. [9,10].

The UUV design shared in Figure 1.2 below is by Sun et al. It was designed by the biomimicry method for civilian use in 2021 [11].



Figure 1.2. The Sample UUV Design [11]

1.1.Literature

As in every field, there are new developments in submarine design with the advancement of technology. Especially the progress in computer-aided engineering has paved the way for measuring the performance of submarine designs with CFD. However, the foundations of today's modern submarine technologies have been laid with the work done in the last 20 years. Therefore, experimental studies by Liu and Huang on behalf of the Defense Advanced Research Projects Agency (DARPA) in 1998 are very important for the literature. In these studies, drag force measurement tests were carried out at different speeds for 11 submarine configurations, which are shared in Figure 1.3 below [12].

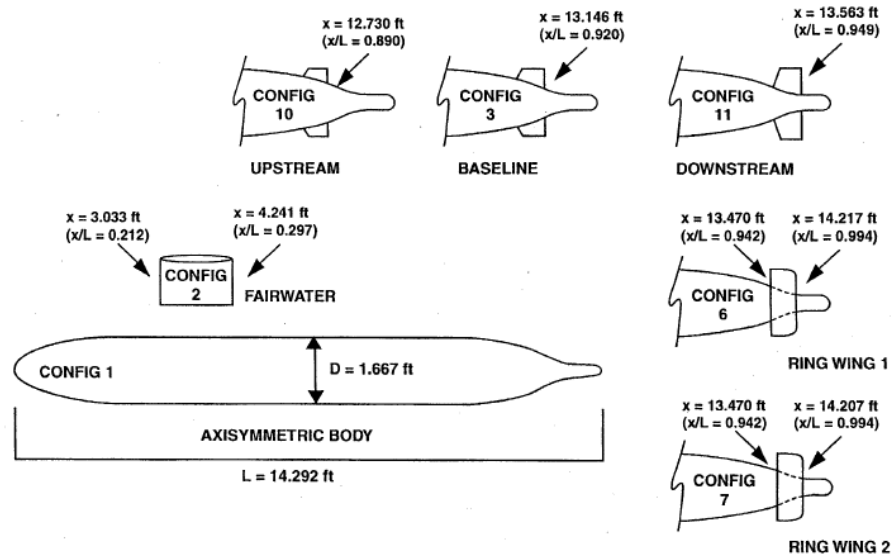


Figure 1.3. Hydrodynamic Test Geometries of DARPA SUBOFF Experimental Program [12]

Following these experimental studies, experimental verification studies were carried out with CFD and simulation methods that gave the most accurate results and started to be researched. In a study by Marshallay and Eriksson in 2012, the experiences obtained in CFD studies carried out until that year were summarized. In addition, all the details necessary for obtaining the simulation results closest to the experimental result with the Reynolds-Averaged Navier-Stokes Equations (RANS) model are summarized [13].

Although successful results were obtained with RANS, more advanced CFD solution methods were also tried. A study was conducted for the fully appendaged version of the DARPA SUBOFF model with Large Eddy Simulation (LES) by Qu et al. in 2021 [14].

At the point reached in today's literature, all the essential details of constructing CFD simulation models that give approximate results with experimental studies for DARPA SUBOFF and other submarine forms have been learned. In parallel with these studies, optimization studies have been started to increase the hydrodynamic performance of submarines. Although the studies in this field are pretty new, successful results have been obtained. For example, in a study conducted by Paz and Munoz in 2014, multiobjective optimization was applied to a submarine form, and the hydrodynamic

performance and mobility of the form were increased separately. With this study, the most effective design parameters and design limits on hydrodynamic performance and mobility have been determined. For example, when the initial and optimum forms presented in Figure 1.4 are examined, it is understood in what direction and how the form should change to increase the hydrodynamic performance [15].

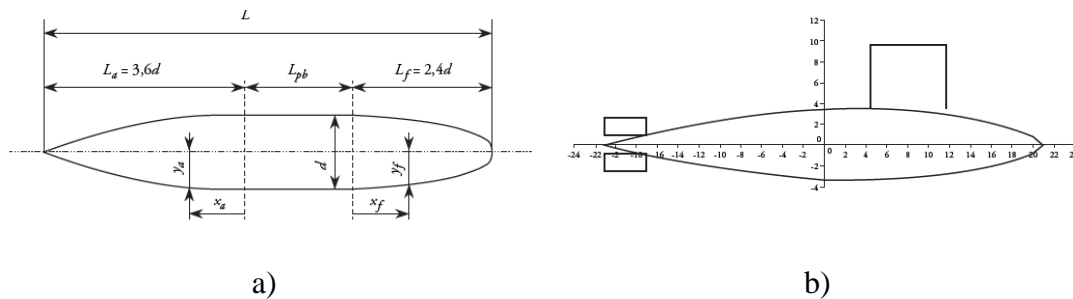


Figure 1.4. a) Initial b) Hydrodynamically Optimal Submarine Forms of Paz and Munoz's Study [15]

Gao et. In 2016, a study was conducted to derive new forms by combining different nose cones and stern forms, measuring the hydrodynamic performance through experimental studies, and then optimizing these forms with a Multi-Island Genetic Algorithm (MIGA), aiming to derive new forms with increased hydrodynamic performance. This study aimed not to find a submarine form to be produced directly but to provide information about the design changes that should be made when a form with increased hydrodynamic performance is desired. Studies were carried out for a maximum Reynolds number of 4.2×10^6 at velocities between 0.3 m/s to 1.5 m/s. After the study, it was suggested that pointed forms should be used as much as possible in both the nose cone and the stern for minimum drag force. Figure 1.5 shares the initial form used in this study and the enhanced hydrodynamic performance form [16].

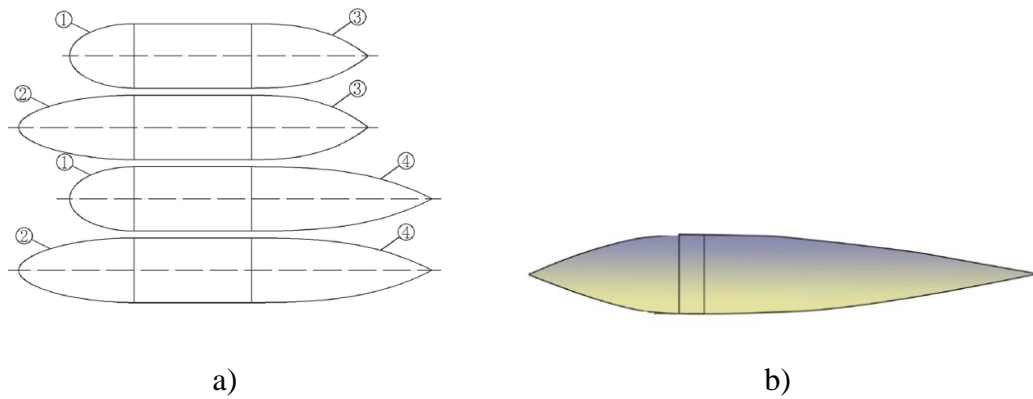


Figure 1.5. a) The test Models b) The Optimized Model's of Gao et. al's Study [16]

Many different studies have been carried out similar to the studies shared above, and the idea of what changes should be made in the design to increase the hydrodynamic performance of a submarine has begun to emerge. The study conducted by Divsalar in 2019 shared results that summarize the optimization studies using different nose cones and stern forms. In this study, the nose cone and stern length of the DARPA SUBOFF AFF-1 model were kept constant while the maximum diameter and middle hull length were changed. The simulation model, confirmed by the DARPA SUBOFF AFF-1 experiment result, was used in all different geometric configurations, and the hydrodynamic performance of all of them was calculated [17].

Although the scope of the study is broad, the results' precision could be higher since full parametric modelling is not performed, and all geometric configurations are created manually. After the different nose cone and stern forms tried in this study, the form that produces 15% less drag force than DARPA SUBOFF AFF-1 at 1.5 m/s is shared in Figure 1.6. While the length of the middle body of the optimum form has been shortened, its maximum diameter has been increased.



Figure 1.6. An Optimum Form of Divsalar's Study [17]

Another topic researched in the current literature on submarines is to make designs that can be affected by supercavitation. In this context, the most extreme point of a submarine hydrodynamic optimization study is to make a design that can create supercavitation because such designs have the highest hydrodynamic efficiency. For this reason, in any hydrodynamic optimization study that is not carried out with the goal of supercavitation, the direction in which the submarine form should be changed can be learned by examining the studies aimed at supercavitation.

Cavitation is a physical phenomenon that occurs when the liquid pressure is lower than the saturated vapour pressure in systems operating in water [18]. Supercavitation is a natural physical phenomenon that occurs when underwater vehicles reach high speeds. The pressure they create around them becomes much lower than the saturated vapour pressure of the water in their volume. In the meantime, a space around the vehicle will enclose almost the whole [19]. At this time, a small part of the nose cone of the vehicle comes into contact with the water, and the rest comes into contact with the cavity.

This significantly reduces the friction on the vehicle and allows the vehicle to accelerate to very high speeds. However, it is necessary to make significant design changes, especially in the nose cone part of the vehicle [20]. Many studies have been done on this phenomenon, and the design changes that need to be made when it is desired to increase the speed of a submarine have started to take place in the current literature. For example, in the study by Kim et al. in 2021, the supercavitation performances of two structures with blunt and conical nose forms were examined, and it was determined that the maximum velocity of the conical form was higher [21]. Two different forms used in the experiments in the study are shared in Figure 1.7.

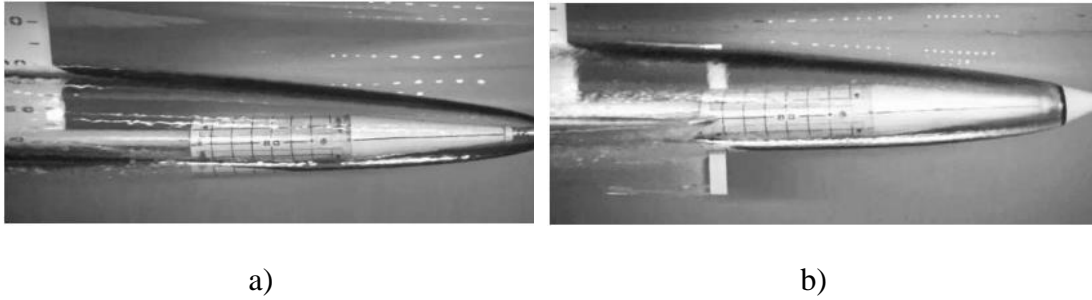


Figure 1.7. Supercavitation with a) Blunt Type b) Cone Type Nose Cavitator [21]

Since the studies shared above summarize similar studies done before them, they are sufficient to understand the meaning of the subject in the literature and to examine innovative submarine designs.

1.2. Motivation

Especially the widespread use of UUV necessitates the development of new designs with different features in this field. Since the common purpose of these designs is to increase the hydrodynamic performance, the relationship between performance and design changes is tried to be learned in the studies.

It is seen that most of the studies in the current literature in the field of submarine design are optimization studies to increase hydrodynamic performance with high-accuracy CFD simulations. Although the way to get maximum efficiency from an optimization study is to work with fully parametric models, according to the author's knowledge, there is no fully parametric study in the literature. Since optimization studies are generally based on trying different nose and stern forms, their efficiencies are controversial.

In addition, there are two crucial parameters in such optimization studies. The first is the difference in the longitudinal centre of buoyancy (LCB) positions between the newly derived and original forms. However, whether the longitudinal centre of buoyancy (LCB) points of the new forms derived in the three optimization studies shared above have been changed is not mentioned.

Another critical parameter is the difference between the displacement of the newly derived forms and the displacement of the first form. Divsalar stated in his study that the displacement was kept constant but did not share any information proving this. In

the other two studies, no information was given about whether the displacement was preserved.

In the following sections, necessary explanations about why these parameters are essential will be made, and information about how they reacted to these parameters will be given in the study conducted within the scope of the thesis.

According to these details, it is clear that there is a need for an optimization study with a fully parametric model in which both parameters mentioned above are taken into account in the literature.

1.3. Purpose of the Thesis

In the previous sections, the limitations of the studies in the literature were mentioned. Therefore, the study conducted within the scope of the thesis aims to conduct a more comprehensive study using the information obtained from the studies in the literature.

In this context, firstly, how to optimize a submarine was investigated. As a result of the research, it has been seen that four different optimization strategies are frequently used.

The first is the studies where the length and diameter do not change, but the displacement is accepted to decrease at specific rates. The second is the studies where the length over diameter ratio and displacement remain the same, but the length and diameter are increased equally.

The third is the studies done by decreasing the length and increasing the diameter.

The fourth and last one is the studies carried out by increasing the length and keeping the diameter constant.

In the study conducted in the thesis, the four optimization strategies mentioned above were also tried using the fully parametric CAD model. In this way, two essential inferences will be made.

i. Determination of the optimization strategy that reduces the drag force the most

When a submarine is desired to be optimized with no constraint, it will be learned which strategy reduces drag more.

ii. Determination of the optimization strategy that will reduce the drag force the most according to the design constraints

Suppose there are design constraints related to length, diameter or displacement. In that case, it will be ensured that the most appropriate strategy for these limits can be determined and an approximate estimation of the optimum design form.

Another highlight of the work to be done in the thesis is keeping the LCB constant in all the forms derived during the optimization studies. This way, a comparison of the drag forces will be made most accurately.

In summary, since the fully parametric CAD model will be used in this study, the scope of the studies can be broad. This way, all optimization studies in the current literature will be summarized, and the most efficient one will be determined by comparing different optimization strategies.

1.4. Outline of the Thesis

In this section, the content of the thesis will be summarized.

In the first chapter, the history of submarines is mentioned, and the studies in the literature are summarized. Then, examining these studies explains what the thesis wants to add to the literature and which methods it will add to the literature by making inferences.

In the second chapter, the terms of hydrodynamics are mentioned, and the turbulence model and Navier-Stokes equations, used as solvent equations, are discussed with basic literature knowledge.

In the third chapter, optimization studies are evaluated, and the fundamental theories of optimization strategies used in the thesis are explained.

In the fourth chapter, the simulation model used in the CFD simulations carried out within the scope of the thesis is shared with details, such as verifying this model with experimental work and making the results independent from the network.

In the fifth chapter, all the details about the setup of the optimization studies to be done in the thesis with CAESES and how the simulations are carried out are shared.

In the sixth chapter, the results of four different optimization studies conducted within the scope of the thesis are shared.

In the seventh chapter, the results obtained were evaluated and discussed, and predictions were made about future work.

2.THEORY AND MODELLING

In this section, hydrodynamic equations and models are shared. The Navier-Stokes equations from which Reynolds Averaged Navier-Stokes (RANS) equations are derived, and the theory of the SST k-w turbulence model are explained.

2.1. Navier-Stokes Equations

Navier-Stokes equations, one of the fundamental equations of fluid mechanics, are obtained by applying Newton's second law of motion for fluid motion. These equations are obtained by calculating the forces acting on a control volume when there is a continuous flow. The Navier-Stokes equations for incompressible flow can be written in Cartesian tensor notation as: [22]

Mass Conservation:

$$\frac{\partial u_i}{\partial x_i} = 0 \quad (2.1)$$

Momentum Equation:

$$\frac{\partial u_i}{\partial t} + u_j \frac{\partial u_i}{\partial x_j} = -\frac{1}{\rho} \frac{\partial p}{\partial x_i} + \nu \frac{\partial^2 u_i}{\partial x_j \partial x_j} \quad (2.2)$$

In the above equation, $\frac{\partial}{\partial t}$, ρ , u , p , t , ν represent the material derivative, density, flow velocity, pressure, time and kinematic viscosity respectively.

The variables here are instantaneous quantities that depend on both time and spatial coordinates.

2.2. Turbulence Modelling

Turbulence can be defined as flow motion without any rules in which it is difficult to distinguish a statistically significant mean in which fluid motions vary in various magnitudes according to space and time [23].

Another definition characterizes turbulence as a three-dimensional time-dependent motion that causes velocity oscillations of eddy elongation to propagate over all wavelengths where viscous forces and boundary conditions determine the minimum and maximum range [24].

Turbulent flow can be characterized as fluctuations in the velocity domain. Therefore, using the finer mesh structure elements than the smallest turbulence length scale and resolving with a shorter time step than the fastest fluctuation ratio (turbulence time scale) in the flow is called DNS (Direct Numerical Simulation). Conservation equations can be time mean, group mean, or controlled to remove small-scale occurrences. As a result, equations to be solved computationally may become more suitable for solution. However, equations modified in this way may contain unknown variables. Therefore, turbulence modelling is necessary to determine these variables in terms of known ones. Generally, the widely used RANS (Reynolds-Averaged Navier-Stokes) and LES (Large Eddy Simulation) turbulence models can be used to solve N-S equations since small-scale agitation may not need to be modelled directly depending on the application [25].

Within the scope of this thesis, a solution was obtained with the SST k- ω turbulence model using RANS methodology.

2.2.1. Reynolds Averaged Navier-Stokes Equations

The Reynolds average of the equation set consisting of mass and momentum equations is the basis for all algorithms that can perform computational fluid dynamics analysis. This mean includes the time average of the solution parameters in the Navier-Stokes equations [25].

According to the RANS mean, the velocity components are decomposed as follows:

$$u_i = \bar{u}_i + u'_i \quad (2.3)$$

To obtain the Reynolds Averaged Navier-Stokes (RANS) equations, equation 2.3 is written in the differential form of the conservation of mass and momentum equations. The Reynolds-averaged Navier-Stokes (RANS) equations for incompressible flow can be written in Cartesian tensor notation as:

Mass Conservation:

$$\frac{\partial u_i}{\partial x_i} = 0 \quad (2.4)$$

Momentum Equation:

$$\frac{\partial \bar{u}_i}{\partial t} + \bar{u}_j \frac{\partial \bar{u}_i}{\partial x_j} = -\frac{1}{\rho} \frac{\partial \bar{p}}{\partial x_i} + \nu \frac{\partial^2 \bar{u}_i}{\partial x_j \partial x_j} + \bar{u}_j' \bar{u}_i' \quad (2.5)$$

\bar{u}_j' and \bar{u}_i' are the fluctuating velocity components in the j-th and i-th directions, respectively

2.2.2. SST k- ω Turbulence Model

Although the standard k- ω model provides high success in boundary layer flows, Menter's comparison of popular turbulence models for boundary layer flows with reverse pressure gradients states that the standard k- ω model calculates excessive shear stress realistic velocity profiles. He stated that the reason for this did not include the calculation of the shear stress transport of the model, and he improved the results with a slight change in the calculation of the turbulent viscosity. The study states that the standard definition of turbulent viscosity causes erroneous results in flows containing reverse pressure gradients [26].

By this idea, Menter made a practical change in calculating the turbulent viscosity, ensuring that the shear stress is not greater than 0.3 (Bradshaw's constant) k . In addition, he added an intelligent function to the calculation of turbulent viscosity, ensuring that this change remains only in the boundary layer region [27].

Accordingly, he changed the calculation of turbulent viscosity as follows:

$$v_t = \frac{a_1 k}{\max(a_1 w; \Omega F_2)} \quad (2.5)$$

Here, a_1 denotes the constant number equal to 0.3. If Ω is considered for a two-dimensional flow in the boundary layer, it shows the derivative $\frac{\partial U}{\partial y}$, but it can be taken as the magnitude of eddy for general complex flows. F_2 , on the other hand, is an intelligent function that is one inside the boundary layer and 0 outside, which ensures smooth formatting in the transition between two values. Accordingly, the F_2 function is defined as:

$$F_2 = \tanh(\text{arg}_2^2) \quad (2.6)$$

$$\text{arg}_2 = \max\left(\frac{\sqrt{k}}{0.09wy}; \frac{500v}{y^2w}\right) \quad (2.7)$$

Here, y is the distance from the wall in the normal direction.

It has been shown that the standard k - ω model, especially in free shear flows, is highly dependent on the values of ω at the inlet boundary and can change the values of turbulent viscosity more than twice. Thus, in the boundary layer, Menter made a significant change in the ω transport equation by using the original k - ω model, which was very successful in this region, and aiming to get rid of the dependence of the model on the free flow values in free shear flows. The equation is used by transforming the variable in the ε transport equation used in the standard k - ε model, and thus the term called "cross-diffusion" is added to the ω transport equation used in the standard k - ω model.

In order for this term not to affect the original form, which is very successful in the boundary layer, it is ensured that it is used only in free flows and in the upper regions of the boundary layer with a smart function. Accordingly, the SST k - ω model uses the original k - ω model in the boundary layer and the standard k - ε model for free

shear flows, except for the change mentioned earlier in the calculation of turbulent viscosity. The turbulent kinetic energy k and specific dissipation ω equations used in the SST model are as follows [27]:

$$\frac{\partial k}{\partial t} + \frac{\partial}{\partial x_j} (kU_j) = \tau_{ij} \frac{\partial U_i}{\partial x_j} - \beta_k \omega k + \frac{\partial}{\partial x_j} \left[\left(\nu + \frac{\nu_t}{\sigma_k} \right) \frac{\partial k}{\partial x_j} \right] \quad (2.8)$$

$$\frac{\partial \omega}{\partial t} + \frac{\partial}{\partial x_j} (\omega U_j) \quad (2.9)$$

$$= \frac{\gamma}{\nu_t} \tau_{ij} \frac{\partial U_i}{\partial x_j} - \beta_w \omega^2 + \frac{\partial}{\partial x_j} \left[\left(\nu + \frac{\nu_t}{\sigma_w} \right) \frac{\partial \omega}{\partial x_j} \right] + 2(1 - F_1) \sigma_{cd} \frac{1}{\omega} \frac{\partial k}{\partial x_j} \frac{\partial \omega}{\partial x_j}$$

3. OPTIMIZATION METHODOLOGY

Optimization can be mathematically explained as the process by which an objective function's maximum or minimum value is found [28]. Especially in recent years, it has become essential to carry out optimization studies as more complex problems have become solvable through simulations. In this part of the thesis, the study's definition as an optimization problem will be made, and it will be explained how to choose the most suitable algorithm for hydrodynamic optimization.

Since this thesis is not a study in the field of statistics, in-depth information about optimization methods and their algorithmic theories is not given. However, only the algorithms of the methods used in the thesis are summarized. In Figure 3.1 below, the optimization steps followed and the algorithms used are shared.

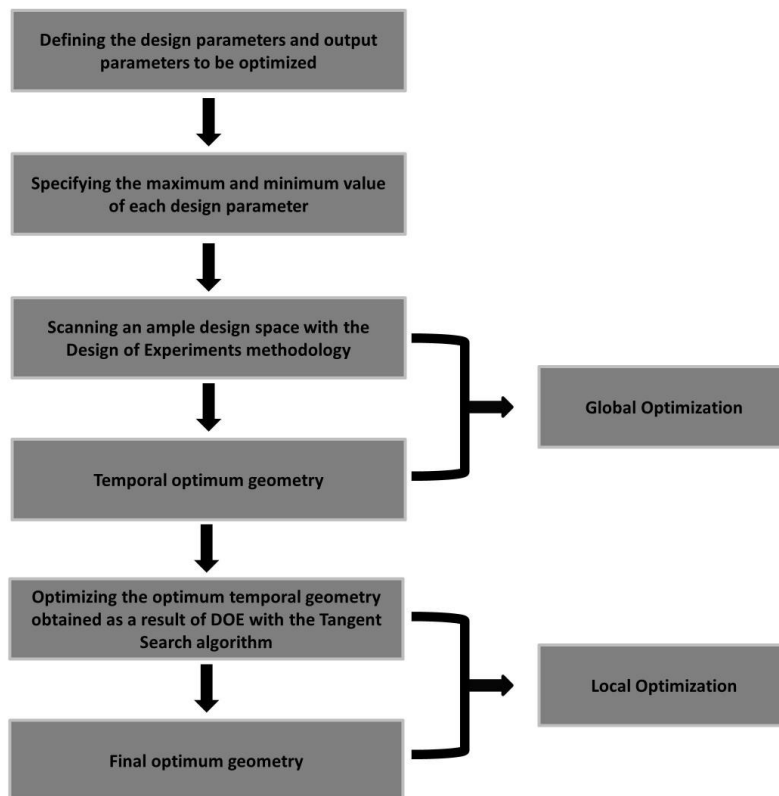


Figure 3.1. Optimization Process Steps Followed in the Thesis

3.1. Theory of Optimization Methodology

As seen in Figure 3.2, many optimisation methods are used in the literature, but these methods are generally divided into two classes: exact and approximate [29]. The method used in the thesis is included in the underlined groups.

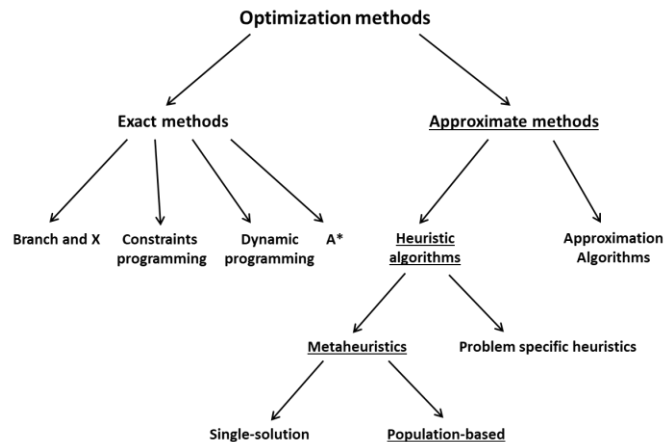


Figure 3.2. Classification of Optimization Methods

Exact methods, as the name suggests, can give exact results. However, these methods are not practical because they require a high computational cost and perform many local optimization works [30-32]. For this reason, approximate methods are more advantageous than exact methods, especially in complex optimization problems. Hence, the most commonly used approximate methods are in the heuristic and metaheuristics classes, respectively [33, 34].

In this thesis, the optimization is performed in two stages. In the first step, the Design of Experiments was performed to collect data. Then, the Tangent Search method in the population-based metaheuristics category was used in the second stage for local optimization.

3.2. Design of Experiment Methodology (DoE)

Regardless of the field of optimization studies, it is necessary to collect data in the first step, and at this point, the best-known method is the Design of Experiment (DoE) method [35,36]. This method collects and analyses data with statistical models such as Latin squares or full factorial [37]. This process aims to keep the data collected to a minimum and to maximize the number of data provided by performing as few tests as possible [38].

This methodology DoEs not have an algorithm directly introduced to the science of statistics, and the underlying terminology is based on the work of Sir Ronald Aylmer Fisher in the 1920s [39]. However, in the following years, this theory was applied by Box and Wilson in industrial experiments, and it became widespread use by the DOE method in the first stage of their post-op optimization studies. This study also paved the way for the correct evaluation of the results by performing Response Surface Modeling studies after DoE [40]. In the following process, more detailed studies were made by Genichi Taguchi, and the DoE terminology was finalized [41].

3.2.1. Terminology in Design of Experiments

To perform DoE in CFD applications, defining the problem and selecting the design parameters is necessary. Then, the range of variability should be defined by subtracting each design parameter's minimum and maximum values. Finally, according to the maximum number of simulations that can be made in these intervals, a design space is created by randomly changing the design parameters at the specified intervals, and the results of all designs are collected. However, this situation brings with it a risk. Since there is no information about the solution space in the first place, the created design space may exclude the optimum design [42].

In this thesis, different designs to be created while doing DoE were created using the Sobol sequence algorithm. This risk was minimized by systematically creating the designs.

3.2.2. Sobol Sequence Algorithm in Design of Experiments

Russian mathematician I.M. Sobol first proposed the Sobol sequence in 1967 [43]. The approach aims to get the most accurate integral result with the Monte Carlo method. For example, the sequence derived by Sobol in equation 3.1 gives the least incorrect result against [44].

$$\int f(x) = \lim_{n \rightarrow \infty} \left(\frac{1}{n} \right) \sum_i f(x_i) \quad (3.1)$$

How this algorithm integrates with DOE can be explained as follows. Since the mathematical basis is not strong in other global optimization methods where Sobol is not used to derive a new design, the derived designs cannot create the correct design space and mislead the optimization. On the other hand, the Sobol sequence has a more advanced mathematical formulation than other methods, thus ensuring more consistent results by creating a suitable design space and ensuring adequate exploration. At the same time, since the Sobol sequence is not entirely random but quasi-random, it can be derived much more quickly from sequences defined in other DOE methods [44].

3.3. Metaheuristics Optimization Methodologies

Metaheuristics methodologies can be defined as stochastic algorithms that continuously evaluate an objective function and repeat the process, thus aiming to progress towards the optimum. They can provide adequate solutions with reasonable levels of computational power but need help to ensure optimality. Nevertheless, these methods are suitable for use in many optimization problems thanks to the advanced abstraction techniques they use [28]. As seen in Figure 3.1, they are generally divided into two classes single-solution and population-based [28]. Single-solution methods are also included in the literature as local search methods, and they need a starting point to start the process. They try to catch the minimality by looping the solution presented at the beginning with continuous algorithms [28]. This indicates that determining the starting point for optimization is critical and can be considered a limitation of the competence of these methods. These methods are divided into two classes gradient search-based (GSB) and gradient-free search (GFS) algorithms. Newton-Raphson algorithm [45] GSB class algorithms; Nelder-Mead simplex [46], random Hill Climbing [47], Simulated Annealing [48], and Pattern Search [49] can be given as examples of algorithms in the GFS class. Single-solution

methods' devotion to the first solution has led scientists working in this field to focus on developing other methods. At this point, we come across population-based or global search methods. Unlike local methods, these methods do not need a starting point. They aim to reach the optimum by considering the optimization problem very generally by finding more than one candidate optimum point [28].

This enables the optimization loop to find the optimum by scanning a much larger space with minimum error. Differential Evolution Algorithms [50], Artificial Bee Colonies [51], and Genetic Algorithms [52] can be given as examples of the most well-known population-based algorithms. However, these methods cannot be described as perfect because they need to use a developed mathematical infrastructure. Therefore, in recent years, metaheuristic algorithms with highly developed mathematical infrastructures have begun to be developed. In this context, high efficiency is obtained in optimization problems that seem pretty complex and challenging by using arithmetic, geometric or analytical functions in the optimization processes of the studies [53-56].

It cannot be said that a single algorithm is more efficient than the others because they work with each other with very different efficiency, although these algorithms use mathematical infrastructure.

At this point, there is a need for a new algorithm that combines the prominent features of different mathematical algorithms without losing the advantage of using mathematical infrastructure to solve optimization problems. The solution is Tangent Search Algorithm, and more detailed information is given in the next section.

3.4. Tangent Search Algorithm

The tangent search algorithm, as the name suggests, is a reasonably new algorithm based on the tangent function, and it was finalized in 2021 by Abdesslem Layeb [28]. It is known that the value of the tangent function changes from $-\infty$ to $+\infty$, which indicates that the tangent search algorithm has a vast space scanning capacity. At the same time, since the tangent function is periodic, this algorithm provides a good balance between scanning and finding. The T-Search algorithm consists of four basic steps, and the step scheme is shared in Figure 3.3 [57].

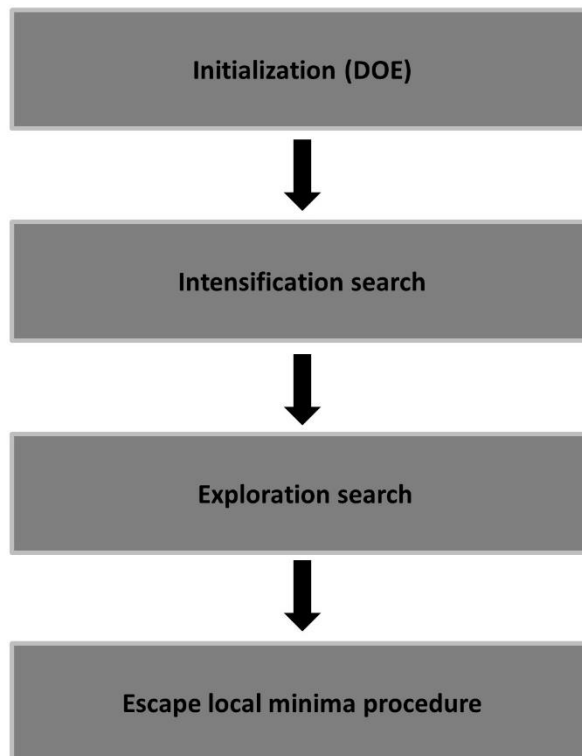


Figure 3.3. Steps of the Tangent Search Algorithm

How this algorithm is used in CFD studies can be explained as follows. First, the output parameter to be minimized is determined in the simulations to be made. Then the lower and upper bound values of all design parameters are determined. Next, the algorithm changes the value of one design parameter while keeping the others constant to understand the effect of each design parameter on the output parameter. After repeating this for each design parameter, the answer to the question of which design parameters should decrease and which should increase. In the ongoing process, it controls the value of the output parameter by simultaneously increasing or decreasing the design parameters. This loop continues until the output parameter is minimized. This algorithm promises to give the optimum result by scanning a considerable space, especially in single-objective optimization studies such as the work done in this thesis [57].

4.SIMULATION MODEL

This section contains all the details of the standard CFD simulation model used to get the result of all geometric variations. These details are flow field and boundary conditions, simulation parameters and solver settings, mesh generation, mesh independence study and comparison of results with experimental data. After completing this section, a simulation model was obtained that gives close results to the results of the empirical studies.

4.1. Geometrical Model

In this study, new designs are derived based on the non-appendages axisymmetric bare hull of the DARPA SUBOFF submarine model (AFF-1), which was used in the SUBOFF project carried out by the Submarine Technology Program Office of the Defense Advanced Research Projects Agency. The performance of these designs is compared with that of the AFF-1 model [58]. The main details of the geometry are shown in Figure 4.1 with symbols, and the main particulars are shared in Table 4.1.

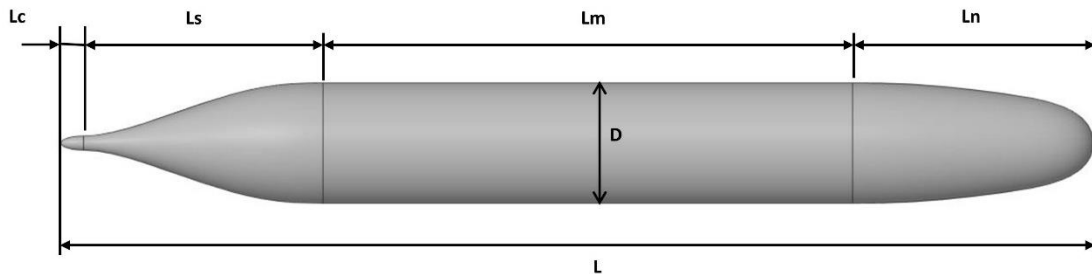


Figure 4.4. The Symbols of the Main Geometric Details

Table 4.1. The Main Particulars of DARPA SUBOFF AFF-1

Description	Symbol	Magnitude	Unit
Total Length	<i>L</i>	4356	mm
Maximum Diameter	<i>D</i>	508	mm
Length of the Nose	<i>L_n</i>	1016	mm
Length of the Middle	<i>L_m</i>	2229	mm
Length of the Stern	<i>L_s</i>	1016	mm
Length of the Cap	<i>L_c</i>	95	mm
Volume of Displacement	<i>Disp</i>	0.708	m ³
Centre of Buoyancy	<i>LCB</i>	0.4621 <i>L</i>	-
Wetted Surface Area	<i>A</i>	5.998	m ²

4.2. Simulation Domain and Boundary Conditions

In CFD analyses of external flows, the size of the computational domain significantly impacts the results. Modelling the volume too small may affect the flow around the submarine and causes results to be inaccurate. On the contrary of this situation, modelling the domain larger than it should increase the number of mesh elements and prolongs the solution time. The form and dimensions of the external computational domain used in this study are shown in Figure 4.2, and its dimensions have been determined by making preliminary simulations.

In these simulations, a very large computational domain was initially chosen, and the dimensions of this volume were systematically reduced to determine where the results were independent of the dimensions of the flow volume. The external flow domain dimensions obtained at the end of the study also coincide with the guide published by ITTC [59].

Since the bare hull model is axisymmetric, it can be modelled periodically and symmetrically. However, since the entire volume is not modelled in periodic modelling, the 3D flow effects are reduced as the defined periodicity angle decreases. On the other hand, this is an optimization study and modelling the entire volume means more mesh elements will be used. Therefore, the volume was modelled symmetrically to keep the mesh element number optimal and minimize the loss of 3D flow effects.

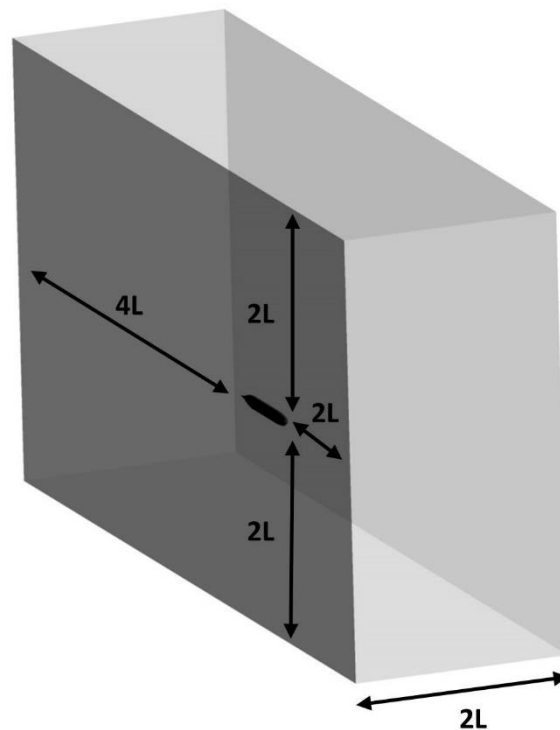


Figure 4.5. Dimensions of the Computational Domain

Boundary conditions used in the validated simulation model are shown in Figure 4.3. The inlet boundary condition for a constant velocity of 3.045 m/s normal to the surface is defined to the right of the flow domain, and the Reynolds number is approximately 12,000,000. All simulations performed within the scope of the optimization study were performed for a speed of 3.045 m/s, and the performance of the optimum form obtained at the end of the study at different speeds is shared in the results section. As in this study, when it is aimed to establish a simulation model that will confirm the experimental results, it is necessary to model the turbulence characteristic of the flow correctly. In this context, the turbulence sensitivity and turbulent viscosity ratio values used in the study are taken from the study, which confirms the RANS model with the experiment of DARPA SUBOFF AFF-1 [60].

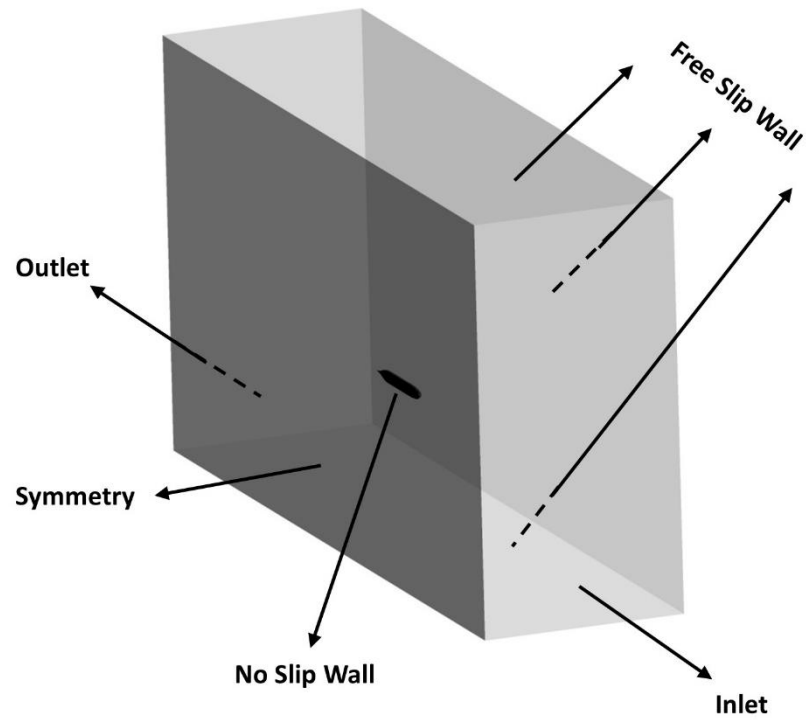


Figure 4.6. Boundary Conditions

The outlet boundary condition is defined to the left of the flow domain with zero-gauge pressure. As mentioned before, half of the submarine hull is modelled, and symmetry condition is defined at the mid-surface. The surfaces of the submarine hull are modelled as no-slip walls, the remaining side surfaces are modelled as free-slip, and all boundary conditions are summarized in Table 4.2.

Table 4.2. Boundary Conditions Details

Name Selection	Boundary Condition Type	Parameter	Value
Inlet	Velocity Inlet	Velocity (m/s)	3.045
		Turbulent Intensity (%)	1
		Turbulent Viscosity Ratio	10
Outlet	Pressure Outlet	Gauge Pressure (Pa)	0
Side Walls	Wall	Free Slip	-
Symmetry	Symmetry	-	-
Bare Hull Surface	Wall	No Slip	-

4.3. Simulation Parameters and Solver Settings

The working fluid used in the simulations is water. Since these simulations are performed at low speed and constant temperature conditions, the density and viscosity of the water are considered constant. Therefore, the fluid properties were defined the same as in the experimental work of Huang et al. [12], and the water density is 998.2 kg/m^3 . The dynamic viscosity is taken as $1.003 \times 10^{-3} \text{ kg/(ms)}$.

These experimental studies were carried out for six different speed values ranging from 3.045 to 9.15 m/s of 8 different DARPA SUBOFF configurations in the fully submerged condition. In the studies, submarine models were used with their actual dimensions, and the volume of the test pool is the same as that recommended in the guide prepared by ITTC.

On the other hand, the turbulence modelling method is one of the most critical parameters affecting the simulation results. When similar studies [61-64] conducted with the RANS approach were examined, it was seen that the turbulence model that gave the most consistent results with the experimental results is SST k-w. Therefore, this model is used in all simulations.

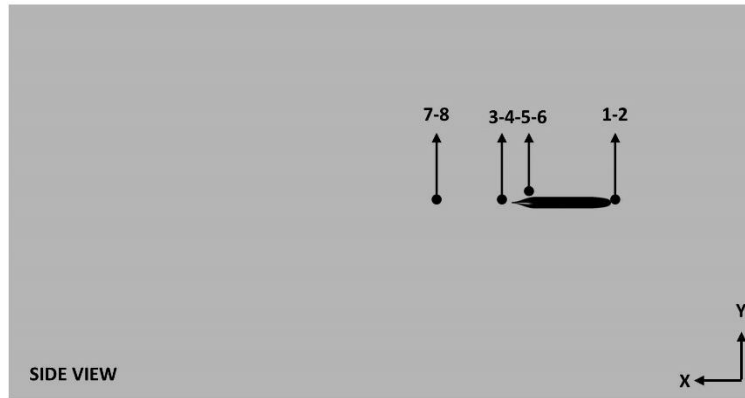
In the study, only the hydrodynamic performance of the submarine is examined, and this evaluation is independent of time. In order to verify this situation, transient solutions were taken, and it was seen that it was independent of time, so a steady formulation was used. The coupled scheme is used for velocity and pressure relation. Gradient discretization is performed using the least squares cell-based method. For pressure, momentum, turbulent kinetic energy and specific dissipation rate, the second-order upwind scheme has been used, and all schemes and discretization methods are shared in Table 4.3.

Table 4.3. Methods and Discretization Schemes Used

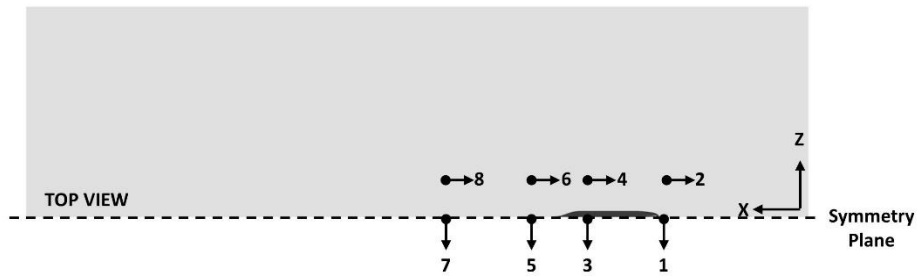
	Methods and Discretization Schemes
Pressure-Velocity Coupling	COUPLED
Gradient	Least Squares Cell-Based
Pressure	Second Order Upwind
Momentum	Second Order Upwind
Turbulence Kinetic Energy	Second Order Upwind
Specific Dissipation	Second Order Upwind

Convergence checks are detailed via residual graphs and additional monitors. Velocity data from 8 different points which are shown in Figure 4.4 and Table 4.4, of the flow domain were continuously checked to ensure that the solution converged, and the velocity became stable at these points. On the other hand, the drag and lift forces of the submarine were also monitored, and these parameters were checked for convergence. Before starting the solution, all simulations were initialized using the Full Multi Grid (FMG) method and it was seen that the validation study converged in about 100 iterations.

For this reason, 150 iterations were performed in all optimization studies to ensure that the results converged. Convergence means that the speed and force values become stable, and the residual values decrease to 10^{-6} .



a)



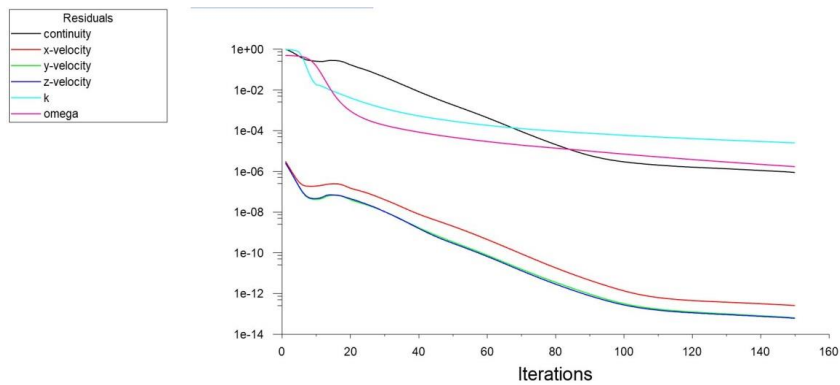
b)

Figure 4.7. Locations of Convergence Control Points a) Side View b) Top View

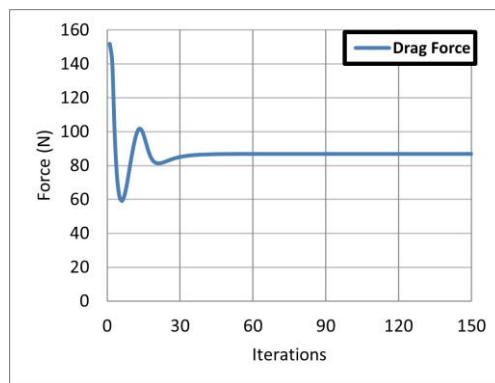
Table 4.4. Coordinates of Convergence Control Points

Points	X Coordinate (mm)	Y Coordinate (mm)	Z Coordinate (mm)
1	-10	0	0
2	-10	0	1000
3	3250	264	0
4	3250	264	1000
5	4366	0	0
6	4366	0	1000
7	7366	0	0
8	7366	0	1000

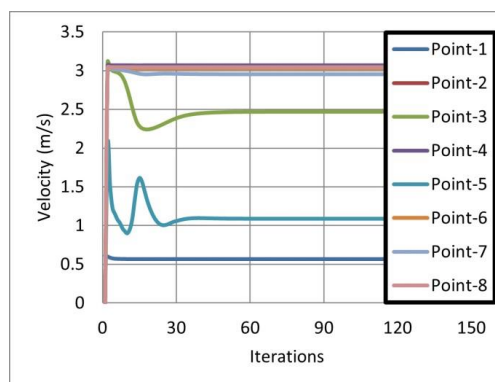
The additional monitors assigned to control the simulations' convergence and the residuals' graphs are shared in Figure 4.5. It is clearly understood from these graphs that residual values have dropped to the highest, approximately 10^{-6} level, and drag force and velocity values at eight control points converged.



a)



b)



c)

Figure 4.8. Convergence Control Graphs a) Residuals b) Drag Force c) Velocity at Control Points

4.4. Mesh Generation

Since this study aims to establish a simulation model that confirms the experimental results and uses this model throughout all optimization studies, a mesh structure is generated with a minimum number of elements to provide maximum accuracy, and the mesh generation steps are shown in Figure 4.6.

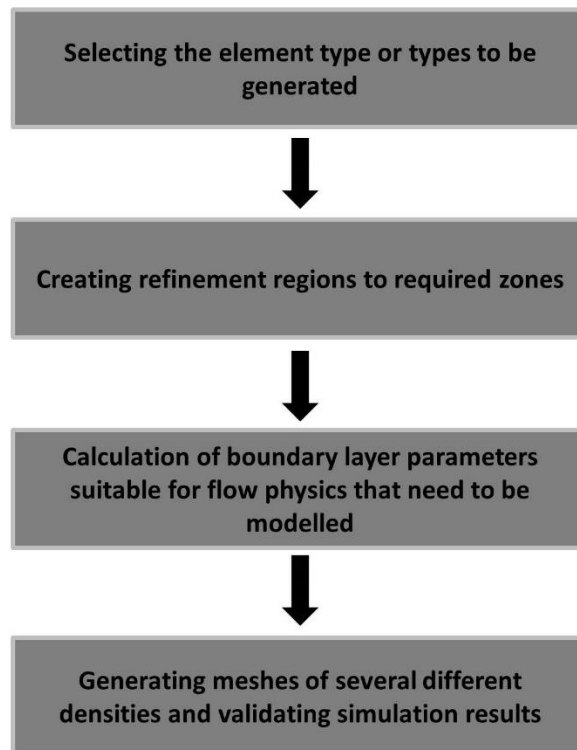


Figure 4.9. Mesh Generation Steps

One parameter that directly affects the result in CFD studies is meshing. Adequate modelling is essential to increase the accuracy of simulation solutions, but at this point, it should be known that the unnecessarily dense mesh will prolong the solution time. Therefore, mesh structures that give maximum accuracy with the optimum number of elements should be created. For this, the physics of the problem should be understood correctly, the requirements should be determined entirely, and a mesh structure should be created according to these requirements. In the first step, the type of element to be used should be decided. These element types are commonly used in Figure 4.7 and summarized as tetrahedral, hexahedral, polyhedral and cartesian with cut cells. Except for a few specific flow problems, there is no specific requirement on the element type.

For this reason, having several choices of mesh element types can be confusing at this stage. However, when the advantages and disadvantages of each element type are known, the element type selection that matches the requirements of the problem can easily be made. In addition, tetrahedral elements model successfully complex geometries but cannot be used in boundary layer modelling and can cause convergence problems. While hexahedral elements can significantly reduce the total number of elements and converge more efficiently, they are unsuitable for high-quality modelling in complex geometries. Another element type is polyhedral, which can significantly reduce the total number of elements and converge more quickly than other elements.

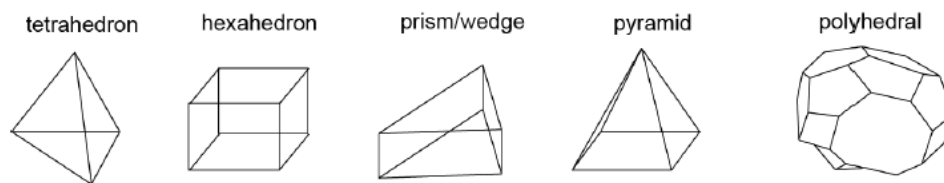
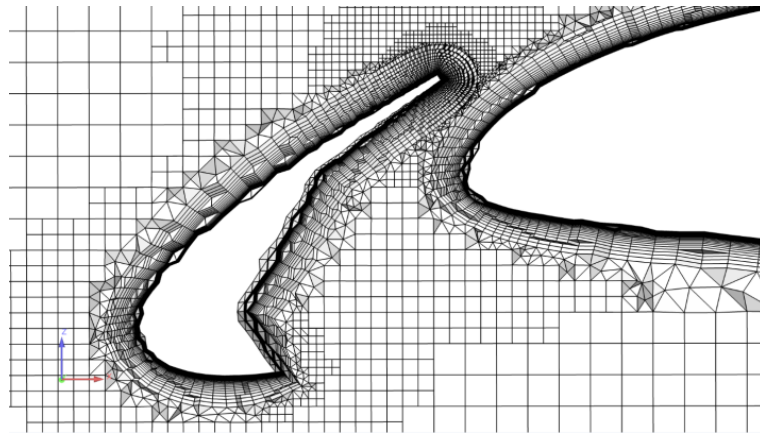
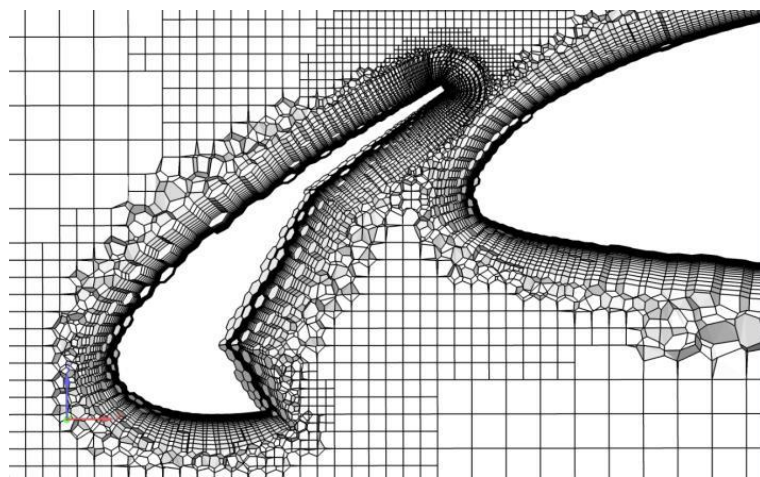


Figure 4.10. Different Types of Mesh Elements [65]

When the advantages and disadvantages of common element types are examined, it is challenging to choose a specific element type for many CFD problems. In this context, hybrid methods that enable the use of different element types have become quite common in industry and academia in recent years. These hybrid methods can serve the needs directly by using different element types. Examples of the most widely used hybrid methods are hexcore using tetrahedral and hexahedral element types and poly-hexcore methods using polyhedral and hexahedral element types. Especially in aerodynamic and hydrodynamic studies, using the poly-hexcore method provides the advantages of reducing the total number of elements, convergence with less iteration and higher accuracy. In the case study of Zore et al.[66], which examined the aerodynamic performance of a high-lift aircraft JSM-WBNP, simulation and experiment results were compared using hexcore and poly-hexcore methods and detailed images of two different mesh structures used are shared in Figure 4.8.



a)



b)

Figure 4.11. Volume Mesh of JSM-WBNP a) Hexcore b) Poly-Hexcore [66]

At the end of the study, it was determined that the total number of elements in the poly-hexcore method was reduced by about half, and accordingly, the solution time was shortened by about 41%. When the results of the two different methods were compared with the experimental results, it was seen that the accuracy rates were very close to each other and the experimental results. Since this thesis is an optimization study, it is necessary to use a simulation model that can converge in a minimum time and provide maximum accuracy. For this reason, it was decided to use the poly-hexcore hybrid method in the simulation model, and a mesh structure was created with this method in all simulations.

The most practical method of minimizing the total number of elements without reducing the accuracy of the solution is to use denser elements in the regions where the flow is disturbed more than in other regions. When this method is adapted to this study, it can be concluded that denser mesh structures should be created for volumes close to the submarine. For this reason, this process was performed with four different refinement regions, the details of which can be seen in Figure 4.9. Several simulations were made and optimized by systematically changing the sizes of these regions, and the results were independent of the sizes of these regions.

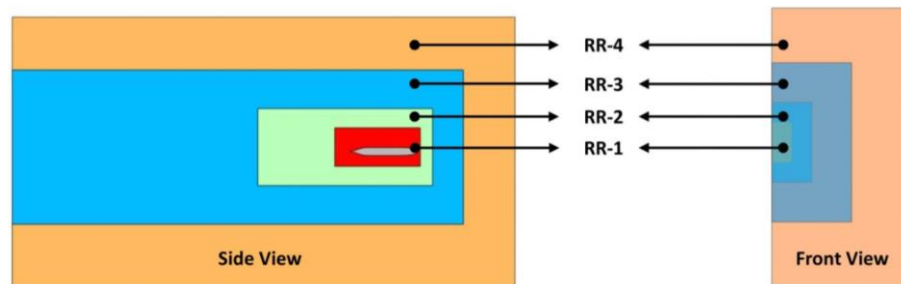


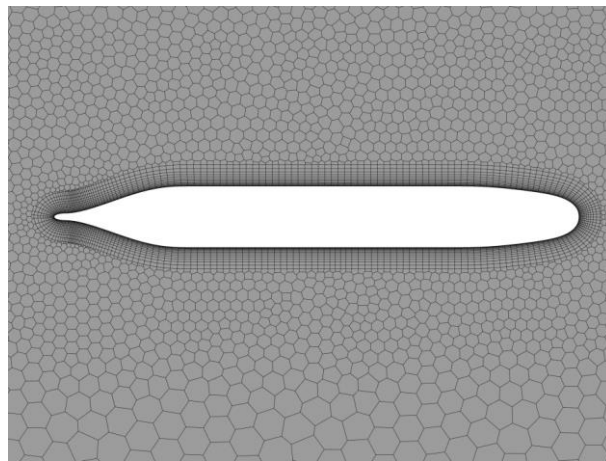
Figure 4.12. Refinement Regions to Control Mesh Density

Another point to be considered in the mesh generation process is near-wall modelling by creating the boundary layers around the walls. It is imperative to make a near-wall modelling that will meet the requirements of the turbulence model and can model the flow physics realistically as closely as possible. At this stage, different studies in the literature in which the experimental results confirmed the CFD simulation results for the DARPA SUBOFF submarine model were examined to establish the optimum y^+ interval and the optimum number of layers [67-71]. In addition, Marshallay and Eriksson prepared a study to summarize all these studies, compared the simulation results for different turbulence models and y^+ intervals with the experimental results, and recommended that the average y^+ value on the hull be approximately 80 for the SST k- ω turbulence model [13]. In line with this information, several preliminary simulations were performed automatically by constantly changing the height of the first boundary layer. As a result, the boundary layer parameters giving the y^+ distribution of approximately 80 on the bare hull were calculated for a speed of 3.045 m/s. Its details are shared in Table 4.5, and detailed views are shared in Figure 4.10.

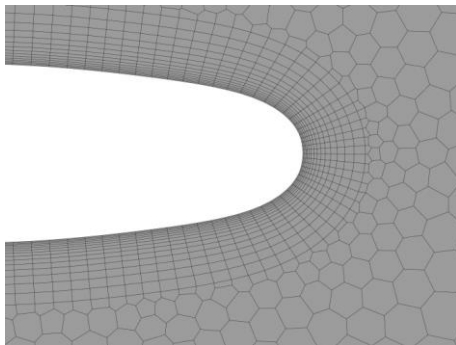
Table 4.5. Details of the Boundary Layer Mesh

Parameter	Value
Number of Layers	15
First Layer Height	1.356×10^{-4} m
Growth Rate	1.1

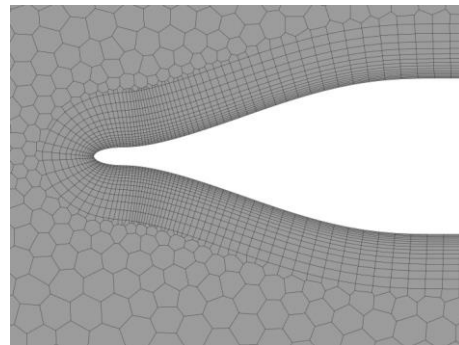
When examining mesh images, it should be known that poly elements are used in the surface mesh in this poly-hexcore hybrid method.



a)



b)



c)

Figure 4.13. Boundary Layer Mesh Around at Different Locations a) the hull b) the nose c) the stern

4.5. Mesh Independence Study

At this thesis stage, the necessary details of the mesh independence study are shared. A detailed mesh study was carried out by creating six different mesh structures. The most critical parameters in the mesh independence study are the upper-lower surface element sizes in the entire computational domain and the average element size in the refinement regions. These parameters are systematically reduced from the coarsest mesh to form different mesh structures. It is aimed to increase the number of elements approximately two times in each new mesh structure. The total number of elements of these mesh structures varies between 37 thousand to 1.6 million, and all the details are shared in Table 4.6.

Table 4.6. Details of Mesh Structures (All sizes are in mm)

	Mesh-1	Mesh-2	Mesh-3	Mesh-4	Mesh-5	Mesh-6	Mesh-7
Lower Element Face Size	40	20	10	7.5	5	2.5	1.25
Upper Element Face Size	8000	4000	2000	1500	1000	750	500
Refinement Region-1	400	200	100	75	50	50	50
Refinement Region-2	1000	500	250	187.5	125	125	125
Refinement Region-3	2000	1000	500	375	250	250	250
Refinement Region-4	6000	3000	1500	1125	750	750	750
Number of Elements	37 K	71 K	178 K	345 K	738 K	1.2 M	1.6 M

For mesh independence control, the drag force was calculated for each mesh structure, and these values were compared with the results of the experimental study of Huang et al. [12]. The equation of the dimensionless drag coefficient is shared in the equation below.

$$C_D = \frac{F_D}{\frac{1}{2}\rho AU^2} \quad (4.1)$$

Where F_R is the total drag force of the axisymmetric bare hull body, ρ is the density, A is the wetted surface area and U is the velocity.

The force values calculated for 3.045 m/s with each mesh structure and the error rates which can be calculated with below equation between these values and the experiment results are shared in Table 4.7.

Table 4.7. Drag Force Values for Calculated Each Mesh Structure and Absolute Errors between Mesh-3 and other Mesh Structures

Mesh	Drag Force (N)	Absolute Error Between Mesh-3
1	90.6947	3.8685 %
2	89.1509	2.101 %
3	87.3168	0
4	87.8746	0.639 %
5	87.6293	0.359 %
6	87.0852	0.265 %
7	87.5147	0.227 %

As seen from the table, when the drag force values of seven different mesh structures were examined, all mesh structures created after Mesh-3 gave results close to each other. Although more mesh structures were tried in the continuation of the study, the results were obtained in this range. Therefore, the results obtained with the simulation model detailed in the previous sections will give close results in this value range. Consequently, the drag force values of 7 different mesh structures created are shared in Figure 4.11, together with the element numbers of these mesh structures.

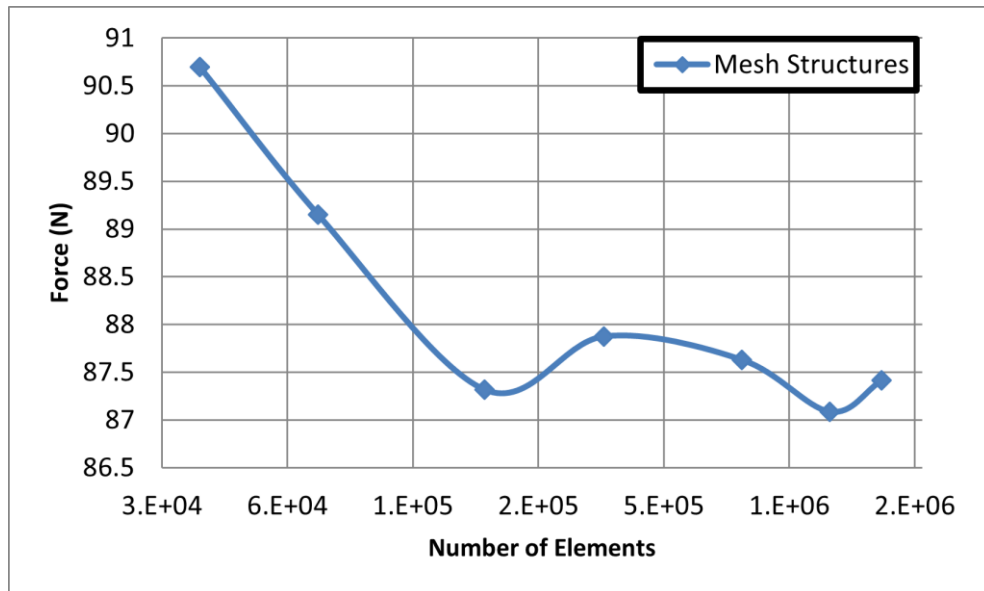


Figure 4.14. Comparison of Seven Different Mesh Structures

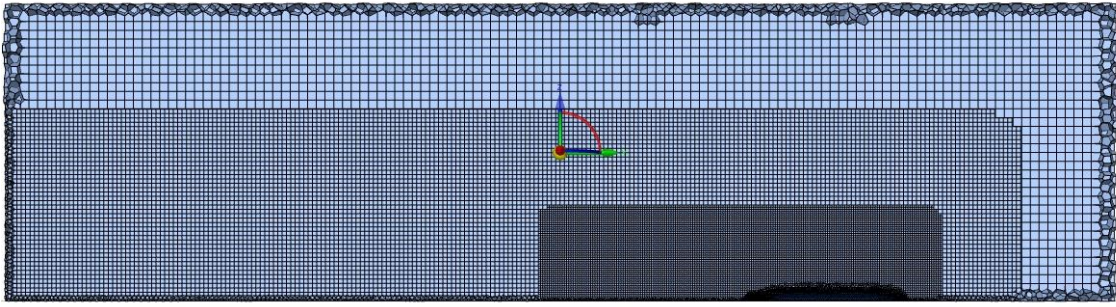
If the drag force values obtained with different mesh structures are close to the test result, one of them can be selected for the verified model. However, if the results are unacceptably far from the experimental result, it will be necessary to change the simulation model.

The drag force value calculated for a speed of 3.045 m/s in the referenced experiment is 87.4 N, and it is seen that the drag force values of all mesh structures created after Mesh-3 are in this range. The absolute error between Mesh-3 and all meshes created after Mesh-3 is below 1 percent.

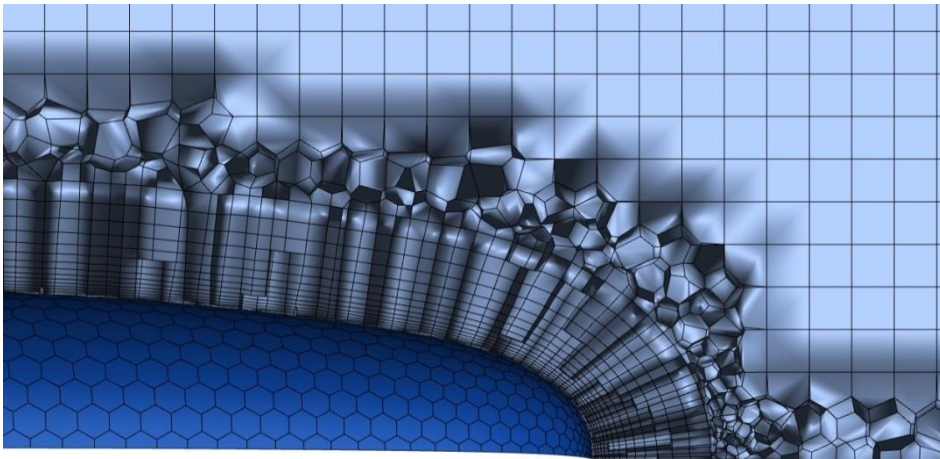
Since the drag force values obtained with different mesh structures are close to each other and the test result, Mesh-3 can be selected as the final mesh structure.

In addition, since this is an optimization study, the total number of elements and every detail that will speed up the simulation is essential. Nevertheless, the primary priority here is accuracy, not speed. For this reason, mesh structures have been studied in great detail.

In summary, there are two reasons for choosing Mesh-3 as the final mesh structure, the details of which are shared in Figure 4.12. The first is that it gives results close to the results of the experiment and the results of the mesh structures created after it. The second is that it has the least number of elements among these five structures.



a)



b)

Figure 4.15. Mesh Structure to be Used in the Validated Simulation Model a) Overview
b) Boundary Layer Transition on the Nose

5. HYDRODYNAMIC OPTIMIZATION PROCESS OF THE SUBMARINE

This chapter of the thesis details the steps of the hydrodynamic optimization process. Initially, the DARPA SUBOFF AFF-1 was modelled in 3-D on CAESES. In the ongoing process, this model has been made parametric and is ready to create a design space. Afterwards, global, and local optimizations with DoE and T-Search algorithms, detailed in Section 3, were carried out using the simulation model shared in Section 4. Finally, the most optimum design is aimed at, and this process is explained in detail in Figure 5.1.

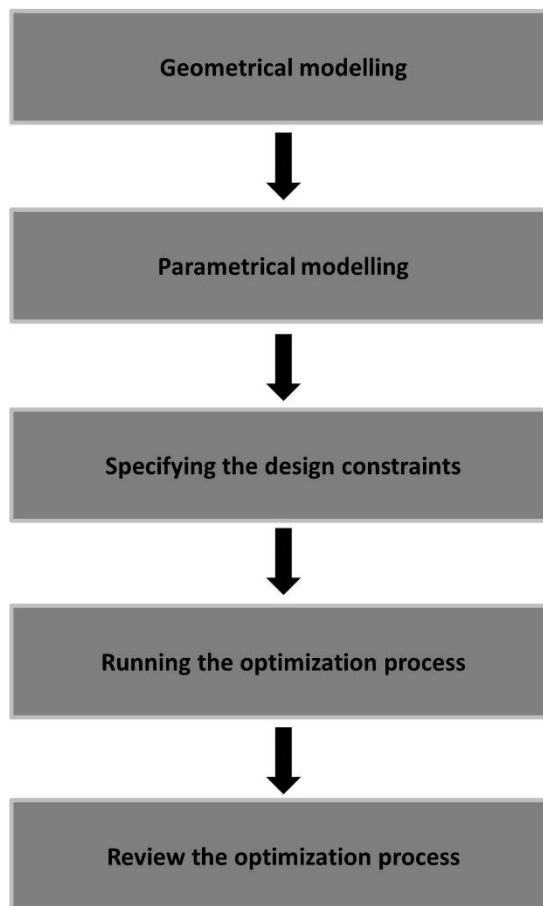


Figure 5.16. Steps of the Optimization Process

5.1. Geometrical Modelling

First, the DARPA SUBOFF AFF-1 model, the primary geometric details shared in section 4, was modelled in 3D in CAESES with the dimensions of the model used by Groves et al. [58]. This modelling has been done using different curve equations that calculate the varying radius of the four main body sections along their lengths: the nose, middle body, stern, and cap. Geometric sections are given in Figure 5.2, and the equations of each curve are shared in below equations. Since the equations are shared by NASA in Feet units, they are scaled in meters after the design is completed.

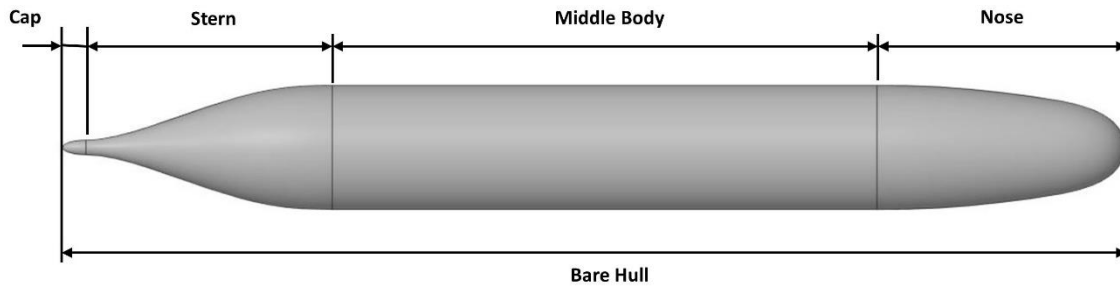


Figure 5.17. Geometric Sections of the DARPA SUBOFF AFF-1 Model

$x = \text{Model Scale Axial Length in Feet}$

$R = \text{Model Scale Radial Length in Feet}$

$\text{Maximum Body Diameter} = 1.666667 \text{ Ft (0.508 m)}$

$\text{Total Body Length} = 14.291667 \text{ Ft (4.356 m)}$

The Equation of the Nose Cone for $0 \text{ Ft} \leq x \leq 3.333333 \text{ Ft}$

$$R = R_{MAX} \{ 1.126395101x(0.3x - 1)^4 + 0.442874707x^2(0.3x - 1)^3 + 1 - (0.3x - 1)^4(1.2x + 1) \}^{1/2.1} \quad (5.1)$$

$$R_{MAX} = \frac{5}{6} \text{ Ft} \quad (5.2)$$

The Equation of the Middle for $3.33333 \text{ Ft} \leq x \leq 10.645833 \text{ Ft}$

$$R = R_{MAX} \quad (5.3)$$

*The Equation of the Stern for 10.645833 Ft ≤ x
 ≤ 13.979167 Ft*

$$R = R_{MAX}\{0.01380625 + 1.175\varepsilon^2 + 0.149075\varepsilon^3 + 7.29568125\varepsilon^4 - 13.821425\varepsilon^5 + 6.1878625\varepsilon^6\}^{1/2} \quad (5.4)$$

$$\varepsilon = \frac{13.979167 - x}{3.333333}, x \text{ in Feet} \quad (5.5)$$

The Equation of the Cap for 13.979167 Ft ≤ x ≤ 14.291667 Ft

$$R = 0.1175R_{MAX}\{1 - (3.2x - 44.733333)^2\}^{1/2} \quad (5.6)$$

5.2. Parametrical Modelling

The full parametrization of the design was again carried out with CAESES. At this stage, only the nose cone has been made parametric from the four different sections detailed in the previous section.

5.2.1. Parametrical Modelling of the Nose Cone

In the process of parameterizing the nose cone, similar studies in the literature were examined, and it was seen that there were two different methods. The first is controlling the stern and nose sections of the existing submarine form over these equations, such as Overpelt and Nienhuis [72], Yazici [73], and Budak [74], with different curve equations. The second is to derive new forms by manually controlling the existing submarine design without using the curve form of the DARPA SUBOFF model, such as Divsalar [17], Paz and Munoz [15].

When both methods are examined in terms of advantages and disadvantages, the first method is weaker in creating design space. Because it is clear that as the order of the curve equations used in this method increases, more detailed designs can be derived, and these designs will not differ much from each other since they use a common curve equation. However, since the design is directly intervened in the second method, the new designs derived can be very different, and a more comprehensive design space can be scanned. Therefore, in the optimization study carried out in the thesis, the way to intervene in the design manually was chosen.

In this context, the nose cone was divided into four equal sections, as seen in Figure 5.3. Then, each section's diameter and the nose cone's shape were controlled with the help of variable coefficients.

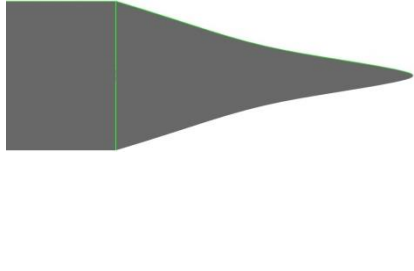
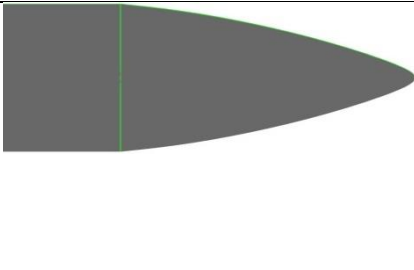
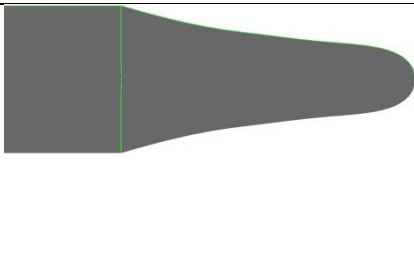


Figure 5.18. Sections in the Nose Cone (CAESES)

These coefficients in the range of 0.15-1 are directly multiplied by the diameter of each section and assigned a new diameter. While choosing this range, the optimum forms obtained in the studies of Budak [74], Yazici [73] and Divsalar [17] were taken, and sample designs taken for different coefficients are shared in Table 5.1.

Table 5.8. Sample Designs Taken for Different Coefficients

Form No	Section	Coefficient	Form
1	1	0.7	
	2	0.8	
	3	0.5	
	4	0.8	
2	1	0.3	
	2	0.5	
	3	0.6	
	4	0.7	
3	1	0.2	
	2	0.5	
	3	0.4	
	4	0.8	

4	1	0.15	
	2	0.3	
	3	0.4	
	4	0.7	
5	1	0.3	
	2	0.6	
	3	0.8	
	4	0.9	
6	1	0.8	
	2	0.6	
	3	0.7	
	4	0.7	

5.2.2. Parametrical Modeling of the Stern

The stern form is not entirely parametric like the nose form and has been optimized using the Lackenby method. This method ensures that the centres of buoyancy of all derived forms are very close to each other. It has been mentioned in the previous sections that the primary goal of the study in the thesis is to keep constant the centres of buoyancy of the optimum form and the DARPA SUBOFF AFF-1 form. This point makes this title one of the most important topics of the thesis, and the theory of the Lackenby method, which is used to keep the centre of buoyancy constant, and how it is applied in the study will be explained respectively.

5.2.3. Lackenby Methodology

5.2.3.1. Development of the the Lackenby Methodology

Based on the work by Lackenby in 1950, the method basically tries to control the whole form with a single curve by combining sub-curves belonging to different parts of naval architectures such as hull and submarine. Furthermore, it allows the design to be changed by allowing the sub-curves to be shifted to the movement along the length axis according to the design goals set by the user [75].

This method continued to be used and developed in the following years. In the literature, the parameterization of the designs of water vehicles such as ships and submarines with this method first started with the work of Nowacki et al. in 1977. In this study, the hull curve of a hull is modelled with a 7-point B-spline using 14 different parameters [76].

Later, this study was further advanced, and Krach parametrically modelled the bulbous bow curve of the same hull form. After this study, when different curves were used, it was determined that the nose cone directly affected the hydrodynamic performance and the position of the centre of buoyancy of structures such as submarines and hulls [77].

In the ongoing process, studies that will expand the scope of these two studies have been carried out. One of them is the study prepared by Jacobsen and Kracht in 1992, and in this study, the hull form was modelled with 12 different curves, six primary and six secondaries [78].

A study that will both summarize and expand the scope of all these studies was prepared by Harries and Abt in 1998. In this study, Sectional Area Curve (SAC) models were made with 24 parameters, including essential parameters such as displacement, centre of buoyancy, slopes in anterior and posterior obliques, and position of the maximum cross-sectional area [79]. In this way, almost all the parameters to be considered in the design of structures, such as submarines and hulls, have been determined, and in the ongoing process, modelling has been started with these parameters.

The meeting of mathematical models in this field with CFD is relatively new. In 2007, Abt and Harries conducted a two-stage study using the Lackenby method and CFD together with the Friendship Framework infrastructure used in this thesis. In the first stage, by shifting the different sections of the hull, designs that provide the desired hydrodynamic performance parameters were obtained. In the second stage, they both increased their hydrodynamic performance by aiming these designs to have the same buoyancy centre and displacement as the first design. As a result, they obtained an optimum hull design with the same hydrostatic properties as the first design [80].

5.2.3.2. Theory of the Lackenby Methodology

Since the Lackenby method was first developed for a hull form, its theory is explained over the hull form. In the next section, the integration of this method into the work done in the thesis will be detailed. First, the terms used in the methodology and the calculation methods of these terms will be explained.

i. Sectional Area Curve (SAC):

Sectional area curve (SAC) forms the basis of naval architectures as it directly controls the design. The sections with significant changes in the design are treated as separate sections to create this curve, and a single curve connecting these sections is created [75]. The literature studies detailed in the previous section aimed to bring this curve to the maximum change with the minimum parameter.

The SAC of the hull, which Lackenby considered as two different sections, is shown in Figure 5.4.

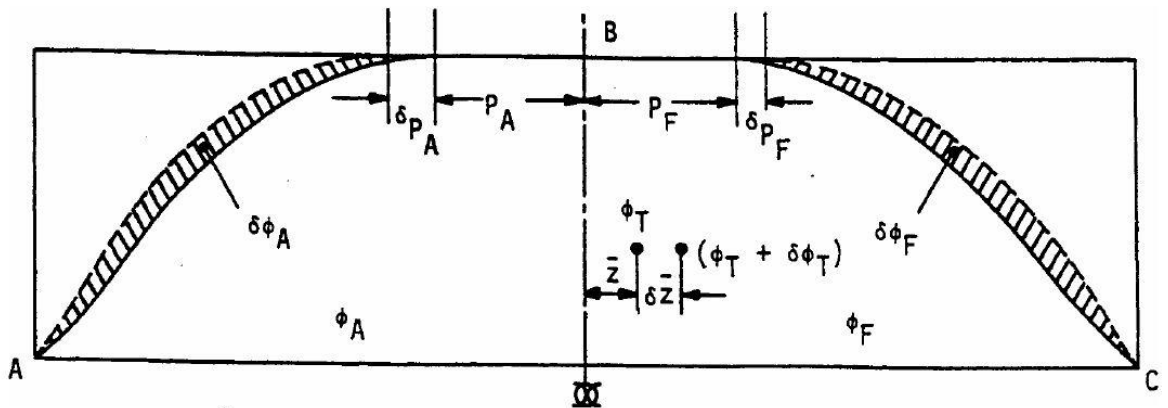


Figure 5.19. First Sectional Area Curve Derived by Lackenby [75]

ii. Length between perpendiculars (LPP):

It is the length of a ship or submarine from the initial point along the longitudinal axis to the beginning of the stern. The distance between the start and end points of the cross-sectional area curve is equal to this length. Figure 5.5 shows the LPP measurement over the DARPA SUBOFF AFF-1 model.

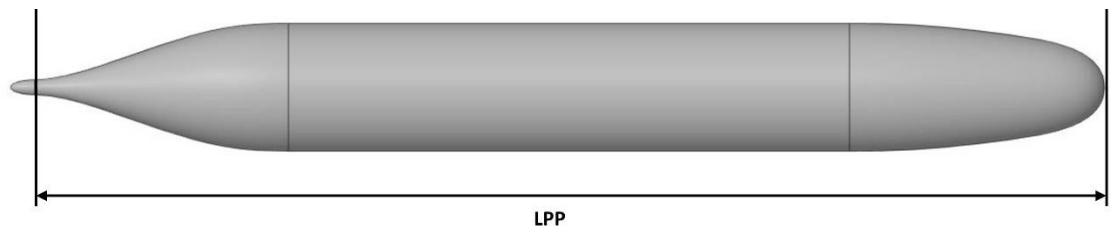


Figure 5.20. LPP of the DARPA SUBOFF AFF-1

iii. Prismatic Coefficient (CP)

The prismatic coefficient is also an essential parameter for naval architecture. It is the ratio of the volume of the ship or submarine to the volume of the smallest prism that these structures can fit [81]. This ratio can be calculated for a hull with the parameters shared in the Figure 5.6 below. This coefficient directly changes the form of the sectional area curve created for the Lackenby method. However, this change varies according to the method of obtaining the curve, and its effect in this study is explained in the next section.

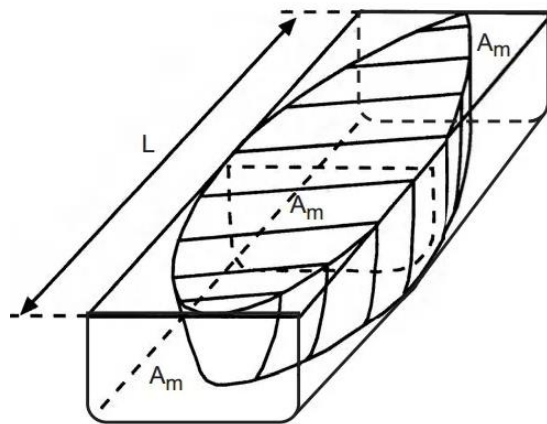


Figure 5.21. Parameters of Prismatic Coefficient [81]

L: Length of the ship

A_M: Cross sectional area of the middle of the ship

$$\text{Volume of the prism } (V_P) = L \times A_M \quad (5.7)$$

Volume of the ship (V_S) = Displacement of the ship

$$\text{Prismatic coefficient } (C_P) = V_S / V_P \quad (5.8)$$

iv. Longitudinal Centre of Buoyancy (LCB)

Naval architectures are not just designed for hydrodynamic performance concerns. At the same time, the stability of these structures is of great importance in the design phase. Especially in submarine designs, the stability of the submarine at complete submergence, surfaced and transition travel depths are studied separately. As seen in Figure 5.7, the forces that a submarine is exposed to are the gravitational force acting from the centre of gravity and the buoyancy force acting from the buoyancy centre. All stabilization calculations are made by calculating these forces [82].

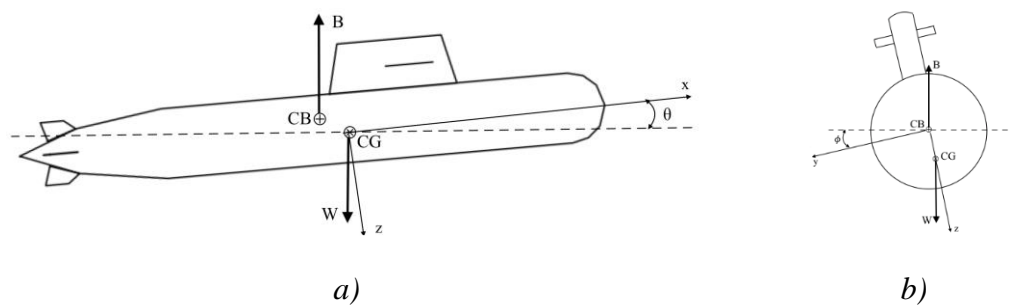


Figure 5.22. Gravity and buoyancy forces acting on a submarine a) Side view b) Front view [82]

Since there is no aim on the stability of the submarine in the study conducted in the thesis, it is aimed that the buoyancy centres of all the derived designs are the same. The Lackenby method calculates the position of the buoyancy centre of the new form obtained after the change on the sectional area curve. After that, it calculates the difference in the distance along the length between the buoyancy centres of the first and last forms. After that, by shifting the form by this difference, the buoyancy centres equalize their positions. In this study, designs with the same stability capability but different hydrodynamic performances were derived by the Lackenby method.

For this, first, the buoyancy centre of the first form was calculated, then the buoyancy centres of all the forms derived with the same formulation were calculated, and the difference between them was found. In the next step, the Lackenby method is aimed to minimize this difference.

The LCB calculation method is shown below for a ship in its simplest form. First, the volume is calculated by taking the definite integral of all cross-sectional areas along the length, as seen in Figure 5.8 [83].

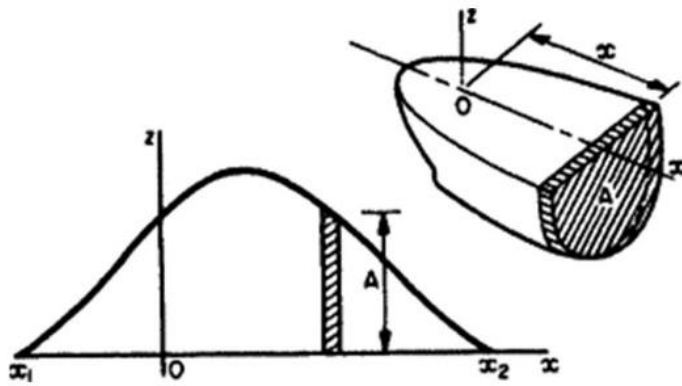


Figure 5.23. Parameters of the Longitudinal Centre of Buoyancy [83]

$$\nabla = \int_{x_1}^{x_2} A dx \quad (5.9)$$

$$LCB = \frac{1}{\nabla} \int A x dx \quad (5.10)$$

5.2.3.3. Application of the Lackenby Methodology

This chapter will be detailed how the Lackenby method was included in the optimization work for this thesis in the CAESES environment. In the first stage, geometric changes in the initial form are carried out without concern for hydrostatic properties. Then, the new form is updated with the Lackenby method to obtain the final form. In order to make this process easier to conceptualize, the steps are shared in Figure 5.9.

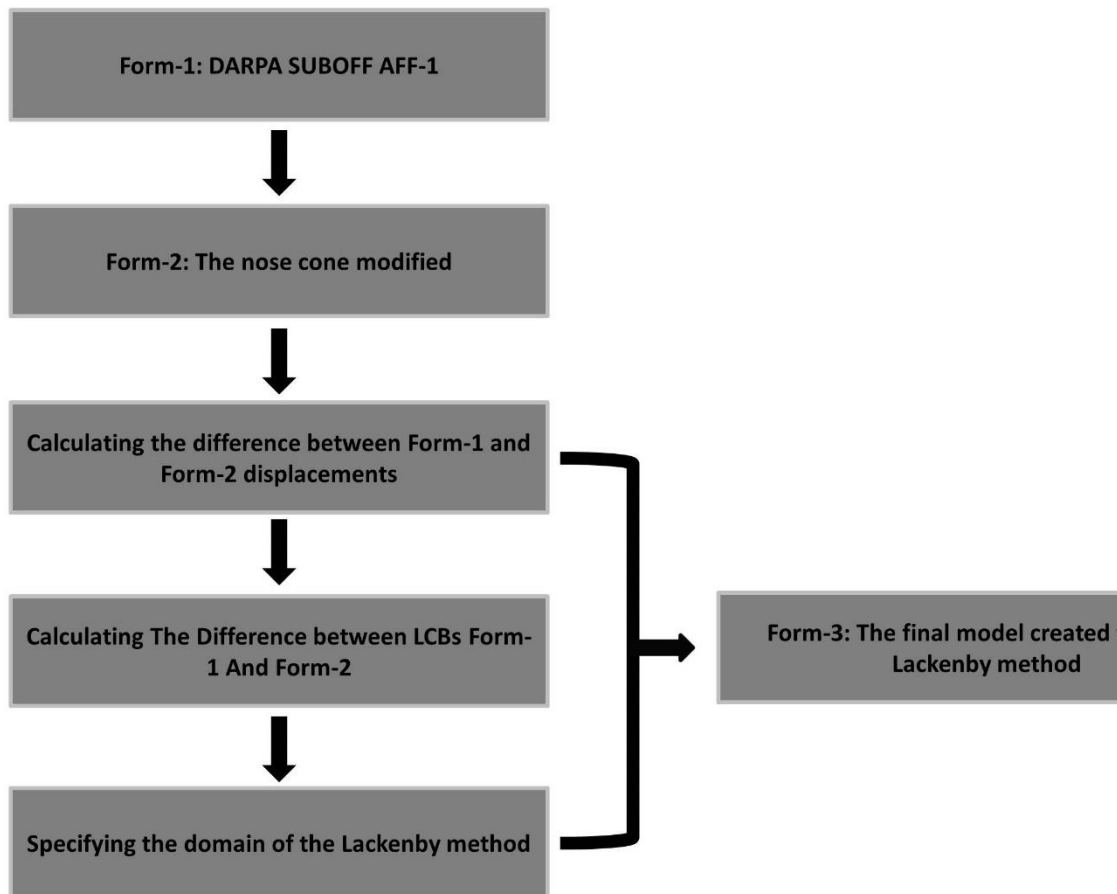


Figure 5.24. Steps of the Parametrization

After the geometric changes in the first form are made, the sectional area curve (SAC) should be calculated as described in the theory of the method. CAESES allows the use of several different methods in the creation of this curve, and the last method in the literature is the one used in the study of Abt and Harries [79]. In this method, an initial sectional area curve is created with the Lackenby formulation by using the length between the perpendicular and the volume of the submerged part of the submarine. The first curve created for the thesis study is shared in Figure 5.10.

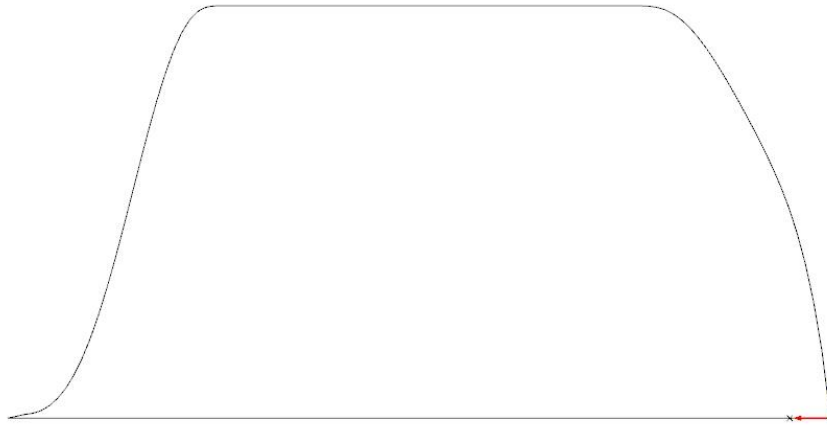

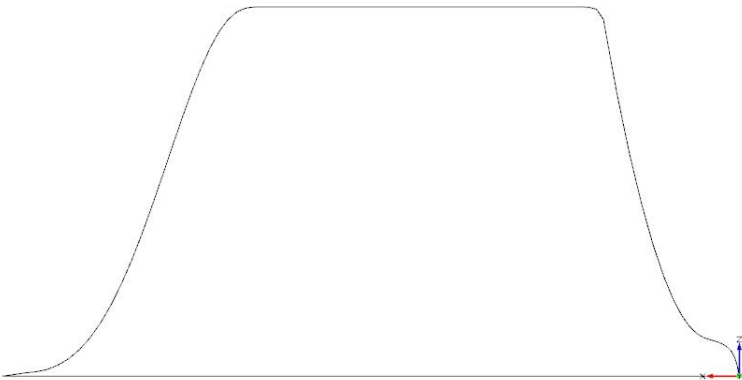


Figure 5.25. The first Sectional Area Curve

Step 1: Calculating the Difference Between Form-1 and Form-2 Displacements:

The Lackenby method tries to approximate the displacements of Form-1 and Form-3. First, the prismatic coefficient values for Form-1 and Form-2 are calculated using the equation which was given in previous section. The difference between these values affects the area scanned by the SAC form. If the prismatic coefficient of Form-1 is higher than Form-2, the Lackenby method should move toward increasing the displacement, and the area covered by the SAC form should be increased. In Table 5.2, how the same initial SAC form is affected by the Form-1 and Form-2 prismatic coefficients and the curves created for Form-3 are explained in more detail.

Table 5.9. Change of the SAC Form According to The Displacement Difference Between Form-1 And Form-2

Comparison of the prismatic coefficients	The new SAC forms created for Form-3
Form-1 < Form-2	
Form-1 > Form-2	

Step 2: Calculating the Difference between Longitudinal Centres of Buoyancy Form-1 and Form-2:

At this step, the buoyancy centres of Form-1 and Form-2 are calculated, and the difference between them is found. In order for Form-3 to have the same coordinated buoyancy centre as Form-1, Form-2 must be shifted by the difference.

Step 3: Specifying the Domain of The Lackenby Method:

As mentioned in the previous titles, in this thesis, the nose cone of the DARPA SUBOFF AFF-1 form was made parametric, and the stern form was optimized using the Lackenby method to restore the hydrostatic changes (centre of buoyancy) made by the nose cone to the design.

For this reason, the SAC has been divided into two different sections, and the nose cone has been excluded from the Lackenby method because the method should be provided to work only in the stern form. This strategy will affect the displacement holding performance of the Lackenby method. In Figure 5.11, the last SAC form and the working area of the Lackenby method are shared.

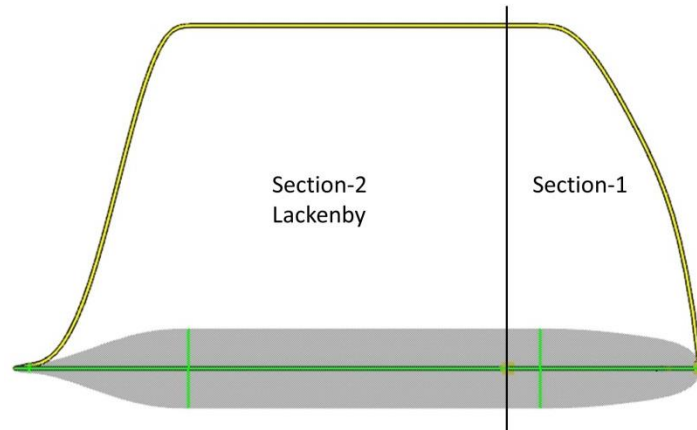


Figure 5.26. The Last SAC Form and the Working Area of the Lackenby Method

In Table 5.3 shared below, the full images of the Form-2 forms with nose cones in Table 5.2 and the images of the Form-3 forms obtained after applying the Lackenby method are shared. In all designs, the diameter and length between the perpendicular (LPP) are constant.

In addition, the displacement and LCB differences of these forms with Form-1 are also shared in Table 5.4.

Δ LCB-1: The absolute value of the LCB difference between Form-1 and Form-2;

Δ LCB-2: The absolute value of the LCB difference between Form-1 and Form-3;

Δ Disp-1: The absolute value of the Displacement difference between Form-1 and Form-2;

Δ Disp-2: The absolute value of the Displacement difference between Form-1 and Form-

Table 5.10. Centers of Buoyancy Positions without the Lackenby Method


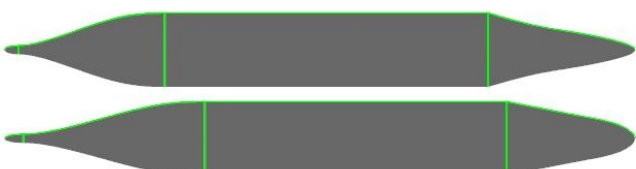
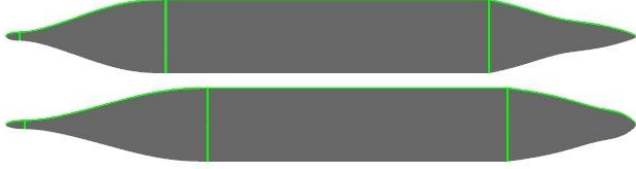

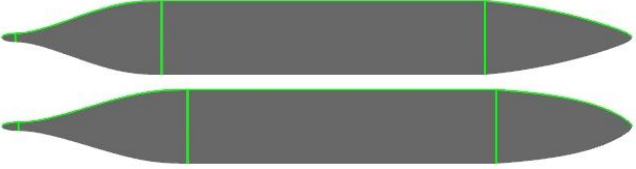

Design	Form	Figure
1	2	
	3	
2	2	
	3	
3	2	
	3	
4	2	
	3	
5	2	
	3	
6	2	
	3	

Table 5.11. LCB and Displacement Differences of Derived Designs

Design	$\Delta\text{LCB-1}$ (m)	$\Delta\text{LCB-2}$ (m)	$\Delta\text{Disp-1}$ (m ³)	$\Delta\text{Disp-2}$ (m ³)
1	0.237	0.001	0.059	0.058
2	0.284	0.001	0.076	0.075
3	0.293	0.002	0.079	0.078
4	0.322	0.002	0.090	0.089
5	0.220	0.001	0.049	0.049
6	0.246	0.001	0.063	0.062

As seen from the table, the Lackenby method is crucial to keep the centres of buoyancy almost the same. On the other hand, working the method only in the stern is not efficient in keeping the displacement the same. Additional studies have been carried out on this subject and will be detailed in the following sections.

5.3. Constraints of the Optimization Process

The DARPA SUBOFF AFF-1 model is fully parametrically modelled in the CAESES environment using the methods detailed in the previous chapters, and the design spaces have been created.

In the study conducted in this thesis, four different optimization studies were carried out considering several different constraints, which are displacement, the length between the perpendicular, diameter, and centre of buoyancy and four optimum designs were found. By examining similar studies in the literature with these criteria, it is aimed to scan all design targets that can be set in a submarine optimization.

All the optimization processes in this thesis performed were aimed at keeping the centre of buoyancy constant, and the stability of the forms was kept the same. In this way, all forms can be easily compared with each other without any doubt, and Table 5.5 shared below shows the design constraints of four different optimization studies.

Table 5.12. Design Constraints of the Optimization Processes

Optimization Process	LPP	Diameter	L/D	LCB	Displacement
1	Constant	Constant	Constant	Constant	±10%
2	Increased	Increased	Constant	Constant	Constant
3	Decreased	Increased	Decreased	Constant	±10%
4	Increased	Constant	Increased	Constant	±10%

Optimization Process-1: This is the first process described above. Then, the resulting Form-2 is rederived with the Lackenby method. It is aimed that the displacement will remain the same at about 10 percent.

Optimization Process-2: In this process, after the displacement difference between Form-2 and Form-1 is calculated, the ratio of this difference to the first displacement is found. Then, Form-3 obtained by the Lackenby method is scaled with this ratio throughout the diameter and length. Therefore, as LPP and diameter increase, all other constraints are constant.

Optimization Process-3: In this process, the submarine model is optimized by increasing its diameter and decreasing its LPP.

Optimization Process-4: In this process, the submarine model is optimized with constant diameter and increased LPP.

The design constraints values used in these processes will be detailed in Section 6.

5.4. Running the Optimization Process

After the fully parametric geometry is created and the design spaces are determined, optimization studies should start. In this section, CAESES and Fluent integration for creating the automated workflow have been detailed.

At this stage of the study, using the optimization methods detailed in Chapter 3, single-objective optimization studies were carried out to reduce the drag force under certain design constraints of the first model.

CAESES provides ready-made DoE and T-Search methods used in this study. However, the design spaces to be scanned by the optimization works must be specified by the user at the DoE stage. At this point, 1000 designs were scanned for the first study in four optimization studies. However, in this study, the details of which will be shared in the next section, it was seen that scanning 1000 designs could not significantly affect the results, and other studies were conducted by scanning 500. The optimum design found after each DoE scan was optimized with the T-Search method, and the most optimum design was found.

After the methods are determined, CAESES should automatically derive the geometries in the determined design space. Then, fluent should automatically re-establish the simulation model for each design and transfer these results to CAESES so that these results can be evaluated. This loop can be set up in the CAESES environment and can be done with the help of the SoftwareConnector interface shared in Figure 5.12 below.

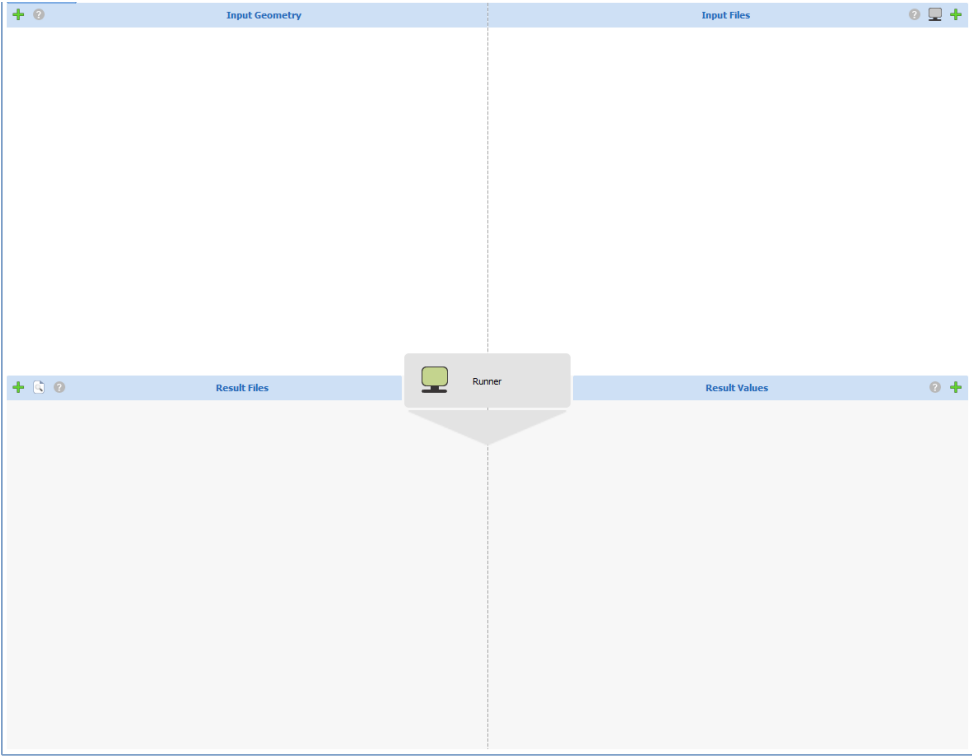


Figure 5.27. SoftwareConnector Interface on CAESES

The interface consists of four panels, and their functions are as follows.

i. Input Geometry:

This panel enables CAESES to derive new designs according to the specified design constraints and variable values to export these designs in formats that can be opened by the software to be used in the simulation.

ii. Input Files:

This panel covers the stages of creating a mesh structure and running the simulation of the obtained geometry. Two files were attached to this panel for the study carried out within the scope of the thesis. First, the journal file was prepared in the language of FLUENT for the simulation model, the details of which are shared in Chapter 4, and the second one is the batch file that will run FLUENT. Then, the mesh structures were created to the derived geometries by CAESES with the previously clarified settings of FLUENT, and simulations were performed.

iii. Result Files:

This panel ensures that the desired result images are taken from the same angle after each simulation. In this way, result images of all simulations can be collected.

iv. Result Values:

This panel allows the output parameters to be transferred to CAESES after the simulations are performed. In this study, the drag force values of the submarine designs were calculated in each simulation, and optimization studies were carried out according to these values.

5.5. Review the Optimization Process

As mentioned in the previous section, all automatically generated geometries were simulated, and the results were collected in the CAESES environment.

After the DoE stage, Pareto analyses were performed to determine the Pareto frontier. This way, the effects of the different design variables used on the submarine performance and other targeted design criteria can be seen, and the order of magnitudes and optimum ranges of these variables can be calculated.

Pareto analyses create a frontier by calculating the points that allow all objectives to intersect in multi-objective problems and are very useful in reaching the optimum design. This method calculates the percentage deviations from the objectives and obtains a curve, as shared in Figure 5.6, and on this curve, the design points where all objectives are met at the maximum rate can be determined [84].

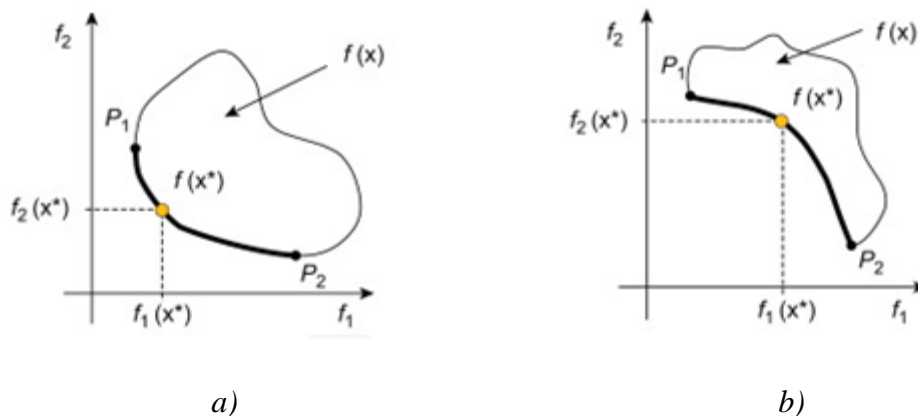


Figure 5.28. Pareto frontiers for the multiobjective optimizations a) convex b) nonconvex

The work done in the thesis should be described as something other than as a multi-objective optimization study. Because as a result of simulations, only the submarine's hydrodynamic performance is wanted to be optimized. Form-2 is derived according to the design variable values shared in the previous sections. Then the Lackenby method is performed to derive Form-3, ensuring that all parameters except the drag forces are within the desired ranges.

In other words, if f_2 is considered as the drag force in the graph above and f_1 is the difference of hydrostatic parameters between the initial design and the final design, the points f_1 are already evident before the simulations.

However, Pareto analyses performed on the optimum form obtained after DoE can provide efficient T-Search scanning in a smaller design space. Because in this way, the optimum values of the upper and lower bounds of the defined design variables can be calculated. On the other hand, it can also show the effect of the Lackenby method on hydrodynamic performance and whether it works efficiently.

Because there is a possibility that the defined design variables will work inefficiently in the Lackenby method, for example, suppose the diameter changes on the nose cone are larger or smaller than a specific coefficient. In that case, it may cause the Lackenby method not to work and cause deviations from the hydrostatic properties. However, thanks to the Pareto frontier, more efficient work can be done in the T-Search stage.

After all these steps, designs with improved hydrodynamic performance and the design variable values of these designs can be calculated by using two different optimization methodologies.

6. RESULTS

This section will share and examine the results of the optimization studies detailed in the previous section. Since four different optimization studies were carried out, each is discussed in separate sections.

6.1. Optimization Process-1

The first optimization study aims to decrease the drag force of the DARPA SUBOFF AFF-1 model without changing hydrostatic parameters other than displacement. For this, as stated in the previous section, the diameters of the four different parts of the nose cone shared in Figure 6.1 were controlled with constant coefficients and the Lackenby method was defined in the stern part.



Figure 6.29. Workfields of Optimization Process-1

The bounds of the design variable values and design constraints used to control the diameters of the nose cone sections are shared in Table 6.1 and Table 6.2, respectively.

Table 6.13. Design Variables of Optimization Process-1

Design Variable	Coefficient
S-1	$0.15 \leq S-1 \leq 1$
S-2	$0.15 \leq S-2 \leq 1$
S-3	$0.15 \leq S-3 \leq 1$
S-4	$0.15 \leq S-4 \leq 1$

Table 6.14. Design Constraints of Optimization Process-1

Design Constraints	Objective Functions
L	Keep constant
Diameter	Keep constant
L/D	Keep constant
LCB	Keep constant
Displacement	Can change $\pm 10\%$

6.1.1. DoE-1 Results

This is the optimization study in which the most drag reduction is expected in the study conducted in the thesis. Therefore, this study was done before the others, and 1000 different designs were scanned by keeping the design space huge at the DoE stage.

The Table 6.3 below shows the design variable values of the best 20 designs with LCB and displacement changes.

$$\Delta LCB = \frac{(LCB_2 - LCB_1)}{LCB_1} * 100 \quad (6.1)$$

$$\Delta Disp = \frac{(Displacement_2 - Displacement_1)}{Displacement_1} * 100 \quad (6.2)$$

Table 6.15. Top 20 Designs of DoE-1

No	S-1	S-2	S-3	S-4	ΔLCB (%)	ΔDisp (%)	Drag Force (N)
951	0.277002	0.172412	0.277002	0.851416	0.013086	-9.28707	76.4174
847	0.25376	0.262061	0.419775	0.814893	0.009568	-8.70243	76.4921
575	0.172412	0.277002	0.305225	0.922803	0.011863	-8.29996	76.5712
143	0.239648	0.299414	0.206445	0.658008	0.017158	-10.9086	76.5785
287	0.194824	0.347559	0.347559	0.882129	0.012344	-8.24054	76.7146
455	0.324316	0.244629	0.404004	0.812402	0.009967	-8.80373	76.7213
519	0.311865	0.203955	0.192334	0.650537	0.016929	-11.1845	76.8057
791	0.286963	0.228857	0.532666	0.755127	0.016294	-8.81889	76.8131
383	0.158301	0.291113	0.516895	0.765918	0.01686	-8.66725	76.8787
215	0.299414	0.239648	0.319336	0.916992	0.009402	-8.28569	76.8805
359	0.347559	0.194824	0.234668	0.689551	0.016414	-10.7205	76.934
699	0.388232	0.233838	0.262061	0.773389	0.013752	-9.78581	77.0208
479	0.178223	0.178223	0.57666	0.905371	0.009508	-7.29015	77.1753
167	0.35918	0.36582	0.166602	0.857227	0.011	-9.13089	77.2067
631	0.265381	0.396533	0.345068	0.697021	0.013692	-9.68443	77.2112
7	0.309375	0.415625	0.415625	0.734375	0.01242	-8.90482	77.3039
639	0.162451	0.220557	0.647217	0.866357	0.010421	-7.16433	77.3198
719	0.248779	0.187354	0.36167	0.527686	0.015293	-11.5021	77.3361
119	0.262891	0.183203	0.488672	0.581641	0.01165	-10.5631	77.3869
23	0.282813	0.282813	0.601562	0.867188	0.011748	-7.12987	77.4098

When the results are examined in terms of displacement and LCB, it is seen that the displacement is in the 10% change band as expected, and the LCB remains almost constant with little change.

On the other hand, as mentioned before, it is possible to examine the effect of the constant coefficient with which each section is multiplied on the drag force value with Pareto parameter sensitivity analysis. Figure 6.2, shared below, shows the Pareto analysis results of the top 50 designs detailed above.

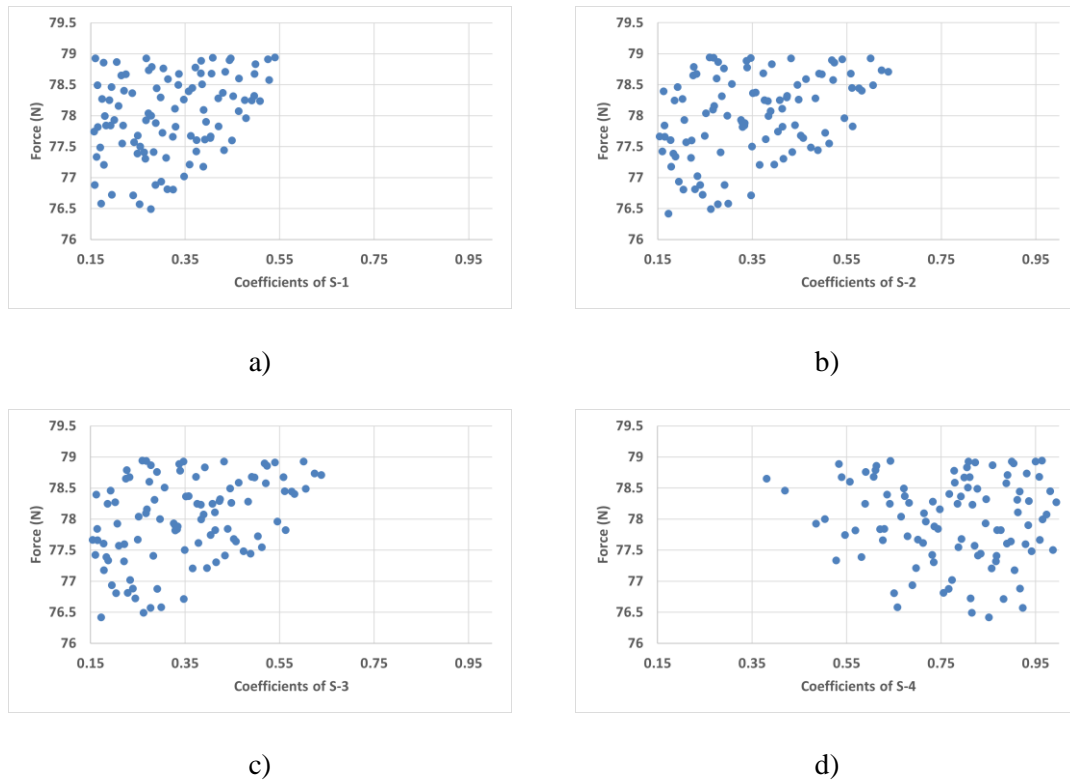


Figure 6.30. Pareto Analyses of DoE-1 a) S-1 b) S-2 c) S-3 d) S-4

When the graphs are examined, it is seen that the optimum coefficient range for S-1, S-2, and S-3 is between 0.15-0.55, while this range for S-4 is 0.55-1.







In optimum design, S-1, S-2, and S-3 may have values close to each other, but S-4 will necessarily have a more excellent value than them.

If a different optimization method were used instead of T-Search after this stage, it would be essential to determine the optimum values of these design variables, but this is not a requirement for T-Search.

On the other hand, since the limits defined for the hydrostatic parameters (LCB, Displacement) for this process are primarily provided, and the deviation rates of these parameters are very close to each design, it is not necessary to examine them in detail with Pareto.

In Table 6.4 below, the visuals of the five designs and the first design that creates the lowest drag force obtained from DoE are shared with the drag force values obtained in the simulations.

Table 6.16. Top 5 Designs of DoE-1

Design	Drag Force (N)	Figure
DARPA SUBOFF AFF-1	87.3168	
DoE-1 287	76.7146	
DoE-1 143	76.5785	
DoE-1 575	76.5712	
DoE-1 847	76.4921	
DoE-1 951	76.4174	

When the designs are examined, it is seen that the nose cone designs are similar to each other in general, but they are different enough to be distinguished by the eye. This indicates that the optimization study achieves almost have the same drag force with different values and therefore gives very successful results.

6.1.2. T-Search-1 Results

It was stated in Section-3 that a starting point is needed for the T-Search method. Therefore, at this point, a design should be chosen as a starting point among the optimum designs obtained in the DoE phase. Among all the designs shared in Table 6.4, no one has a form different from the optimum forms suggested in the literature. For this reason, five different designs can be selected as the starting point for T-Search because T-Search will find the intersection of these five designs. At this point, DoE-1 951 design, the most optimal form obtained due to DoE, was chosen as the initial form for the T-Search method.

On the other hand, since the T-Search method will repeat the parameter sensitivity analysis within itself, the design variable bounds have not been changed.

The T-Search method has found the most optimum form by scanning additional 44 designs, and in Table 6.5 shared below, the design variable values of all scanned designs are shared with LCB and displacement changes. The change in LCB and displacement values was calculated by equations 6.1 and 6.2 respectively.

When the table is examined in detail, the working principle of the T-Search method is more clearly understood. As explained before, this method first examines the effects on the parameter to be optimized by increasing or decreasing all design variable values. After this stage, it decides whether all design variables should increase or decrease for optimum design. When the table is examined, it is understood that the design variable values were tested one by one in the first seven designs, and it was determined in which direction they should be changed. Afterwards, all design variables were changed in the selected direction at the same time, and the optimum design was found.

Table 6.17. Results of T-Search-1

No	S-1	S-2	S-3	S-4	ΔLCB (%)	ΔDisp (%)	Drag Force (N)
0	0.277002	0.172412	0.277002	0.851416	0.0130862	-9.28707	76.4174
1	0.319502	0.172412	0.277002	0.851416	0.0135078	-9.25772	76.6468
2	0.234502	0.172412	0.277002	0.851416	0.0131752	-9.31569	76.2781
3	0.234502	0.214912	0.277002	0.851416	0.0138795	-9.21873	76.2833
4	0.234502	0.15	0.277002	0.851416	0.0133208	-9.36745	76.2878
5	0.234502	0.172412	0.314502	0.851416	0.012985	-9.14463	76.2319
6	0.234502	0.172412	0.314502	0.888916	0.011642	-8.79368	76.52
7	0.234502	0.172412	0.314502	0.813916	0.009107	-9.45821	76.1163
8	0.176064	0.172412	0.366064	0.762354	0.011644	-9.72821	76.0786
9	0.15	0.172412	0.436963	0.691455	0.018137	-10.0469	76.382
10	0.197979	0.172412	0.366064	0.762354	0.011543	-9.7154	76.1991
11	0.15415	0.172412	0.366064	0.762354	0.011059	-9.73421	76.117
12	0.176064	0.194326	0.366064	0.762354	0.011285	-9.67187	76.0628
13	0.176064	0.194326	0.3854	0.762354	0.012705	-9.58468	76.2416
14	0.176064	0.194326	0.346729	0.762354	0.011436	-9.75975	76.1472
15	0.176064	0.194326	0.366064	0.781689	0.010946	-9.50499	76.1728
16	0.176064	0.194326	0.366064	0.743018	0.015333	-9.86713	76.0798
17	0.176064	0.224458	0.366064	0.762354	0.010924	-9.59056	76.1094
18	0.184282	0.194326	0.366064	0.762354	0.010934	-9.66429	76.1637
19	0.167847	0.194326	0.366064	0.762354	0.011161	-9.67592	76.0875
20	0.176064	0.202544	0.366064	0.762354	0.01112	-9.64994	76.1369
21	0.176064	0.186108	0.366064	0.762354	0.011236	-9.69206	76.1005
22	0.176064	0.194326	0.373315	0.762354	0.011326	-9.64001	76.2189
23	0.176064	0.194326	0.358813	0.762354	0.011339	-9.70519	76.1565







24	0.176064	0.194326	0.366064	0.769604	0.011098	-9.60888	76.1186
25*	0.176064	0.194326	0.366064	0.755103	0.011515	-9.73555	76.0449
26	0.176064	0.194326	0.366064	0.745132	0.015397	-9.83267	76.1717
27	0.179146	0.194326	0.366064	0.755103	0.011568	-9.73413	76.0693
28	0.172983	0.194326	0.366064	0.755103	0.011472	-9.73701	76.1056
29	0.176064	0.197408	0.366064	0.755103	0.011466	-9.7274	76.1968
30*	0.176064	0.191245	0.366064	0.755103	0.011517	-9.74321	76.0298
31	0.176064	0.191245	0.368784	0.755103	0.011584	-9.73064	76.1253
32	0.176064	0.191245	0.363345	0.755103	0.011532	-9.75549	76.1501
33	0.176064	0.191245	0.366064	0.757822	0.011487	-9.72011	76.1283
34	0.176064	0.191245	0.366064	0.752383	0.011497	-9.76627	76.1698
35	0.176064	0.187007	0.366064	0.755103	0.011558	-9.75334	76.2639
36	0.17722	0.191245	0.366064	0.755103	0.011531	-9.74268	76.1517
37*	0.174909	0.191245	0.366064	0.755103	0.011499	-9.74378	76.001
38	0.174909	0.1924	0.366064	0.755103	0.0116	-9.74098	76.0829
39*	0.174909	0.190089	0.366064	0.755103	0.011491	-9.74653	76.022
40*	0.174909	0.191245	0.367084	0.755103	0.011505	-9.73916	76.0581
41	0.174909	0.191245	0.365045	0.755103	0.0115	-9.7484	76.1161
42	0.174909	0.191245	0.366064	0.756122	0.011483	-9.7351	76.1945
43	0.174909	0.191245	0.366064	0.754083	0.011524	-9.75241	76.1854
44	0.17332	0.191245	0.366064	0.755103	0.011473	-9.74451	76.2341

*: Top 5 Designs of T-Search-1

After the local optimization with the T-Search method, it was observed that there was a slight decrease in the drag force values. At the same time, the lowest drag force value obtained after DoE was 76.4174 N, which decreased to 76.0010 after T-Search.

The five designs with the lowest drag force value were examined, and the optimum design was decided. The drag force values obtained in the simulations are shared in Table 6.7 from the largest to the smallest.

Table 6.18. Top 5 Designs of T-Search-1

Design	Drag Force (N)	Figure
DoE-1 951	76.4174	
T-Search-1 40	76.0581	
T-Search-1 25	76.0449	
T-Search-1 30	76.0298	
T-Search-1 39	76.0220	
T-Search-1 37	76.0010	

When the designs are examined, it is seen that they have forms that are clearly different from DoE-951 but very similar to each other. As the previous section shared, the designs intersect the five most optimal forms proposed after DoE.

On the other hand, it is seen that the drag forces are not much different compared to DoE-951. This result shows that the T-Search method can optimize the targeted performance parameter and the form. For this reason, it is crucial to benefit from the T-Search method in the study.

6.1.3. Specifying Optimum Design-1

The optimum design was determined after the DoE and T-Search optimization results, the details of which were shared above. Since the optimum forms obtained after T-Search are very similar to each other and show intimate performance at the point of meeting all design limits, it was deemed appropriate to choose the design with the least calculated drag force as the final design. At this point, while the first optimum design was DoE-1 951, the final optimum design was chosen as T-Search-1 37.

The optimum design's hydrostatic characteristics and the drag force are compared with the DARPA SUBOFF AFF-1 in Table 6.7 below.

Table 6.19. Comparison between DARPA SUBOFF AFF-1 and the Optimum Design-1

Design	LCB (m)	Disp (m³)	L (m)	D (m)	L/D	Drag Force (N)
DARPA SUBOFF AFF-1	2.013	0.708	4.356	0.508	8.57	87.3168
Optimum Design-1	2.013	0.639	4.356	0.508	8.57	76.0010

When the table is examined, it is seen that the hydrostatic parameters have not changed much, and the drag performance has been significantly improved. Therefore, the rates of change of hydrostatic and hydrodynamic parameters are shared in Table 6.8 below. The rate of change of hydrostatic parameters was calculated by Equations 6.1 and 6.2, the change of drag performance parameter was calculated with following Equation 6.3.

$$\Delta F_D = \frac{(F_{D1} - F_{D2})}{F_{D1}} * 100 \quad (6.3)$$

Table 6.20. Comparison of Hydrostatic and Hydrodynamic Parameters between Optimum Design and Initial Design

Parameters	Values
$\Delta\text{LCB} (\%)$	0.0115
$\Delta\text{Disp} (\%)$	-9.7439
$\Delta\text{FD}(\%)$	-12.9595

Hydrostatic parameters, longitudinal centre of buoyancy and displacement values changed as intended. While the LCB remained almost constant, the displacement change did not exceed 10%. On the other hand, an improvement in drag performance is observed in the band of about 13%.

The figures from different angles are shared in Figure 6.3 below for a more accessible examination of the Optimum Design-1 form.

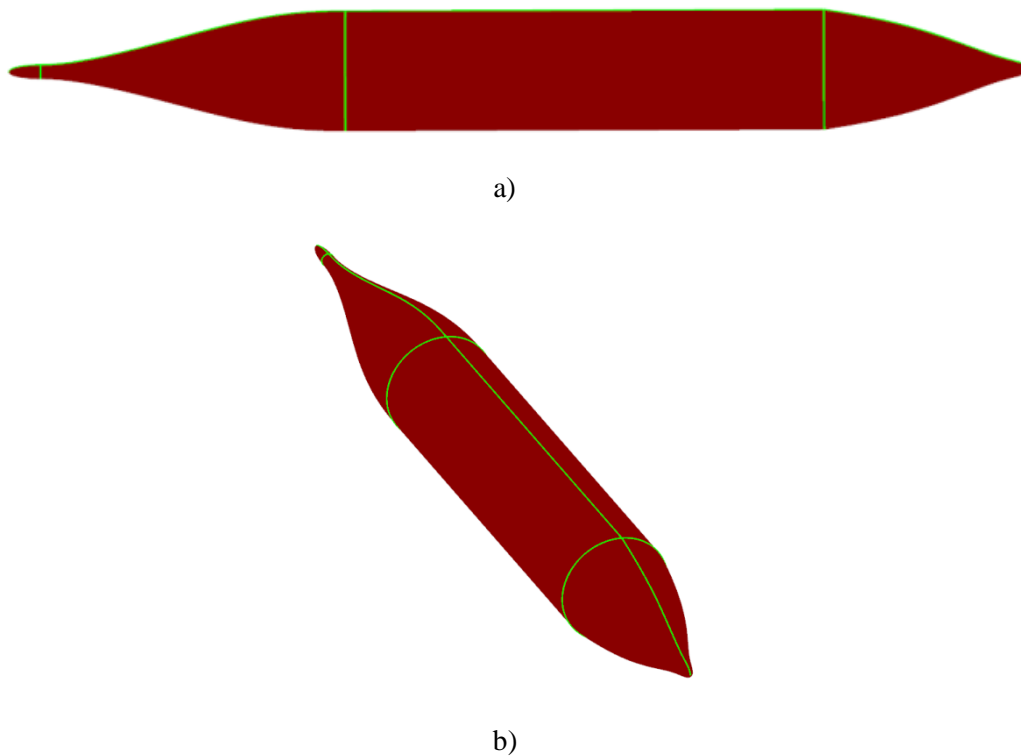


Figure 6.31. Optimum Design-1 a) Section View b) Isometric View

6.2. Optimization Process-2

The second optimization study aims to keep the displacement of the DARPA SUBOFF AFF-1 model constant. For this, the form obtained after Lackenby is modified again without entering the simulation. The steps are explained in detail to understand this process better.

i. After Lackenby

The displacement ratio between the form obtained after Lackenby and the DARPA SUBOFF AFF-1 forms is calculated with the help of the following Equation 6.4.

$$Ratio_{Disp} = \frac{Disp_{DARPA}}{Disp_{Lackenby}} \quad (6.4)$$

ii. Scaling

The form obtained after Lackenby is scaled in all axes with the ratio calculated above. In this way, since the LCB position is preserved, there is no need to use the Lackenby method again. This stage is detailed in Figure 6.4, shared below.

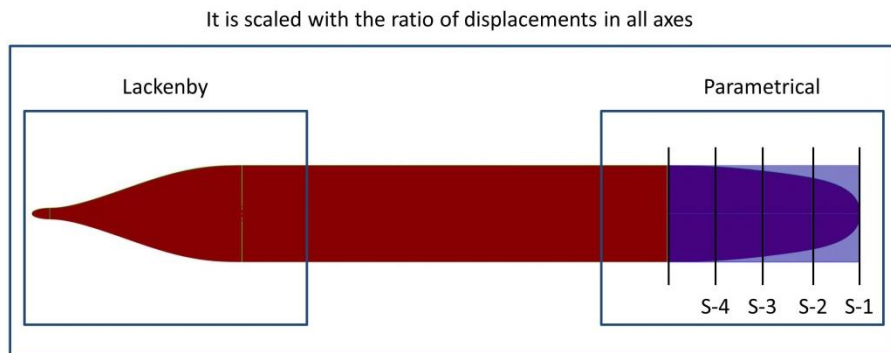


Figure 6.32. Workfields of Optimization Process-2

The bounds of the design variable values and design constraints used to control the diameters of the nose cone sections are shared in Table 6.9 and Table 6.10, respectively.

Table 6.21. Design Variables of Optimization Process-2

Design Variable	Coefficient
S-1	$0.15 \leq S-1 \leq 1$
S-2	$0.15 \leq S-2 \leq 1$
S-3	$0.15 \leq S-3 \leq 1$
S-4	$0.15 \leq S-4 \leq 1$

Table 6.22. Design Constraints of Optimization Process-2

Design Constraints	Objective Functions
L	Increased
Diameter	Increased
L/D	Keep constant
LCB	Keep constant
Displacement	Keep constant

6.2.1. DoE-2 Results

In the first optimization process, a space covering 1000 designs was scanned in the DoE stage, but when the top 25 forms were examined, it was seen that most of them were in the first 500 forms, and a space of 500 designs was scanned in this process.

The Table 6.11 below shows the design variables and scaling coefficients (SC) values of the best 20 designs obtained due to DoE being shared with the LCB and displacement changes. These changes are calculated with the same methods as Process-1.

Table 6.23. Top 20 Designs of DoE-2

No	S-1	S-2	S-3	S-4	Δ LCB (%)	Δ Disp (%)	SC	Drag Force (N)
439	0.277832	0.384082	0.556738	0.965137	0.0088	1.1×10^{-5}	1.03	81.5106
127	0.159961	0.432227	0.817383	0.950195	0.0068	7.1×10^{-8}	1.02	81.6825
103	0.342578	0.528516	0.780859	0.926953	0.0090	1.8×10^{-4}	1.02	81.7357
047	0.216406	0.349219	0.375781	0.986719	0.0104	3.9×10^{-7}	1.03	81.7552
215	0.299414	0.239648	0.319336	0.916992	0.0094	8.1×10^{-5}	1.04	81.7973
399	0.237988	0.423926	0.755957	0.845605	0.0088	3.4×10^{-7}	1.03	81.8078
63	0.169922	0.488672	0.528516	0.833984	0.0074	2.6×10^{-4}	1.03	81.8415
383	0.158301	0.291113	0.516895	0.765918	0.0169	1.6×10^{-3}	1.04	81.8712
379	0.374121	0.221387	0.47373	0.928613	0.0101	9.3×10^{-6}	1.03	81.9156
238	0.233008	0.598242	0.651367	0.983398	0.0071	3.2×10^{-7}	1.02	81.9184
287	0.194824	0.347559	0.347559	0.882129	0.0123	4.6×10^{-7}	1.04	81.9408
455	0.324316	0.244629	0.404004	0.812402	0.0100	1.1×10^{-6}	1.04	81.9944
267	0.420605	0.413965	0.440527	0.868848	0.0078	5.8×10^{-5}	1.03	82.0796
443	0.384082	0.277832	0.875488	0.858887	0.0069	1.5×10^{-5}	1.02	82.104
375	0.267871	0.540137	0.79248	0.822363	0.0109	5.8×10^{-7}	1.02	82.186
459	0.430566	0.563379	0.935254	0.918652	0.0052	6.0×10^{-8}	1.01	82.2269
171	0.46543	0.25957	0.697852	0.963477	0.0075	4.4×10^{-5}	1.02	82.2606
335	0.25459	0.47373	0.194824	0.941895	0.0107	1.9×10^{-5}	1.03	82.3214
418	0.410645	0.729395	0.742676	0.938574	0.0060	3.5×10^{-7}	1.02	82.3469
6	0.25625	0.68125	0.89375	0.89375	0.0073	2.1×10^{-7}	1.02	82.3753

When the results are examined in terms of displacement and LCB, it is seen that both remain almost constant.

In this process, Pareto parameter sensitivity analyzes were made, and the effect of form change on the drag force value was examined. The Figure 6.5, shared below, shows the Pareto analysis results of the top 50 designs detailed above.

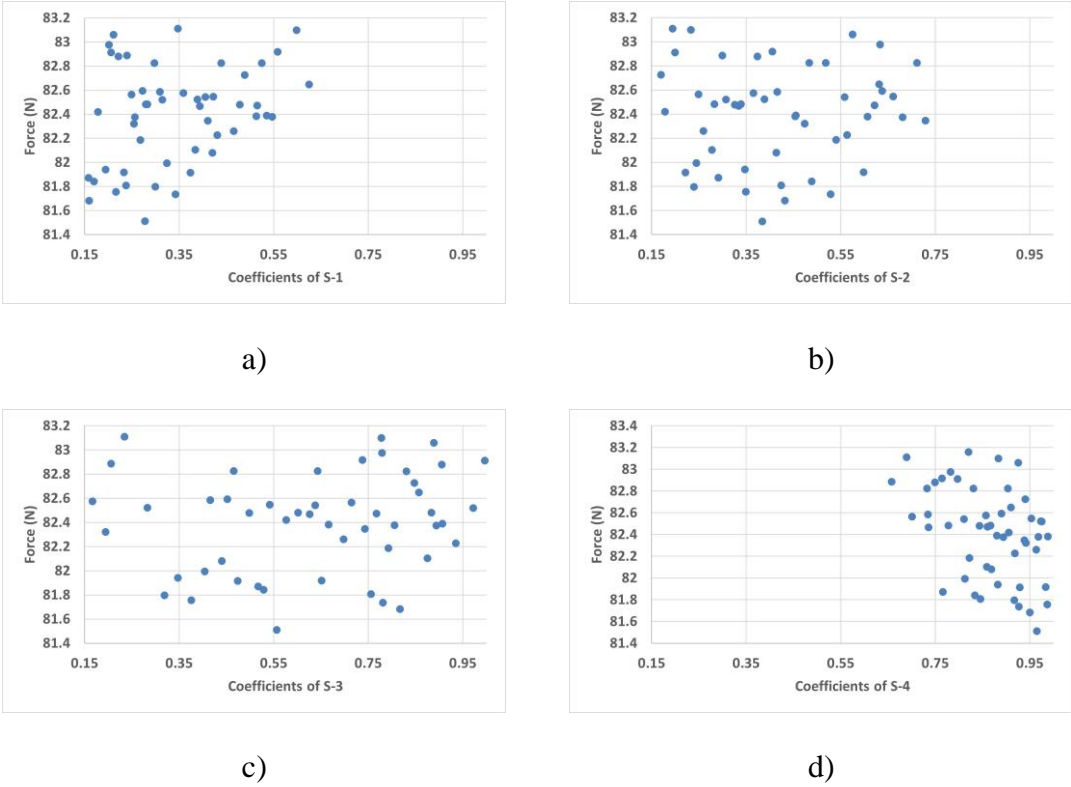








Figure 6.33. Pareto Analyses of DoE-2 a) S-1 b) S-2 c) S-3 d) S-4

When the graphs are examined, it is observed that the S-1 value varies between 0.15-0.55, the S-2 value varies between 0.15-0.75, and the S-4 value varies between 0.75-1. At the same time, there is no specific range for S-3 in the most optimal designs.

In the optimum design, S-1, S-2, and S-3 may have values close to each other, just as in Process-1, S-4 will necessarily have a more excellent value than them.

In Table 6.12 below, the visuals of the five designs and the first design that creates the lowest drag force obtained from DoE are shared with the drag force values obtained in the simulations.

Table 6.24. Top 5 Designs of DoE-2

Design	Drag Force (N)	Figure
DARPA SUBOFF AFF-1	87.3168	
DoE-2 215	81.7973	
DoE-2 47	81.7552	
DoE-2 103	81.7357	
DoE-2 127	81.6825	
DoE-2 439	81.5106	

When the designs are examined, it is seen that they are different from each other, just like in DoE-1, but the drag force values are very close. For this reason, at this stage, one of these five designs can be chosen as the starting point of the T-Search method.

6.2.2. T-Search-2 Results

While choosing the initial design for the T-Search method, the experience gained in Optimization Process-1 was used. As a result, it was seen that the optimum form obtained after T-Search in that process was the intersection of the first five optimum forms obtained after DoE. In this way, it was ensured that the method works efficiently.

In order to increase the reliability of the method, two different T-Searchs were run, starting with DoE-2 103, DoE-2 215 and DoE-2 439. The processes that started with DoE-2 215, 103 and 439 reached almost the same optimum form by scanning 57, 32 and 46 new designs, respectively. For this reason, the result will not change no matter what form is given to the T-Search method.

In this way, it has been proven that the result of the T-Search method is independent of the initial form, and the results of the optimization started with DoE-2 103 are shared.

On the other hand, since the T-Search method will repeat the parameter sensitivity analysis within itself, the design variable values have not been changed.

The T-Search method has found the most optimum form by scanning additional 32 designs, and in Table 6.13 shared below, the design variable values of all scanned designs are shared with LCB and displacement changes. The change in LCB and displacement values was calculated by Equations 6.1 and 6.2 respectively.

Table 6.25. Results of T-Search-2

No	S-1	S-2	S-3	S-4	Δ LCB (%)	Δ Disp (%)	SC	Drag Force (N)
0	0.342578	0.528516	0.780859	0.926953	0.0090	1.8×10^{-4}	1.02	81.7357
1*	0.385078	0.528516	0.780859	0.926953	0.0073	1.3×10^{-5}	1.02	81.4955
2	0.385078	0.571016	0.780859	0.926953	0.0084	1.3×10^{-5}	1.02	81.4268
3	0.385078	0.571016	0.823359	0.926953	0.0063	2.5×10^{-7}	1.02	81.9662
4	0.385078	0.571016	0.738359	0.926953	0.0094	4.6×10^{-7}	1.03	81.8460
5	0.385078	0.571016	0.780859	0.969453	0.0066	1.1×10^{-4}	1.02	81.9690
6	0.385078	0.571016	0.780859	0.884453	0.0090	4.2×10^{-7}	1.03	81.9661
7	0.443515	0.629453	0.780859	0.926953	0.0083	4.4×10^{-7}	1.02	82.1849
8	0.401015	0.571016	0.780859	0.926953	0.0091	2.2×10^{-7}	1.02	80.9654
9*	0.36914	0.571016	0.780859	0.926953	0.0083	3.5×10^{-7}	1.02	80.1686
10	0.36914	0.586954	0.780859	0.926953	0.0086	3.1×10^{-5}	1.02	81.9365
11	0.36914	0.555078	0.780859	0.926953	0.0089	2.7×10^{-7}	1.02	81.8857
12	0.36914	0.571016	0.796797	0.926953	0.0082	7.5×10^{-7}	1.02	81.9605
13	0.36914	0.571016	0.764921	0.926953	0.0090	2.3×10^{-4}	1.02	81.9036
14	0.36914	0.571016	0.780859	0.942891	0.0082	2.8×10^{-7}	1.02	81.8815
15*	0.36914	0.571016	0.780859	0.911015	0.0085	2.4×10^{-7}	1.02	80.8034
16	0.347226	0.571016	0.780859	0.926953	0.0091	1.1×10^{-5}	1.02	81.8588
17	0.375117	0.571016	0.780859	0.926953	0.0083	3.5×10^{-7}	1.02	81.9281
18	0.363164	0.571016	0.780859	0.926953	0.0091	1.9×10^{-6}	1.02	81.9397







20	0.36914	0.565039	0.780859	0.926953	0.0084	4.3*10 ⁻⁷	1.02	81.8497
21	0.36914	0.571016	0.786836	0.926953	0.0082	4.6*10 ⁻⁷	1.02	81.8394
22	0.36914	0.571016	0.774882	0.926953	0.0083	4.5*10 ⁻⁷	1.02	81.8396
23*	0.36914	0.571016	0.780859	0.93293	0.0080	4.2*10⁻⁷	1.02	81.1203
24	0.36914	0.571016	0.780859	0.920976	0.0083	4.5*10 ⁻⁷	1.02	81.8887
25	0.371382	0.571016	0.780859	0.926953	0.0083	4.4*10 ⁻⁷	1.02	81.8462
26	0.366899	0.571016	0.780859	0.926953	0.0083	4.2*10 ⁻⁷	1.02	81.8530
27	0.36914	0.573257	0.780859	0.926953	0.0082	3.2*10 ⁻⁷	1.02	81.8608
28	0.36914	0.568775	0.780859	0.926953	0.0083	3.8*10 ⁻⁷	1.02	81.6339
29	0.36914	0.571016	0.7831	0.926953	0.0083	4.3*10 ⁻⁷	1.02	81.8376
30	0.36914	0.571016	0.778618	0.926953	0.0083	6.0*10 ⁻⁷	1.02	81.8421
31	0.36914	0.571016	0.780859	0.929194	0.0083	2.2*10 ⁻⁷	1.02	81.8473
32*	0.36914	0.571016	0.780859	0.924712	0.0083	4.1*10⁻⁷	1.02	80.8030

*: Top 5 Designs of T-Search-2

After the local optimization with the T-Search method, it was observed that there was a slight decrease in the drag force values. While the lowest drag force value obtained after DoE was 81.5106 N, this value decreased to 80.1686 after T-Search. Compared to the Optimization Process-1, more improvements have been made at this stage.

The five designs with the lowest drag force value were examined, and the optimum design was decided. The drag force values obtained in the simulations are shared in Table 6.14 from the largest to the smallest.

Table 6.26. Top 5 Designs of T-Search-2

Design	Drag Force (N)	Figure
DoE-2 103	81.7357	
T-Search-2 1	81.4955	
T-Search-2 23	81.1203	
T-Search-2 15	80.8034	
T-Search-2 32	80.8030	
T-Search-2 9	80.1686	

When the forms are examined, it is seen that they are very similar to each other. This is an indication that very delicate work has been done. Therefore, the optimum five designs obtained after T-Search-2 are candidates for being the most optimal design.

6.2.3. Specifying Optimum Design-2

The optimum form was determined after the DoE and T-Search optimization results, the details of which were shared above. All suggested optimum forms are very similar to each other. Therefore, T-Search-2 9 form, which has the lowest drag force, was chosen as the optimum form since it provides the other design limits at almost the same rates.

Table 6.15 below compares the hydrostatic properties and drag forces of the optimum form with the DARPA SUBOFF AFF-1.

Table 6.27. Comparison between DARPA SUBOFF AFF-1 and the Optimum Design-2

Design	LCB (m)	Disp (m³)	L (m)	Diameter (m)	L/D	Drag Force (N)
DARPA SUBOFF AFF-1	2.013	0.708	4.356	0.508	8.57	87.3168
Optimum Design- 2	2.013	0.708	4.460	0.520	8.57	80.1686

When the table is examined, it is seen that LCB, displacement, and L/D parameters remain constant. Therefore, the target design limits for this process have been successfully achieved.

However, the drag force has not been reduced as much as the Optimization Process-1. Therefore, the rates of change of hydrostatic and hydrodynamic parameters are shared in Table 6.16 below. The rate of change of hydrostatic parameters was calculated with Equations 6.1 and 6.2, the change of drag force parameters was calculated with Equation 6.3.

Table 6.28. Comparison of Hydrostatic and Hydrodynamic Parameters between DARPA SUBOFF AFF-1 and the Optimum Design-2

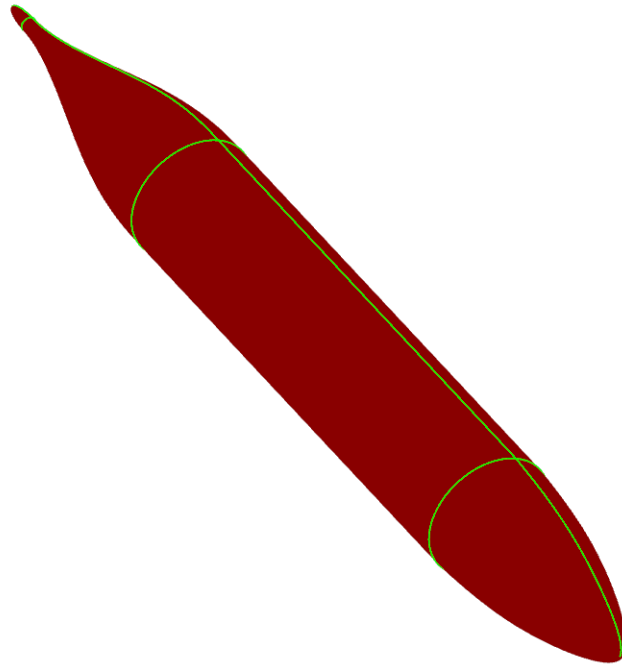
Parameters	Values
Δ LCB (%)	0.0083
Δ Disp (%)	$3.52 \cdot 10^{-7}$
Δ FD(%)	-8.1867

While the LCB and displacement remain nearly the same, the drag force is decreased by about 8 percent, much less than the Optimization Process-1.

Figures from different angles are shared in Figure 6.6 below for a more accessible examination of the Optimum Design-2 form.



a)



b)

Figure 6.34. Optimum Design-2 a) Section View b) Isometric View

6.3. Optimization Process-3

The third optimization process aims to decrease the drag force of the DARPA SUBOFF AFF-1 by reducing its length and increasing its diameter. The four forms described in the diagram shared in Figure 6.7 will be used until the final form is obtained.

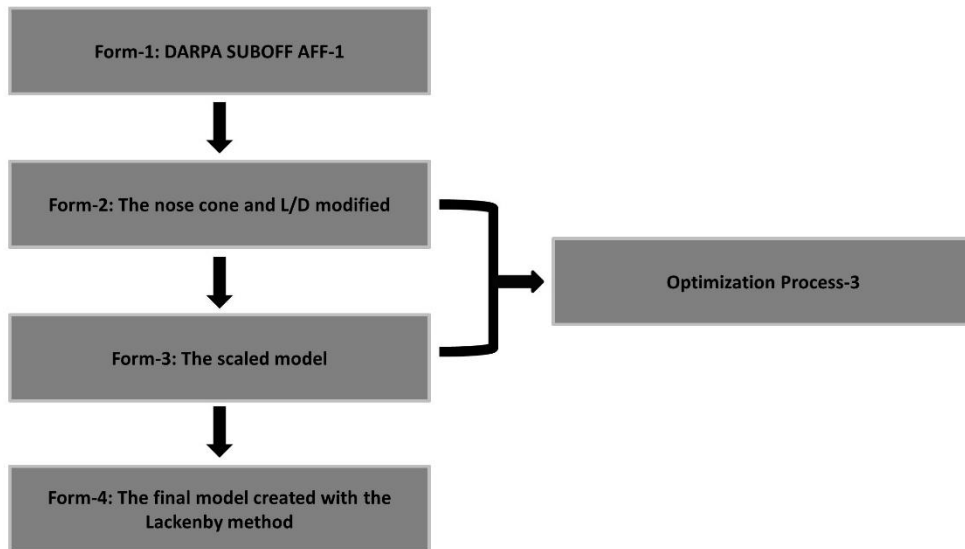


Figure 6.35. The Forms Derived in Optimization Process-3

In this process, while the nose cone is changed like in other processes, the stages of obtaining the optimum form differ. Nevertheless, the general summary of the process is shared in Figure 6.8.

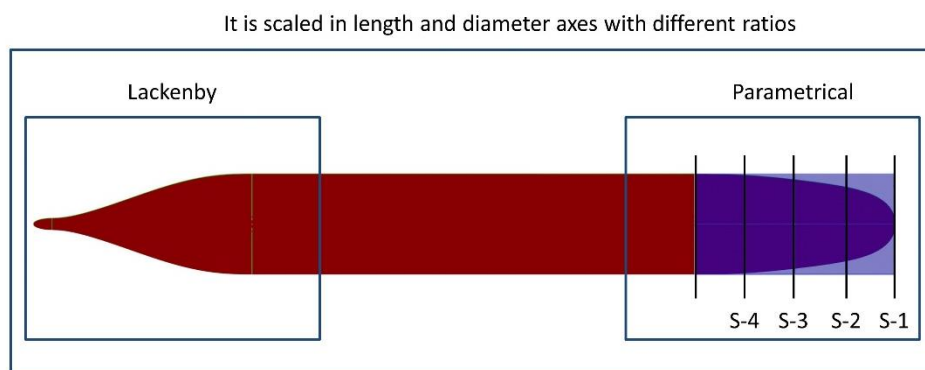


Figure 6.36. Workfields of Optimization Process-3

The bounds of the design variable values and design constraints used to control the diameters of the nose cone sections are shared in Table 6.17 and Table 6.18, respectively.

Table 6.29. Design Variables of Optimization Process-3

Design Variable	Coefficient
S-1	$0.15 \leq S-1 \leq 1$
S-2	$0.15 \leq S-2 \leq 1$
S-3	$0.15 \leq S-3 \leq 1$
S-4	$0.15 \leq S-4 \leq 1$
DV5	$7 \leq DV5 \leq 8.5$

Table 6.30. Design Constraints of Optimization Process-3

Design Constraints	Objective Functions
L	Decreased
Diameter	Increased
L/D	Decreased
LCB	Keep constant
Displacement	Can change $\pm 5\%$

Since this process is more complex than the others, it is explained step by step through an example process for proper understanding.

i. Changing the nose cone form and L/D ratio:

This step is the same as the other processes. Form-2 is obtained by making changes to Form-1. The following content will give the lower and upper limits of the design variables in which the nose cone is controlled.

At this point, Form-2, chosen as an example, was created with the parameters in Table 6.19, and the design is shared in Figure 6.9.

Table 6.31. Design Variables of Sample Form-2

Design Variables	Coefficients
S-1	0.3
S-2	0.5
S-3	0.8
S-4	0.9



Figure 6.37. Sample Form-2

ii. Changing the L/D ratio of Form-2

It has been shared in the previous sections that the L/D ratio of the DARPA SUBOFF AFF-1 model is 8.57. In this process, a displacement difference will occur as the length of the submarine is reduced. This displacement difference will be tried to be eliminated by increasing the diameter. At this point, the L/D ratio of the submarine is assigned as a design variable, as are the cross sections of the nose cone. Therefore, the L/D ratio will decrease due to the decrease in the height of the design. However, the optimum L/D range has been investigated to determine how much it will reduce.

At this point, the study prepared by Moonesun et al. by comparing the drag forces of submarine hulls with different L/D ratios was examined, and it was learned that this range is between 7-10 [85].

The L/D ratio, which CAESES automatically changes, obtains Form-3 by changing the geometry with a few parameters.

Firstly, Form-3 is considered a cylinder with the same volume but different diameter and length, as shared in Figure 6.10. The length and diameter, in this case, are calculated with the following method.

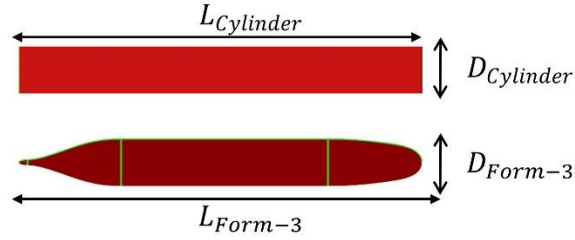


Figure 6.38. A Cylinder Created for Dimension Calculation for Form-3

$$Displacement_{Form-1} = Displacement_{Cylinder} \quad (6.5)$$

$$Displacement_{Cylinder} = \pi \frac{D_{Cylinder}^2}{4} L_{Cylinder} \quad (6.6)$$

$$\frac{L_{Cylinder}}{D_{Cylinder}} = \text{The fifth design variable of this process (DV5)} \quad (6.7)$$

$$D_{Cylinder} = \frac{L_{Cylinder}}{DV5} \quad (6.8)$$

$$Displacement_{Cylinder} = \pi \frac{L_{Cylinder}^2}{4(DV5^2)} L_{Cylinder} \quad (6.9)$$

$$L_{Cylinder} = \left(\frac{Displacement_{Cylinder} 4(DV5^2)}{\pi} \right)^{\frac{1}{3}} \quad (6.10)$$

$L_{Cylinder}$ and $D_{Cylinder}$ are calculated by performing these calculations again for each changed L/D ratio. However, there is much difference between the cylinder and submarine form, which may reduce the performance of the Lackenby method to keep the displacement difference within the desired range in the next step. For this reason, an additional coefficient was initially calculated for DARPA SUBOFF AFF-1 (C_{Disp}), and the calculated cylinder length value for each derived form was multiplied by this coefficient.

$$C_{Disp} = \frac{L_{Form-1}}{L_{Cylinder (Form-1)}} = 1.081 \quad (6.11)$$

$$L_{Form-3} = C_{Disp} L_{Cylinder} \quad (6.12)$$

$$D_{Form-3} = C_{Disp} D_{Cylinder} \quad (6.13)$$

For Form-2, chosen as an example, when the L/D ratio is changed to 8, the parameters shared in Table 6.20 are reached.

Table 6.32. The parameters of Form-2

$L_{Cylinder}$	$D_{Cylinder}$	L_{Form-3}	D_{Form-3}
3.864 m	0.483 m	4.177 m	0.522 m

iii. Scaling

After calculating the length and diameter of Form-3, the coefficients required to scale Form-2 are summed to obtain this form.

$$C_{Length} = \frac{L_{Form-3}}{L_{Form-1}} \quad (6.13)$$

$$C_{Diameter} = \frac{D_{Form-3}}{D_{Form-1}} \quad (6.14)$$

The calculated length and diameter coefficients for Form-2, shared in Figure 6.9, are 0.959 and 1.028, respectively, and the resulting Form-3 is shared in Figure 6.11.



Figure 6.39. Sample Form-3

iv. Lackenby

As in the other processes, the final geometry was obtained by working on Form-3 with the Lackenby method. There is no change in the Lackenby procedure, and the Form-3 shared above is transformed into Form-4 Figure 6.12 after Lackenby.

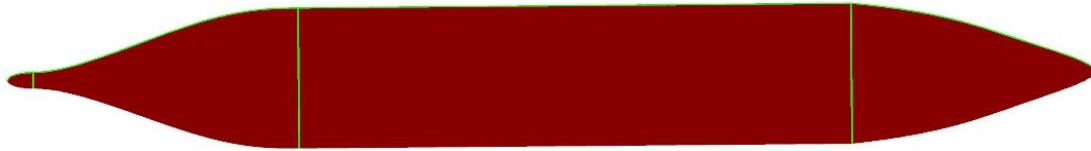


Figure 6.40. Sample Form-4

To see the process's effect, the hydrostatic properties of all forms are shared in Table 6.21.

Table 6.33. Comparison of Hydrostatic Properties of Sample Forms

Design	LCB (m)	Disp (m³)	L (m)	Diameter (m)	L/D
Form-1 (DARPA SUBOFF AFF-1)	2.013	0.708	4.356	0.508	8.57
Form-2	2.074	0.6871	4.356	0.508	8.57
Form-3	2.042	0.6918	4.177	0.522	8
Form-4	2.013	0.6986	4.177	0.522	8

6.3.1. DoE-3 Results

In this process, a space of 250 designs is created at the DoE stage. In Table 6.22, shared below, the drag forces, design variables and L/D values of the best 20 designs obtained as a result of DoE are shared with LCB and displacement changes. These changes are calculated with the same methods as Process-1.

Table 6.34. Top 20 Designs of DoE-3

No	S-1	S-2	S-3	S-4	DV5	Δ LCB (%)	Δ Disp (%)	Drag Force (N)
24	0.367188	0.367188	0.648438	0.882812	7.88281	-0.019	-3.37	80.3925
48	0.308594	0.425781	0.449219	0.988281	7.98828	-0.021	-3.42	80.7166
68	0.548828	0.267578	0.865234	0.947266	7.87695	-0.005	-0.88	81.5459
8	0.390625	0.484375	0.484375	0.765625	7.67188	-0.023	-5.15	82.8564
30	0.648438	0.273438	0.929688	0.789062	7.97656	-0.015	-2.34	83.4322
14	0.671875	0.578125	0.390625	0.859375	7.76562	-0.016	-3.74	83.5057
80	0.337891	0.337891	0.748047	0.736328	7.61914	-0.008	-4.07	83.7909
91	0.572266	0.666016	0.794922	0.876953	7.75977	0.018	-0.66	83.9440
47	0.332031	0.777344	0.378906	0.824219	7.63672	-0.002	-3.34	84.1566
36	0.566406	0.355469	0.425781	0.777344	7.49609	-0.007	-5.24	84.3091
32	0.285156	0.449219	0.707031	0.683594	7.77734	-0.026	-4.93	84.3122
7	0.34375	0.71875	0.90625	0.90625	7.71875	0.035	-2.40	84.6472
28	0.460938	0.460938	0.367188	0.976562	7.41406	0.050	-1.70	85.2608
64	0.267578	0.548828	0.583984	0.853516	7.4082	0.060	-1.15	85.5372
82	0.900391	0.525391	0.560547	0.923828	7.80664	-0.001	-1.30	85.5747
34	0.847656	0.261719	0.519531	0.871094	7.58984	0.001	-3.51	85.6081
57	0.730469	0.941406	0.683594	0.847656	7.94141	0.007	-1.26	86.2141
54	0.777344	0.332031	0.355469	0.707031	7.89453	-0.041	-7.03	86.2720
75	0.595703	0.970703	0.537109	0.806641	7.92383	-0.003	-0.79	86.3346
17	0.695312	0.976562	0.507812	0.929688	7.83594	0.015	-1.15	86.5900

A result not seen in previous processes is examined when the table is scanned. While the drag performance of all the first 25 designs is better than the first form in other processes, there are those with worse performance than the first form among the first 25 designs.

This indicates that the design space should be at least 250. Suppose a multi-purpose optimization study was carried out. In that case, the DoE study of this process could be repeated, but the T-Search method used from now on will eliminate this situation by scanning more designs. Although the results lag behind Optimization Process-1 in terms of drag performance, the fact that the displacement has changed very little indicates that this process will bring a different perspective.

Since there are forms with worse performance than the first form in the first 50 designs, the Pareto analyses to be made in this process were made for the first 20 designs and the graphics are shared in Figure 6.13.

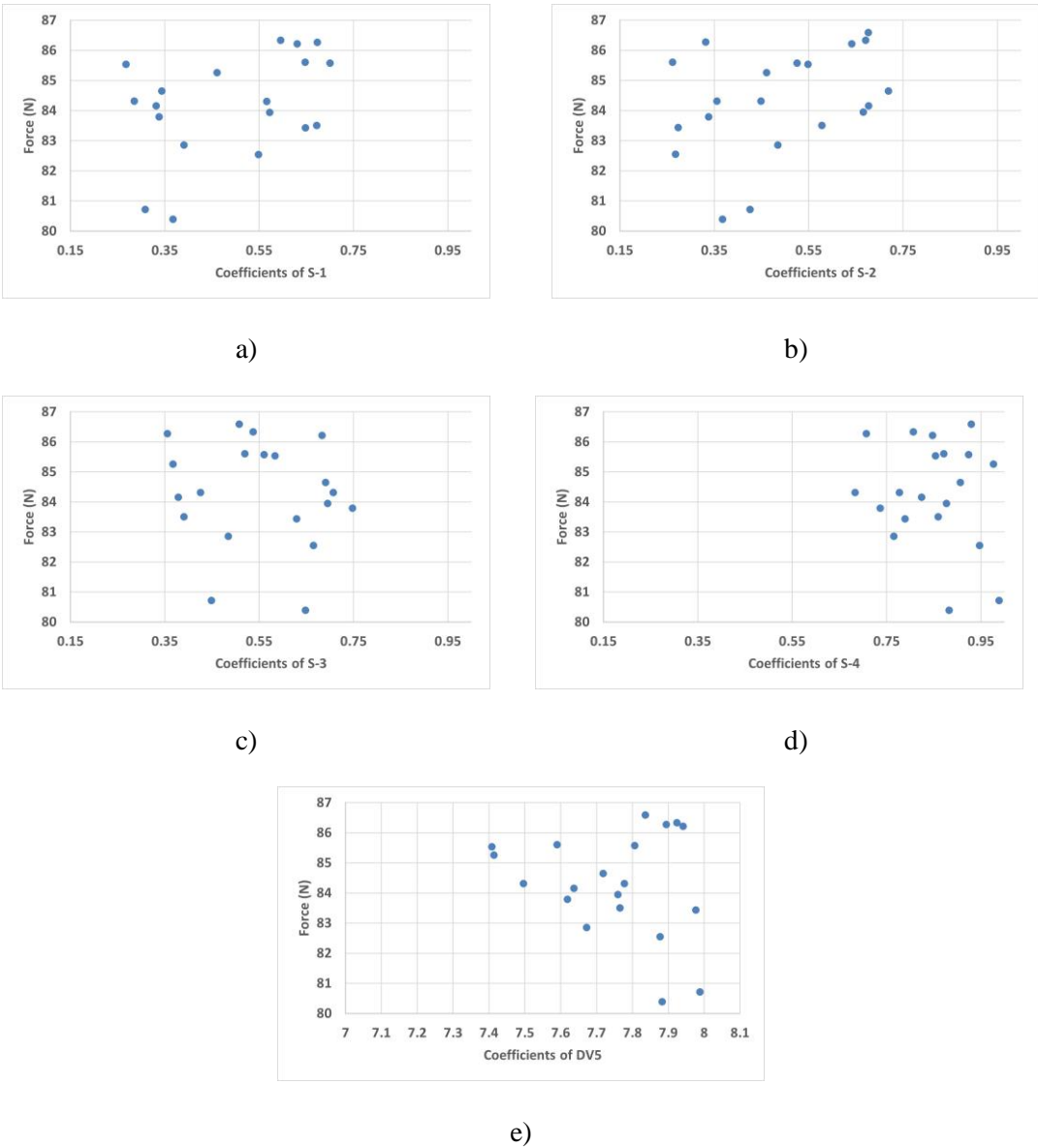


Figure 6.41. Pareto Analyses of DoE-3 a) S-1 b) S-2 c) S-3 d) S-4 e) DV5







When the graphs are examined, it is observed that the S-1 value varies between 0.25-0.65, the S-2 value varies between 0.25-0.75, the S-3 value varies between 0.35-0.75, and the S-4 value varies between 0.75-1 in the most optimal designs.

In optimum design, as in other processes, S-1, S-2, and S-3 may have values close to each other, but S-4 will necessarily have a more excellent value than them.

It is seen that the value of the DV5 variable controlling the L/D ratio is at least 7.5, and the drag force decreases as it approaches 8.

In Table 6.23 below, the visuals of the five designs that create the lowest drag force obtained from DoE and the first design are shared together with the resistive force values obtained in the simulations.

Table 6.35. Top 5 Designs of DoE-3

Design	Drag Force (N)	Figure
DARPA SUBOFF AFF-1	87.3168	
DoE-3 30	83.4322	
DoE-3 8	82.8564	
DoE-3 68	81.5459	
DoE-3 48	80.7166	
DoE-3 24	80.3925	

When the designs and parameters are examined, it is seen that the drag forces are not very close to each other, unlike other processes. DoE-3 24 and DoE-3 48 have better performance than other designs. When these two designs are examined among themselves, it is seen that the parameters are almost the same in terms of hydrodynamics and hydrostatics. For this reason, the DoE-3 24 design with the best performance was chosen as the initial design for T-Search-3.

6.3.2. T-Search-3 Results

Due to scanning a smaller space compared to other processes, DoE-3 could not give as accurate results as other processes. For this reason, T-Search-3 took longer than other processes to scan a space of 97 designs.

All designs scanned in the T-Search stage in other processes were shared, but as more designs were reviewed, the results of the top 10 designs were shared in Table 6.24.







Table 6.36. Top 10 Designs of T-Search-3

No	S-1	S-2	S-3	S-4	DV5	Δ LCB (%)	Δ Disp (%)	Drag Force (N)
23	0.330631	0.249757	0.390992	0.882812	7.91937	-0.035	-5.88	79.467
16	0.330631	0.249757	0.390992	0.882812	7.88281	-0.036	-5.89	79.5467
19	0.330631	0.249757	0.427549	0.882812	7.88281	-0.034	-5.66	79.5785
62	0.25011	0.282813	0.601562	0.867188	8.09375	-0.024	-4.48	79.5825
44	0.282813	0.320313	0.639062	0.867188	8.09375	-0.022	-4.01	79.6197
71	0.320313	0.282813	0.601562	0.867188	8.09375	-0.024	-4.41	79.632
56	0.282813	0.320313	0.639062	0.904688	8.14375	-0.019	-3.51	79.6574
83	0.282813	0.320313	0.601562	0.867188	8.09375	-0.023	-4.28	79.6759
35	0.282813	0.320313	0.639062	0.904688	8.09375	-0.021	-3.54	79.7754
47	0.282813	0.371875	0.690625	0.95625	8.2125	-0.014	-2.21	80.3142

After the local optimization with the T-Search method, it was observed that there was a slight decrease in the drag force values. While the lowest drag force value obtained after DoE was 80.3925 N, this value decreased to 79.467 N after T-Search. This decrease is more significant than that achieved in the T-Search phase in the two previous optimization processes.

The five designs with the lowest drag force value were examined, and the optimum design was decided. The drag obtained in the simulations is shared in Table 6.25 with the force values from the largest to the smallest.

Table 6.37. Top 5 Designs of T-Search-3

Design	Drag Force (N)	Figure
DoE-3 24	80.3925	
T-Search-3 44	79.6197	
T-Search-3 62	79.5825	
T-Search-3 19	79.5785	
T-Search-3 16	79.5467	
T-Search-3 23	79.4670	

When the forms are examined, it is seen that there is a different result from the T-Search studies carried out in the previous processes. While in other processes, the forms are pretty similar to each other, and the forms are visibly different in this process. Since their drag forces are very close to each other, all five designs are candidates for being the most optimum design.

6.3.3. Specifying Optimum Design-3

The optimum form was determined after the DoE and T-Search optimization results, the details of which were shared above. The fact that the proposed forms are visibly different indicates that the design limits defined in this process may differ for each design.

When Table 6.24 is examined, the displacement differences of T-Search-3 23,16 and 19 designs with DARPA SUBOFF AFF-1 are over five percent.

The LCB rate of change is very close in all designs. For this reason, the displacement difference is less than five percent and T-Search-3 62 design with the best drag performance was chosen as the most optimum form.

Table 6.26 below compares the hydrostatic properties and the drag forces of the optimum form with the DARPA SUBOFF AFF-1.

Table 6.38. Comparison between DARPA SUBOFF AFF-1 and the Optimum Design-3

Design	LCB (m)	Disp (m³)	L (m)	Diameter (m)	L/D	Drag Force (N)
DARPA SUBOFF AFF-1	2.013	0.708	4.356	0.508	8.57	87.3168
Optimum Design-3	2.013	0.676	4.192	0.536	7.82	79.5825

When the table is examined, it is seen that the volume changes little while the LCB remains constant.

The drag performance is improved less than Optimization Process-1 but more than Optimization Process-2. The rates of change of hydrostatic and hydrodynamic parameters are shared in Table 6.27 below. The rate of change of hydrostatic parameters was calculated with Equations 6.1 and 6.2, the change of the drag force parameters was calculated with Equation 6.3.

Table 6.39. Comparison of Hydrostatic and Hydrodynamic Parameters between Optimum Design-3 and DARPA SUBOFF AFF-1

Parameters	Values
Δ LCB (%)	-0.0239
Δ Disp (%)	-4.4834
Δ FD(%)	-8.8579

While the hydrostatic parameters and longitudinal centre of buoyancy remained almost constant, the displacement variation did not exceed 5%. On the other hand, an improvement in drag performance is observed in the band of about 9%. Images from different angles are shared in Figure 6.14 below for a more accessible examination of the Optimum Design-3 form.

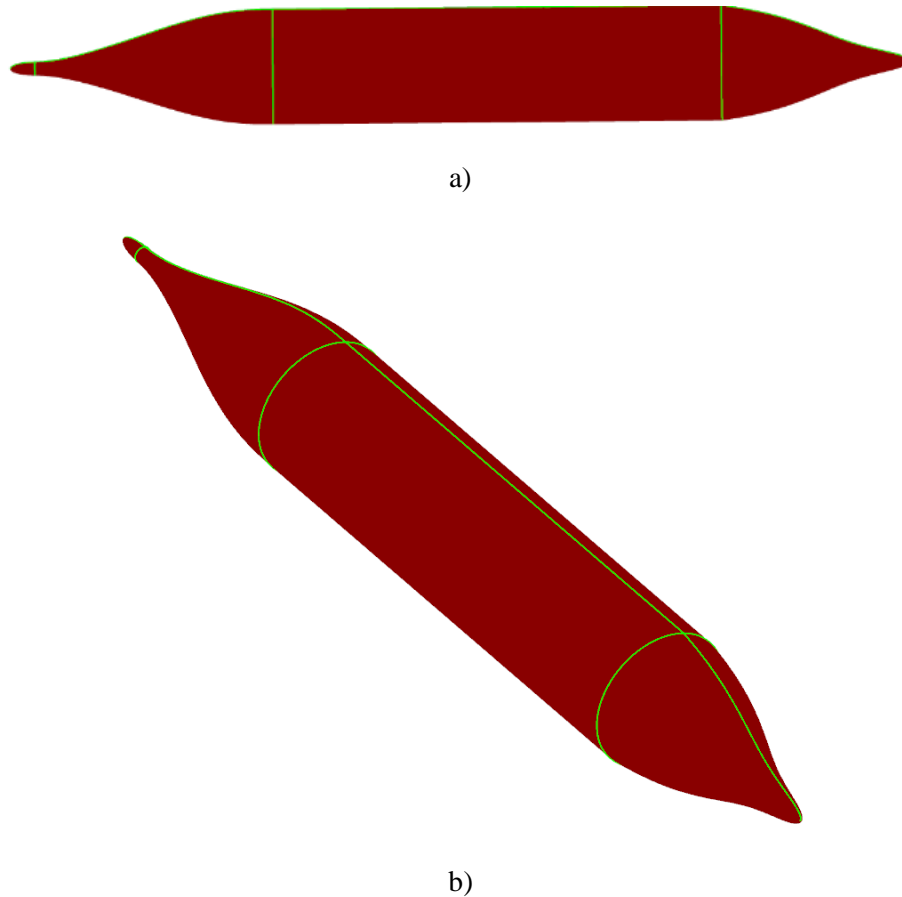


Figure 6.42: Optimum Design-3 a) Section View b) Isometric View

6.4. Optimization Process-4

The fourth and final optimization process is the same as the Optimization Process-3. However, in this process, the length of the submarine is extended, and the diameter is kept constant. Therefore, while the L/D ratio was decreased in the previous process, it was increased in this process. Since the diameter is kept constant in this process, the length of Form-3 can be calculated directly at each L/D ratio that is changed. Therefore, there is no need to perform extended operations as in Optimization Process-3 to reach the C_{Length} coefficient. Instead, form-3 is obtained by scaling Form-2 along the length axis with this coefficient, which is calculated by dividing the length of Form-3 by the length of Form-1, and then the Lackenby method generates Form-4.

The Figure 6.15, shared below, shows the working areas of this process.

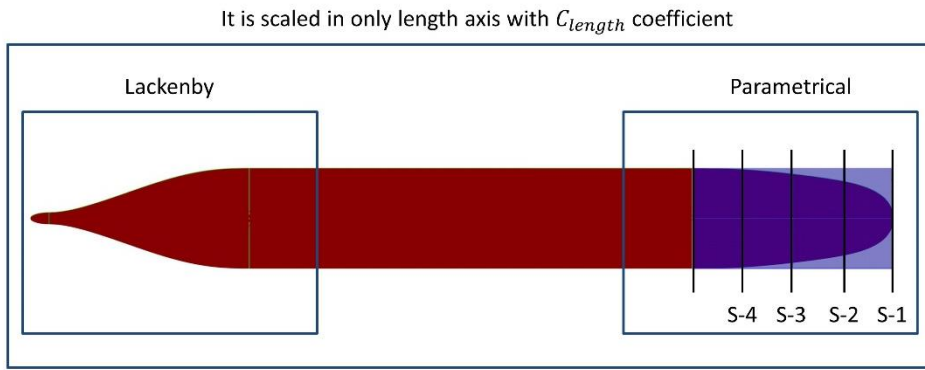


Figure 6.43. Workfields of Optimization Process-4

The bounds of the design variable values and design constraints used to control the diameters of the nose cone sections are shared in Table 6.28 and Table 6.29, respectively.

Table 6.40. Design Variables of Optimization Process-3

Design Variable	Coefficient
S-1	$0.15 \leq S-1 \leq 1$
S-2	$0.15 \leq S-2 \leq 1$
S-3	$0.15 \leq S-3 \leq 1$
S-4	$0.15 \leq S-4 \leq 1$
DV5	$8.5 \leq DV5 \leq 10$

Table 6.41. Design Constraints of Optimization Process-4

Design Constraints	Objective Functions
L	Increased
Diameter	Keep constant
L/D	Increased
LCB	Keep constant
Displacement	Can change $\pm 5\%$

6.4.1. DoE-4 Results

In line with the experience gained in previous processes, it is known that the space to be scanned at the DoE stage should contain at least 250 designs.

DoE studies can be completed by performing multiple simulations simultaneously according to the computational power. However, the T-Search method DoEs not allow this as it changes the design according to the simulation result. Therefore, optimization work gains great speed when an ample design space is scanned by performing multiple simulations simultaneously in the DoE phase.

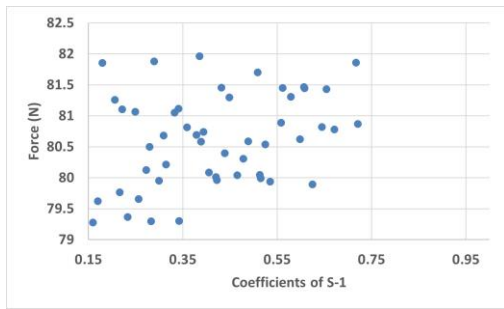
For this reason, a design space containing 500 designs was scanned in this process, just like Process-2. In Table 6.30, shared below, the drag forces, design variables and L/D values of the best 20 designs obtained as a result of DoE are shared with LCB and displacement changes. These changes are calculated with the same methods as other processes.

When the table is examined, it is seen that the displacement and LCB changes are as targeted, and the drag forces have decreased. Therefore, the drag performance improvement is the second best among the four processes.

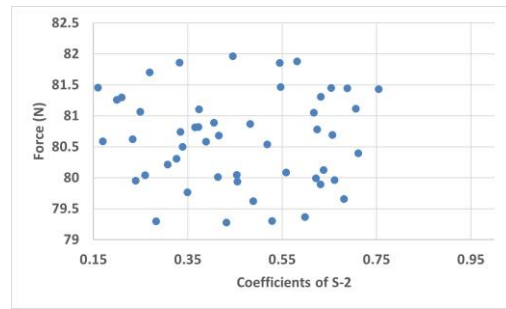
A more detailed analysis has been done with Pareto analyses for the top 20 designs shared in Figure 6.16.

Table 6.42. Top 20 Designs of DoE-4

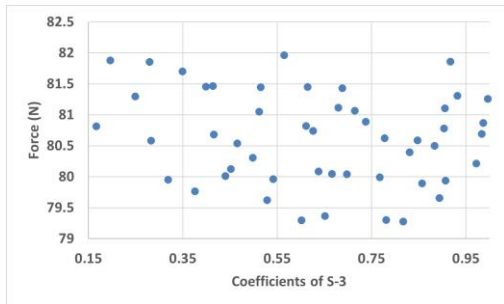
No	S-1	S-2	S-3	S-4	DV5	Δ LCB (%)	Δ Disp (%)	Drag Force (N)
127	0.159961	0.432227	0.817383	0.950195	8.77913	0.010	-4.57	79.277
23	0.282813	0.282813	0.601562	0.867188	8.96372	0.023	-4.74	79.2947
103	0.342578	0.528516	0.780859	0.926953	8.769	0.009	-4.59	79.3031
238	0.233008	0.598242	0.651367	0.983398	8.77603	0.009	-4.57	79.3667
63	0.169922	0.488672	0.528516	0.833984	8.96907	0.023	-4.75	79.6227
6	0.25625	0.68125	0.89375	0.89375	8.69007	0.005	-4.48	79.6556
47	0.216406	0.349219	0.375781	0.986719	8.95934	0.023	-4.70	79.765
160	0.624805	0.631445	0.857227	0.910352	8.67649	0.005	-4.47	79.8922
51	0.535156	0.455469	0.907031	0.880469	8.74852	0.008	-4.55	79.9367
215	0.299414	0.239648	0.319336	0.916992	9.04214	0.030	-4.75	79.9538
114	0.422266	0.661328	0.541797	0.953516	8.81064	0.012	-4.62	79.9616
90	0.515234	0.621484	0.767578	0.860547	8.77421	0.010	-4.62	79.989
267	0.420605	0.413965	0.440527	0.868848	8.98279	0.024	-4.74	80.0109
171	0.46543	0.25957	0.697852	0.963477	8.85157	0.014	-4.63	80.0418
291	0.513574	0.453809	0.666309	0.988379	8.78703	0.010	-4.59	80.0446
219	0.405664	0.558398	0.638086	0.810742	8.8998	0.019	-4.74	80.0839
198	0.272852	0.638086	0.452148	0.89043	8.91382	0.019	-4.70	80.1229
263	0.314355	0.307715	0.971777	0.975098	8.71241	0.006	-4.47	80.2145
131	0.478711	0.325977	0.498633	0.843945	8.99426	0.026	-4.75	80.3083
178	0.438867	0.711133	0.830664	0.830664	8.7391	0.008	-4.56	80.3969



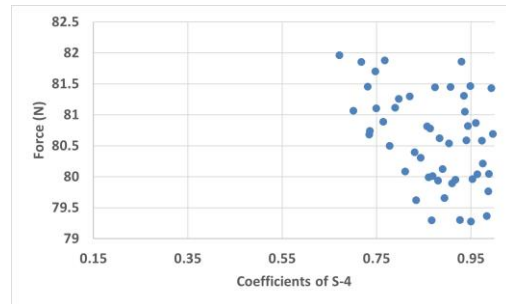
a)



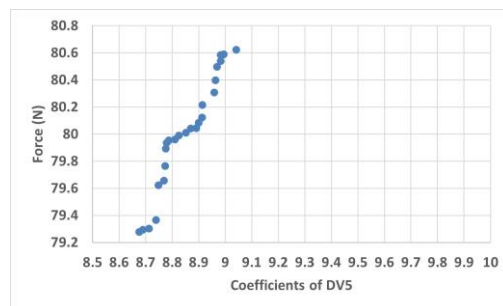
b)



c)



d)



e)

Figure 6.44. Pareto Analyses of DoE-4 a) S-1 b) S-2 c) S-3 d) S-4 e) DV5







When the graphs are examined, it has been observed that the S-1 value varies between 0.15-0.75, the S-2 value between 0.15-0.75, and the S-4 value between 0.75-1 in the most optimal designs. At the same time, there is no specific range for S-3 in the most optimal designs.

In optimum design, as in other processes, S-1, S-2, and S-3 may have values close to each other, but S-4 will necessarily have a more excellent value than them.

It is seen that the value of the DV5 variable controlling the L/D ratio is at least 8.6, and the drag force decreases as it approaches 9.

Table 6.31 below shows the visuals of the five designs that create the lowest resistive force obtained from DoE, and the first design is shared with the drag force values obtained in the simulations.

Table 6.43. Top 5 Designs of DoE-4

Design	Drag Force (N)	Figure
DARPA SUBOFF AFF-1	87.3168	
DoE-4 63	79.6227	
DoE-4 238	79.3667	
DoE-4 103	79.3031	
DoE-4 23	79.2947	
DoE-4 127	79.2770	

When the designs and parameters are examined, it is seen that the drag forces are very close to each other. However, Table 6.29 shows that the $\pm 5\%$ variable target for displacement is close to the limit for all.

There is no problem with being close to the limit at this stage. However, designs that are far from the lowest values of the S-1 and S-2 parameters, especially those that adhere to this evaluation, may deviate from the displacement target if used as a starting form for T-Search.

For this reason, the fact that the DoE-4 127 design has a coefficient of 0.159961 for S-1 indicates that this design may deviate less from the displacement target in the T-Search stage compared to the others.

To explain in more detail, when the S-1 and S-2 values of the DoE-4 103 design are examined, it is seen that they are 0.342578 and 0.528516, respectively. Therefore, if this design is used as the initial form in the T-Search method, these values may approach 0.15 and cause deviation from the displacement target, which is already at the limit.

6.4.2. T-Search-4 Results

As can be understood from the detailed explanations made in the previous section, the DoE-4 127 design was chosen as the initial form of T-Search-4. No changes were made in the design variable ranges, and the T-Search method scanned an additional 32 designs and derived the most optimal form.

T-Search-4 results are shared in Table 6.32 shared below.

Table 6.44. Results of T-Search-4

No	S-1	S-2	S-3	S-4	DV5	Δ LCB (%)	Δ Disp (%)	Drag Force (N)
0	0.159961	0.432227	0.817383	0.950195	8.77913	0.010	-4.57	79.277
1	0.202461	0.432227	0.817383	0.950195	8.77586	0.009	-4.57	79.3645
2	0.15	0.432227	0.817383	0.950195	8.77942	0.010	-4.58	79.341
3	0.159961	0.474727	0.817383	0.950195	8.76555	0.009	-4.58	79.2567
4	0.159961	0.474727	0.859883	0.950195	8.74505	0.008	-4.55	79.3007
5*	0.159961	0.474727	0.774883	0.950195	8.786	0.010	-4.62	78.5201
6	0.159961	0.474727	0.774883	0.992695	8.75463	0.008	-4.54	79.3847
7	0.159961	0.474727	0.774883	0.907695	8.81696	0.013	-4.66	79.1901
8	0.159961	0.533164	0.716446	0.950195	8.79589	0.010	-4.59	79.2216
9	0.175898	0.474727	0.774883	0.950195	8.78498	0.010	-4.59	79.1797
10	0.15	0.474727	0.774883	0.950195	8.78707	0.010	-4.60	79.1987
11	0.159961	0.490664	0.774883	0.950195	8.78123	0.010	-4.60	79.218
12	0.159961	0.458789	0.774883	0.950195	8.79099	0.010	-4.60	79.2175
13	0.159961	0.474727	0.790821	0.950195	8.77827	0.010	-4.60	79.237
14*	0.159961	0.474727	0.758945	0.950195	8.79373	0.011	-4.64	79.1674
15	0.159961	0.474727	0.774883	0.966133	8.77442	0.009	-4.58	79.296
16	0.159961	0.474727	0.774883	0.934257	8.79781	0.011	-4.63	79.2775
17	0.165938	0.474727	0.774883	0.950195	8.78585	0.010	-4.61	79.2069
18*	0.153984	0.474727	0.774883	0.950195	8.78652	0.010	-4.60	79.1598







19	0.159961	0.480704	0.774883	0.950195	8.78424	0.010	-4.60	79.3226
20	0.159961	0.46875	0.774883	0.950195	8.78813	0.010	-4.61	79.2122
21	0.159961	0.474727	0.78086	0.950195	8.78345	0.010	-4.61	79.1806
22	0.159961	0.474727	0.768906	0.950195	8.78883	0.010	-4.60	79.2936
23	0.159961	0.474727	0.774883	0.956172	8.78177	0.010	-4.61	79.1697
24*	0.159961	0.474727	0.774883	0.944218	8.79237	0.011	-4.59	79.0474
25	0.162202	0.474727	0.774883	0.950195	8.78878	0.010	-4.58	79.2698
26	0.15772	0.474727	0.774883	0.950195	8.78643	0.010	-4.61	79.2221
27	0.159961	0.476968	0.774883	0.950195	8.78544	0.010	-4.60	79.2488
28	0.159961	0.472486	0.774883	0.950195	8.7869	0.010	-4.61	79.1953
29	0.159961	0.474727	0.777124	0.950195	8.78515	0.010	-4.61	79.1893
30	0.159961	0.474727	0.772642	0.950195	8.78716	0.010	-4.60	79.2277
31*	0.159961	0.474727	0.774883	0.952436	8.78446	0.010	-4.61	78.8404
32	0.159961	0.474727	0.774883	0.947954	8.78775	0.010	-4.57	79.2551

*: Top 5 Designs of T-Search-2

After the local optimization with the T-Search method, it was observed that there was a slight decrease in the drag force values. While the lowest drag force value obtained after DoE was 79.277 N, this value decreased to 78.5201 after T-Search. Compared to Optimization Process-2 and 3, more improvements have been made at this stage.

The optimum design was decided by examining five designs with the lowest drag force value. In Table 6.33 below, the visuals of the five designs that create the lowest drag force obtained as a result of this method and the optimum design obtained after DoE are shared from largest to smallest, together with the drag force values obtained in the simulations.

Table 6.45. Top 5 Designs of T-Search-4

Design	Drag Force (N)	Figure
DoE-3 24	79.2770	
T-Search-4 14	79.1674	
T-Search-4 18	79.1598	
T-Search-4 24	79.0474	
T-Search-4 31	78.8404	
T-Search-4 5	78.5201	

When the design variable values shared in Table 6.32 are examined, it is seen that they rarely change. For this reason, the forms shared in Table 6.33 are almost identical. For this reason, it will be sufficient to look at the drag force to choose the most optimal form.

6.4.3. Specifying Optimum Design-4

The optimum form was determined after the DoE and T-Search optimization results, the details of which were shared above. The fact that the suggested forms are almost identical to each other facilitates the selection of the optimum form.

It is understood from Table 6.33 that the LCB change rates of all forms are close to each other, and the displacement change rates are below five percent.

For this reason, T-Search-4 5 design, which has the best drag performance among the forms shared in Table 6.33, was chosen as the most optimum form.

Table 6.34 below compares the hydrostatic properties and the drag forces of the optimum form with the DARPA SUBOFF AFF-1.

Table 6.46. Comparison between DARPA SUBOFF AFF-1 and the Optimum Design-4

Design	LCB (m)	Disp (m³)	L (m)	Diameter (m)	L/D	Drag Force (N)
DARPA SUBOFF AFF-1	2.013	0.708	4.356	0.508	8.57	87.3168
Optimum Design-4	2.013	0.675	4.463	0.508	8.79	78.5201

When the table is examined, it is seen that the volume changes little while the LCB remains constant.

The drag reduction is less than Optimization Process-1 but more than other processes. The rates of change of hydrostatic and hydrodynamic parameters are shared in Table 6.35 below. The rate of change of hydrostatic parameters was calculated with Equation 6.1, the change of the drag force parameters was calculated with Equation 6.2.

Table 6.47. Comparison of Hydrostatic and Hydrodynamic Parameters between DARPA SUBOFF AFF-1 and the Optimum Design-4

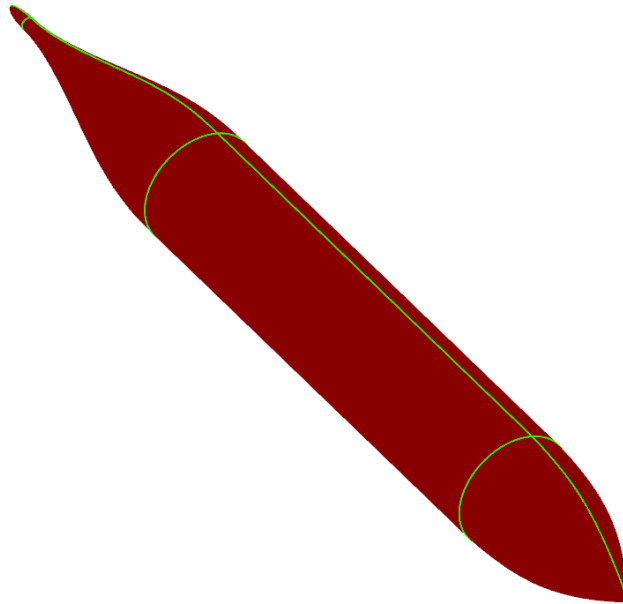
Parameters	Values
Δ LCB (%)	0.0104
Δ Disp (%)	-4.6155
Δ FD(%)	-10.0747

While the hydrostatic parameters and longitudinal centre of buoyancy remained almost constant, the displacement variation did not exceed 5%. On the other hand, an improvement of approximately 10% is observed in the drag force.

In order to examine the Optimum Design-4 form more efficiently, the figures from different angles are shared in Figure 6.17 below.



a)



b)

Figure 6.45. Optimum Design-4 a) Section View b) Isometric View

6.5. Review of the Optimization Processes

Four different optimization process methods and results are shared in detail. In this section, these processes will be summarized and compared with each other. First, however, the design constraints and objective functions defined for all optimization processes are summarized in Table 6.36, which is shared below.

Table 6.48. Design Constraints and Objective Functions

Process	L	Diameter	L/D	LCB	Displacement
Optimization Process-1	Keep constant	Keep constant	Keep constant	Keep constant	Can change $\pm 10\%$
Optimization Process-2	Increased	Increased	Keep constant	Keep constant	Keep constant
Optimization Process-3	Decreased	Increased	Decreased	Keep constant	Can change $\pm 5\%$
Optimization Process-4	Increased	Keep constant	Increased	Keep constant	Can change $\pm 5\%$

6.5.1. Review of Hydrostatic and Geometrical Properties

Although the steps followed in the optimization processes are similar, the optimum designs obtained are geometrically different. Since the changes in the first design are based on the length and diameter change directions shared in Table 6.36, the effects of these changes on the result can be made by examining the LCB and Displacement change rates between the first form and the optimum forms. Table 6.37 below shares the rate of change of these parameters between the first form and the optimum form.

Table 6.49. Rate of Change of LCB and Displacement Compared to DARPA SUBOFF AFF-1

Process	Δ LCB (%)	Δ Disp (%)
Optimization Process-1	0.011499	-9.7439
Optimization Process-2	0.008300	$3.52 \cdot 10^{-7}$
Optimization Process-3	-0.023980	-4.4834
Optimization Process-4	0.010354	-4.6155

When the table is examined, it is seen that the changes in the LCB values in each optimization process are so small that they do not change the initial value. Likewise, displacement changes are below the targeted rates in all processes. For this reason, it can be easily said that all processes reach the target in terms of hydrostatics. The hydrostatic and geometric properties of the optimum designs obtained in all processes are summarized in Table 6.38 below.

Table 6.50. The Hydrostatic and Geometric Properties of All Designs

Design	LCB (m)	Disp (m ³)	L (m)	Diameter (m)	L/D
DARPA SUBOFF AFF-1	2.013	0.708	4.356	0.508	8.57
Optimum Design-1	2.013	0.639	4.356	0.508	8.57
Optimum Design-2	2.013	0.708	4.460	0.520	8.57
Optimum Design-3	2.013	0.676	4.192	0.536	7.82
Optimum Design-4	2.013	0.675	4.463	0.508	8.79

The figures of the optimum designs were shared in the previous titles, but all designs and the DARPA SUBOFF AFF-1 design were shared in Figure 6.18 for more precise comparison.

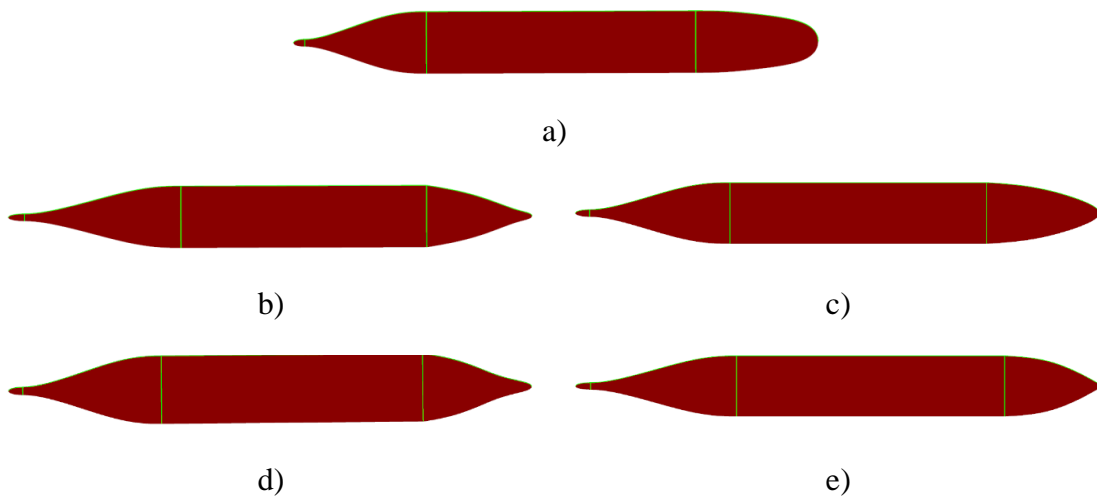


Figure 6.46. Review of all Designs a) DARPA SUBOFF AFF-1 b) Optimum Design-1 c) Optimum Design-2 d) Optimum Design-3 e) Optimum Design-4

When the designs are considered and examined only as forms without being controlled by any parameter in terms of hydrostatics and hydrodynamics, it is clear that they are visibly different from each other. This indicates that the effects of different optimization studies carried out within the scope of the thesis are also different. This will help to determine the design limits correctly when optimizing any submarine design.

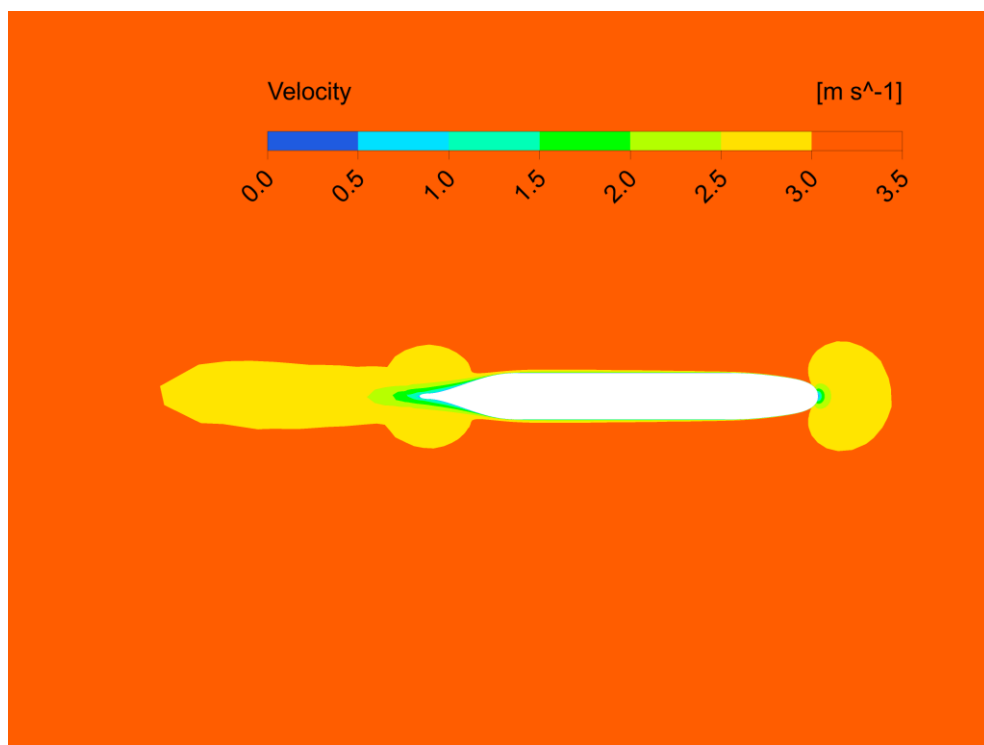
6.5.2. Review of Hydrodynamic Properties

The designs comply with all the design limits set before the hydrostatic optimization studies. Therefore, all four optimization studies are equal in terms of hydrostatics. For this reason, the improvement rates in drag performance should be examined to compare the studies' efficiency. In structures driven by propulsion systems such as submarines, it is more accurate to compare the optimization studies over the drag force. In all of the optimization studies used throughout the thesis, optimization studies were carried out to reduce the drag force. In addition, although the surface areas of all forms are different, it will be helpful to examine the dimensionless drag coefficients to understand the hydrodynamic characteristics of the obtained forms. Table 6.39 shared below shows the drag forces, dimensionless drag coefficients of the designs and the rate of change of these values compared to the first form. The ΔCD calculation was performed with the same method as the ΔFD .

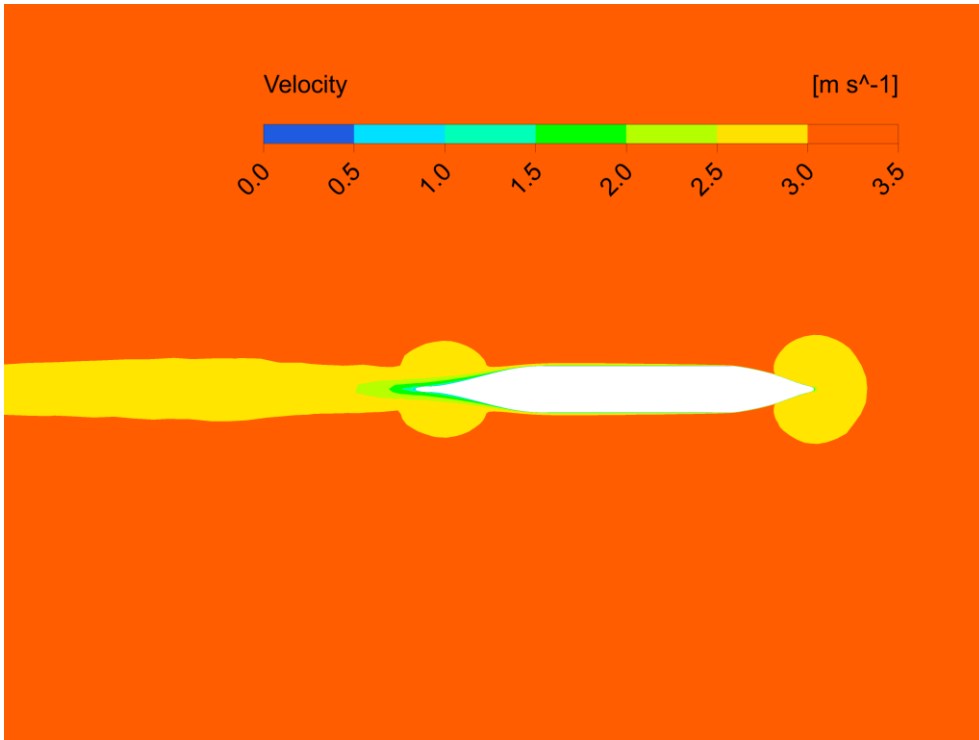
Table 6.51. The Drag Forces and Coefficients of All Designs

Model	Drag Force (N)	$\Delta FD(\%)$	Drag Coefficient	$\Delta CD (\%)$
DARPA SUBOFF AFF-1	87.3168	-	0.003146	-
Optimum Design-1	76.0010	-12.9595	0.002806	-10.7942
Optimum Design-2	80.1686	-8.1867	0.002906	-7.6277
Optimum Design-3	79.5825	-8.8579	0.002934	-6.7243
Optimum Design-4	78.5201	-10.0747	0.002877	-8.5300

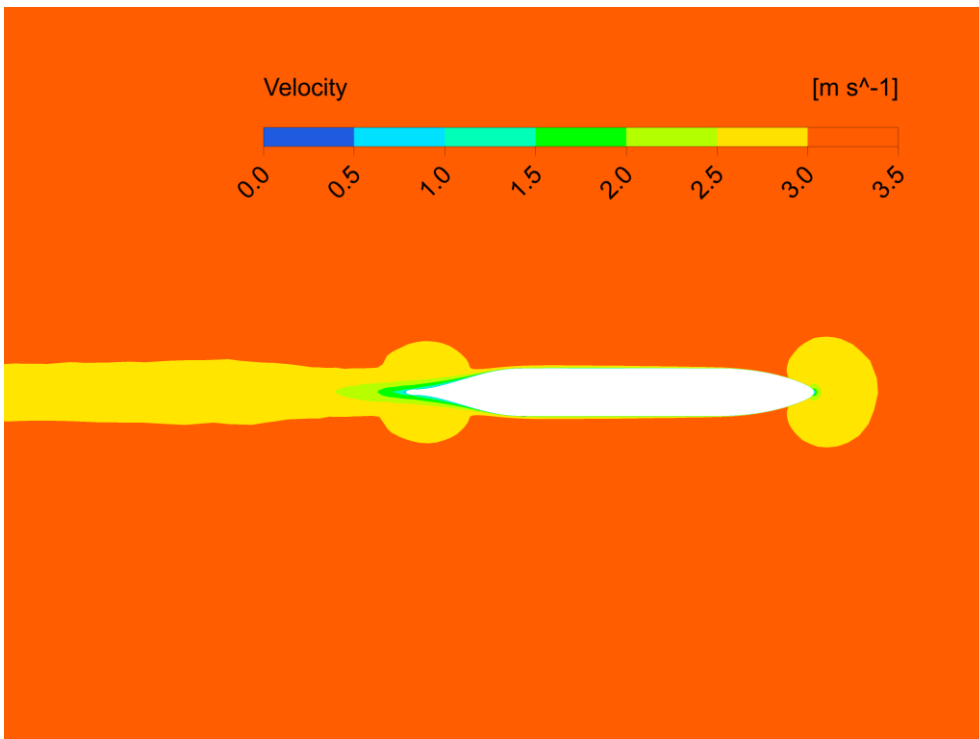
When the results are examined, it is seen that the drag force reduction performance of the processes is between 13 percent and 8 percent; It is seen that the dimensionless drag coefficient reduction performances also vary between 11 percent and 7 percent. Optimization Process-1 is the process with the highest performance of both drag force and dimensionless drag coefficient reduction. This process provides the most improvement among all processes, which indicates that optimization studies are carried out with high efficiency. Because the length and diameter of the submarine were kept constant for Optimization Process-1, a minor intervention in the design was made in this process. The velocity and pressure distributions for 3.045 m/s velocities from the symmetry centres of all designs are shared in Figures 6.19 and 6.20, respectively.



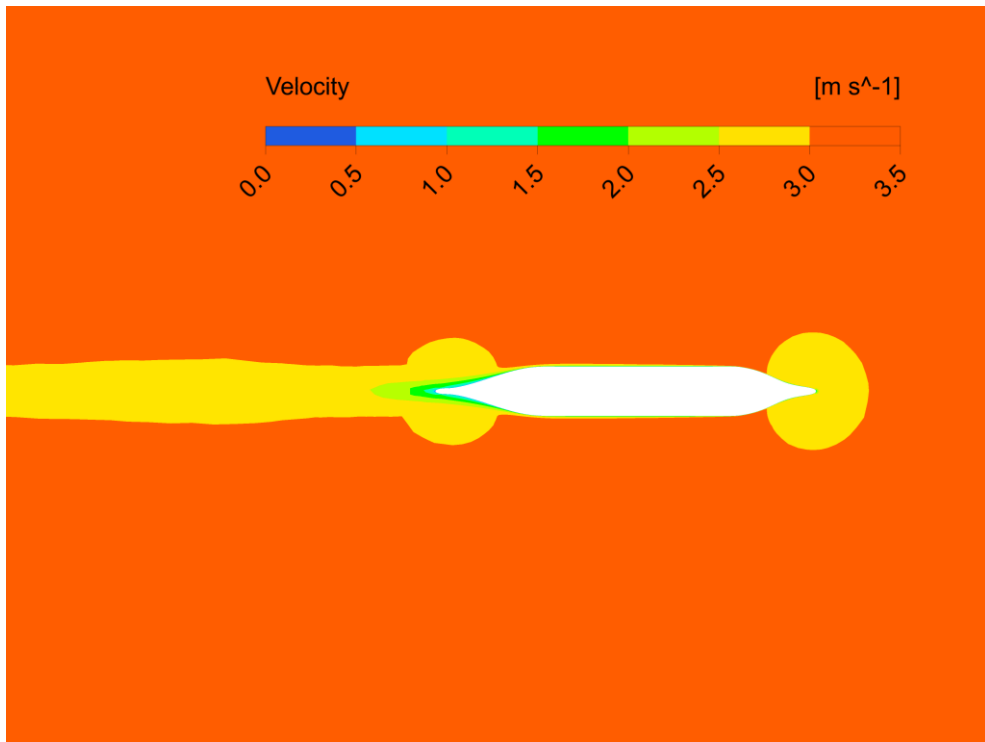
a)



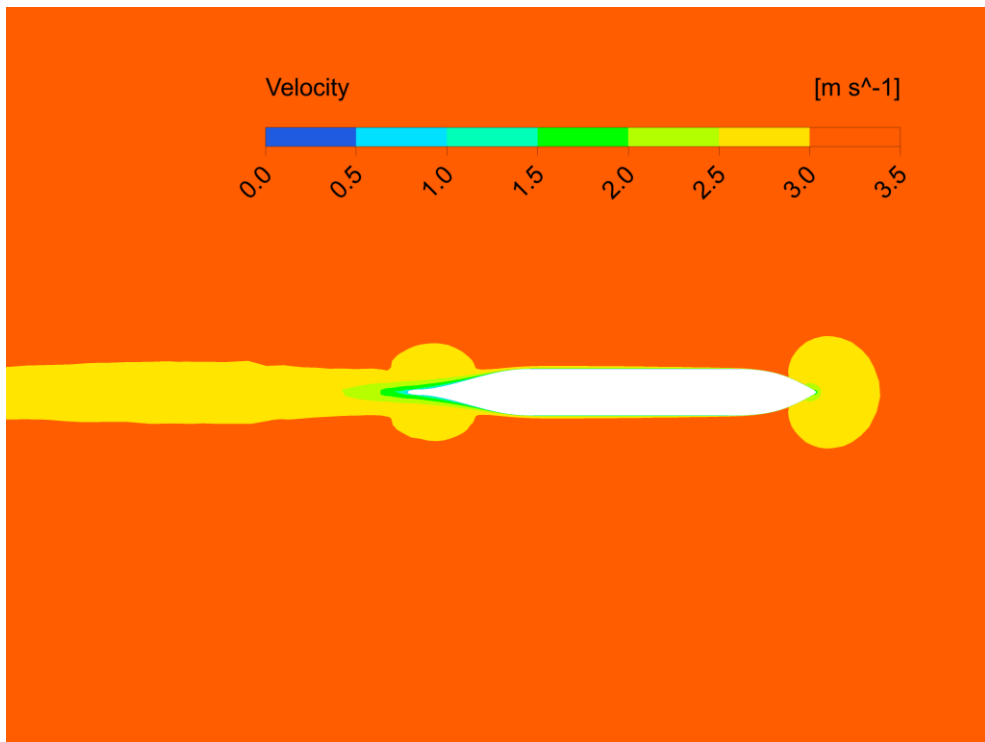
b)



c)

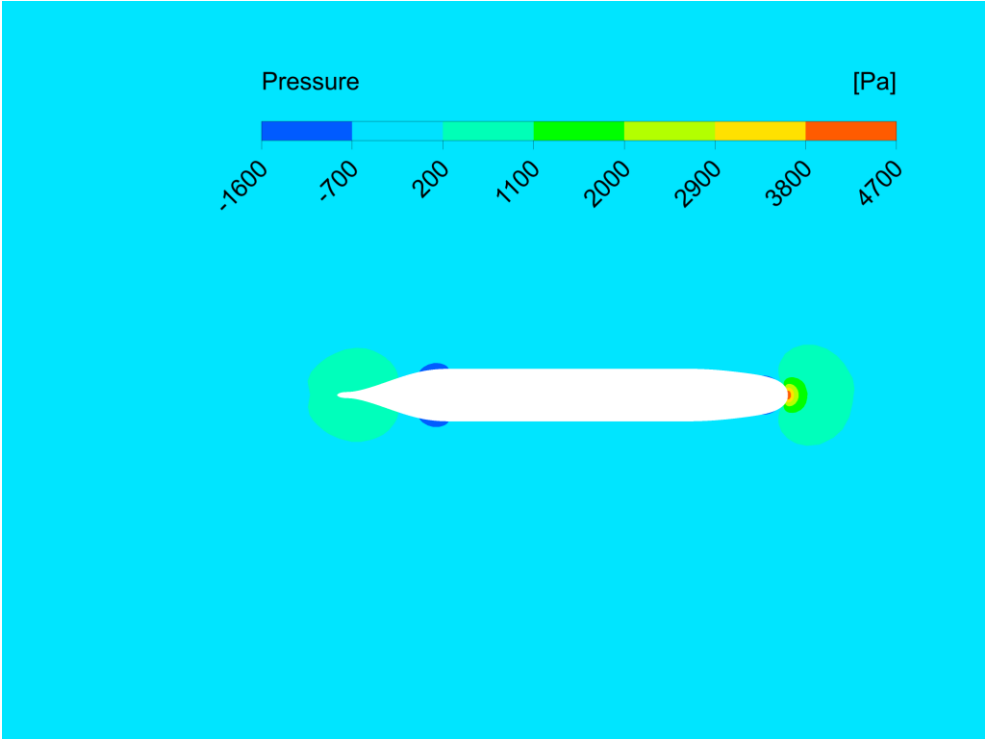


d)

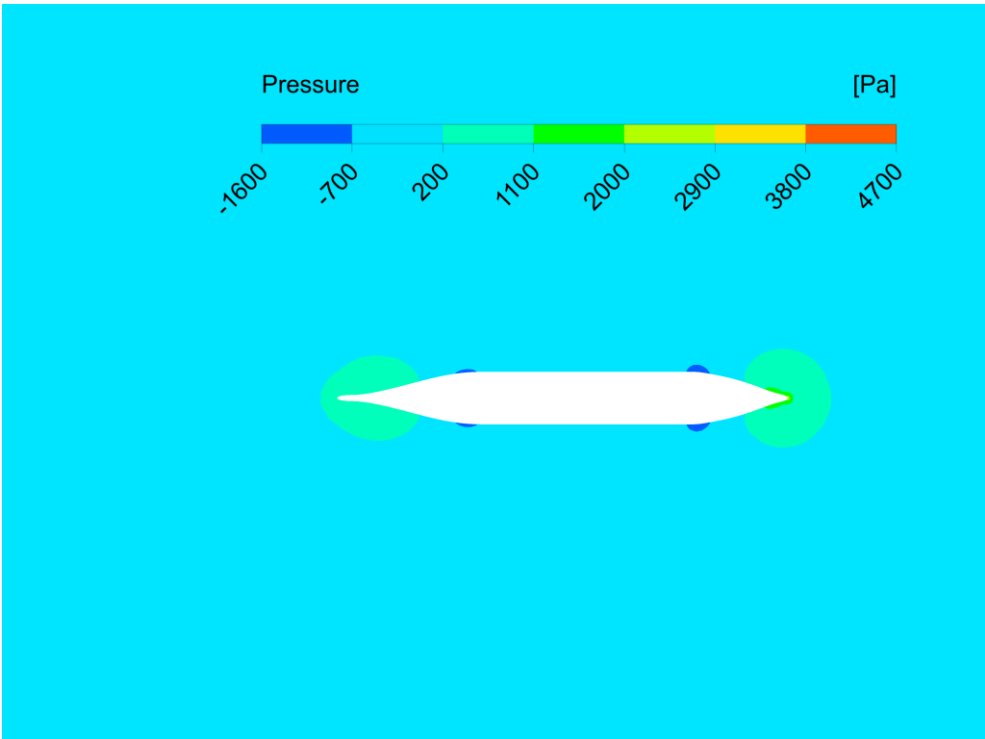


e)

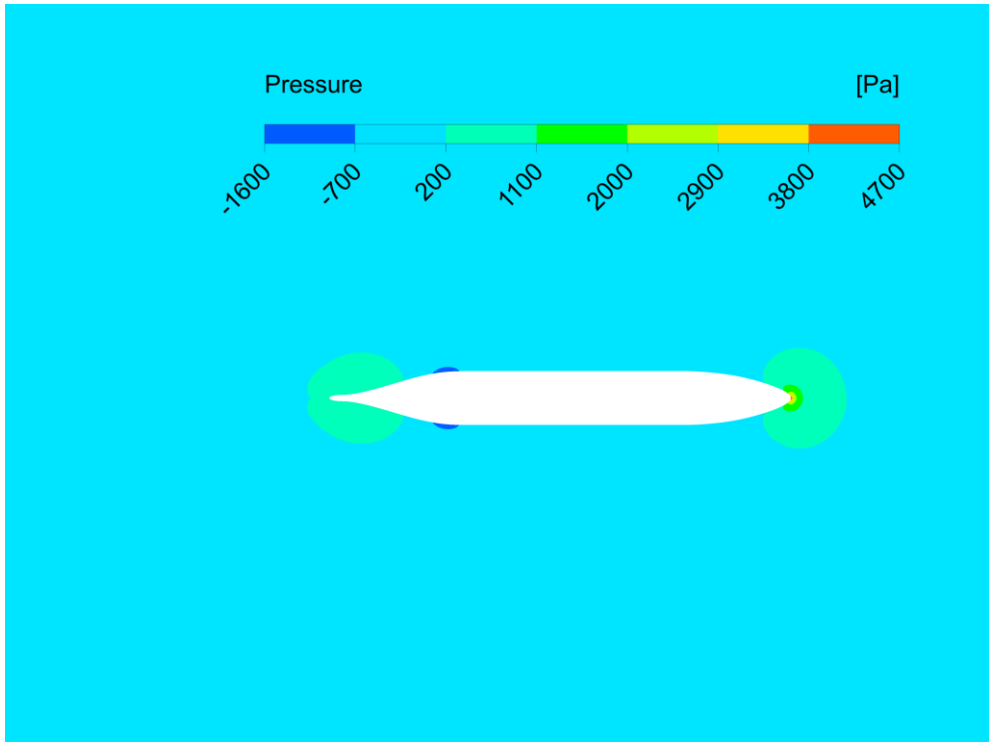
Figure 6.47. Velocity Contours (m/s) for a) DARPA SUBOFF AFF-1 b) Optimum Design-1 c) Optimum Design-2 d) Optimum Design-3 e) Optimum Design-4



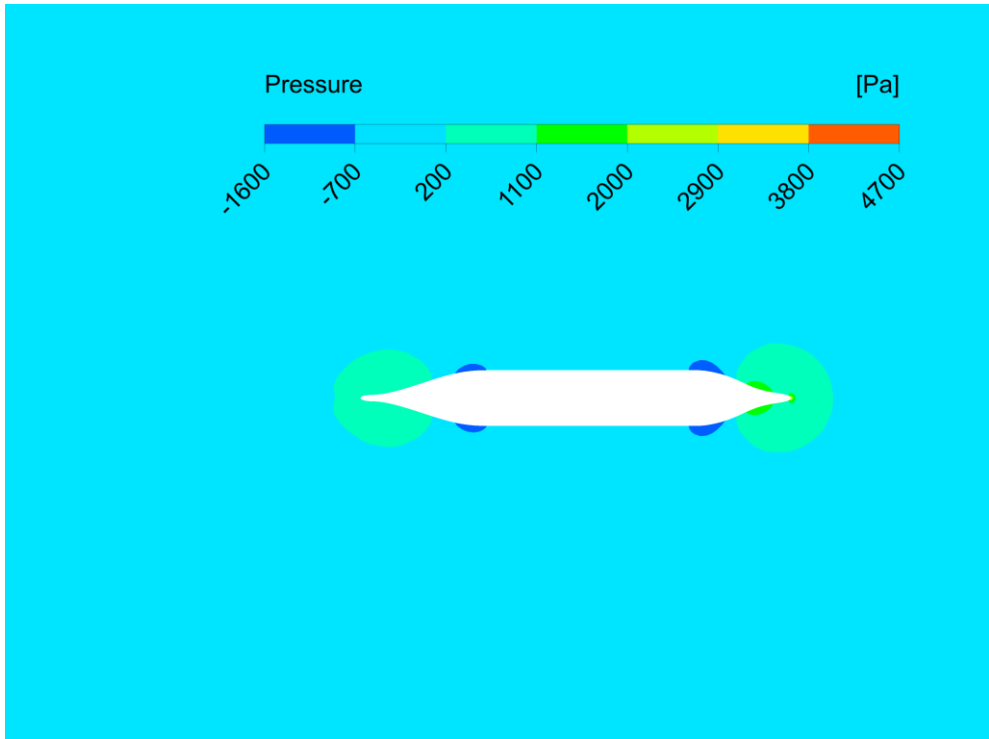
a)



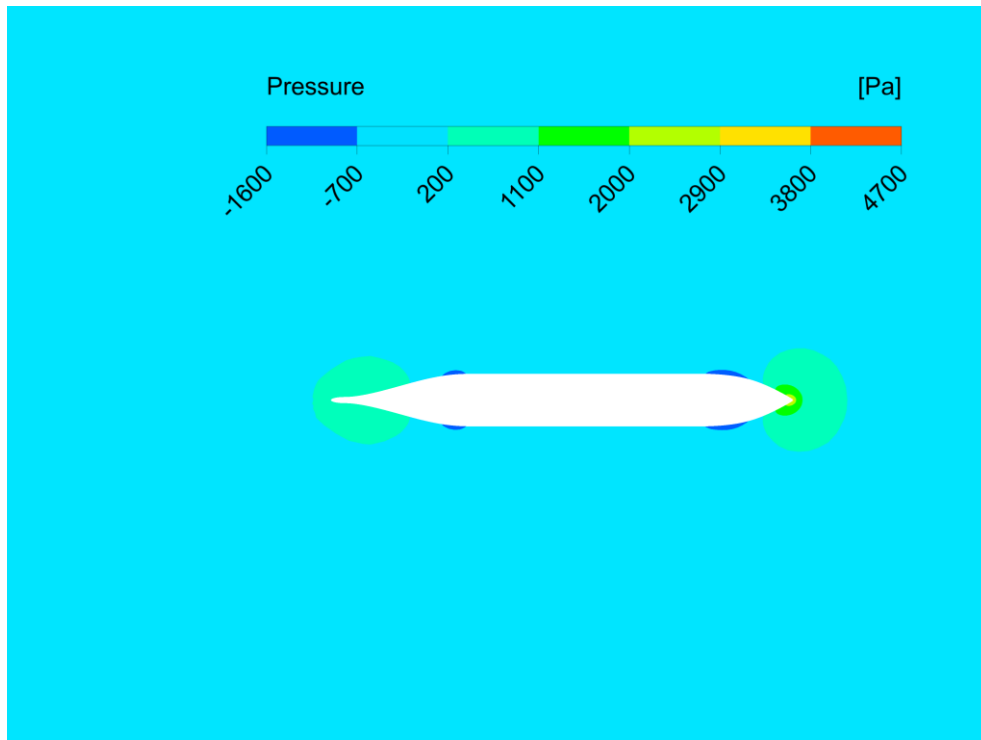
b)



c)



d)



e)

Figure 6.48. Static Pressure Contours (Pa) for a) DARPA SUBOFF AFF-1 b) Optimum Design-1 c) Optimum Design-2 d) Optimum Design-3 e) Optimum Design-4

In all models, the region where the pressure is maximum and the speed is minimum is around the nose cone. When the optimum designs and the initial design are compared, it is seen that the pressure distribution around the nose cone is higher than the distributions in the optimum designs. The fact that the pressure distribution around the nose cone has lower values indicates that the flow separation in this region is stronger. With the flow separation, the boundary layer thickness increases and the drag force due to friction decreases in this area. On the other hand, when the stern forms are examined, it is seen that a trace area is formed in a larger area after the stern in optimum forms. This shows that the flow leaves the submarine body more smoothly in optimum forms. In other words, in optimum forms, the flow leaves the submarine body at smaller angles. This provides a lower drag force in the stern form. Changing the trace area does not pose a problem in a study that aims to reduce the drag force. However, after this study, if the performance of a propeller to be mounted on the stern of the submarine is desired to be examined, these propellers will have to be compatible with the traces of both the optimum forms and the first form.

7. CONCLUSION

7.1. Conclusion and Discussion

Within the scope of the thesis, four optimization studies were performed, and their efficiencies were compared. During these studies, the LCB positions of the derived submarine designs were kept the same as the DARPA SUBOFF AFF-1, so the the drag performance comparison was made with the most accurate method. Since this situation is not considered in most studies in the literature, it is one of the details that make the studies in the thesis unique.

When the four different optimization studies are analyzed separately, it has been observed that the drag reduction has been achieved in the top 13% band at a speed of 3.045 m/s.

These studies have two different achievements. First, it has been learned what the most efficient method is when it is desired to improve the drag performance of a submarine. Optimization Process-1 was the most efficient method, achieving maximum performance improvement without changing the overall length and maximum diameter. Therefore, even if there are no design constraints regarding the total length and maximum diameter, the drag performance of submarines will be maximized by following the Optimization Process-1.

The second gain is determining the most critical design constraints in hydrodynamic optimization studies, where the total length and maximum diameter parameters must be changed separately or simultaneously.

When an optimization study is carried out by keeping the length and diameter constant, the optimum design will be similar to Optimum Design-1. It is seen that the starting point of the stern form was pulled forward to achieve this design. Therefore, when an optimization study is carried out with these targets, the most critical design constraint will be how far forward the starting point of the stern form can be moved. In the thesis, a drag performance improvement of approximately 13% was achieved for this process at a speed of 3.045 m/s.

A form like Optimum Design-2 will be achieved when aiming for a design that is maximally similar to the DARPA SUBOFF AFF-1 but more hydrodynamically efficient than it. The most crucial design constraint will be the maximum dimensions the length and diameter can reach while obtaining the optimum design. In the thesis, the drag reduction approximately 8% was achieved for this process at a speed of 3.045 m/s.

When it is desired to improve the drag performance of the submarine by shortening its length and increasing its diameter, a form similar to Optimum Design-3 will be obtained. Since the length and diameter are changed simultaneously, a study should be carried out by keeping the L/D ratio within the optimum range of 7-10. The most essential design constraint will be how close the L/D ratio of the final design can be to the optimum ratio. In the thesis, the drag reduction of approximately 9% was achieved for this process at a speed of 3.045 m/s.

Finally, it is seen that the sharpest nose cone form is used in Optimum Design-4. Therefore, if the diameter of the submarine is kept constant while extending the length of the submarine, as in the fourth process, the nose cone will need to be sharpened to achieve the optimum form for maximum performance. On the other hand, the L/D ratio is also changed, and since the change in the ratio is only due to the length, it may be challenging to keep this ratio within the optimum ranges. However, when the sizes of Optimum Design-4 and DARPA SUBOFF AFF-1 designs are compared, they seem pretty close. Therefore, it cannot be said that the increase in length directly improves the drag performance. The most essential design constraints will be how much the nose cone can be sharpened and how long the length can be increased. In the thesis, the drag performance improvement of approximately 10% was achieved for this process at a speed of 3.045 m/s.

In addition, other points to be considered in all optimization processes are the dimensions and layouts of the components that must be used in the submarines. For example, if there is a component whose layout will deteriorate when the size of the submarine is reduced, Optimization Process-3 cannot be used. On the other hand, if the design is to be optimized and a component can be placed when the submarine is extended, Optimization Process-4 can be preferred.

When all these inferences are brought together, it has been learned what the most crucial design constraints are according to the geometric and hydrostatic targets set in any

submarine optimization study and what form will be obtained at the end of the study. Therefore, these studies carried out within the scope of the thesis will ensure that the first step of the hydrodynamic optimization study of any submarine in the literature will be completed with maximum efficiency.

7.2. Future Works

It has been mentioned in the previous section that the studies carried out within the scope of the thesis are the first step of the submarine hydrodynamic optimization studies. Therefore, the most efficient optimization process can be selected after this study according to the design limits. A hydrodynamic optimization study can be performed on the fully submerged AFF-8 model of the DARPA SUBOFF. During this study, the appendages in the stern and middle parts of the submarine can also be examined parametrically.

The previous titles mentioned that the submarine has three modes of the voyage: submerged, surfaced and transition. Therefore, a hydrodynamic optimization study can be carried out to minimize the drag force in these three voyage modes.

In addition, hydrodynamic noise is an essential parameter in submarine-style structures. Therefore, after obtaining the most hydrodynamically optimum form covering three different voyage modes, a study can be carried out to increase the hydroacoustic performance of this form, and designs with increased efficiency in all voyage modes can be obtained in terms of both hydrodynamics and hydroacoustics.

8. REFERENCES

1. Fontenoy, P., E., 2007, "*Submarines : An Illustrated History of Their Impact*," First Edition, ABC-Clio, California, USA.
2. Akermann, P., 2002, "*Encyclopaedia of British Submarines 1901-1955*," Penzance:Periscope Publishing.
3. Alden, J., D., 1979, "*The Fleet Submarine in the U.S. Navy: A Design and Construction History*," Annapolis: Naval Institute Press.
4. Verfuss, U., K., Aniceto, A., S., Harris, D., V., Gillespie, D., Fielding, S., Jiménez, G., 2019, "*A review of unmanned vehicles for the detection and monitoring of marine fauna*," *Mar Pollut Bull* 140:17–29.
5. Liu, Z., Zhang, Y., Yu, X., Yuan, C., 2016, "*Unmanned surface vehicles: an overview of developments and challenges*," *Annu Rev Control* 41:71–93.
6. Qian, D., Zhao, J., Yang, Y., 2017, "*Development trend of military UUV: a review of US military unmanned system development plan*," *Unmanned Undersea Syst.* 25:107–50.
7. Kumar, A., Kurmi, J., 2018, "*A review on unmanned water surface vehicle*," *Int. Adv. Res. Comp. Sci* 9:95.
8. Serikawa, S., Lu, H., 2014, "*Underwater image dehazing using joint trilateral filter*," *Comp. Electr. Eng.* 40(1):41–50.
9. Chen, P., Wu X., 2013, "*Optimal extended position call-search method for UUVs' formation*," *Syst. Eng. Electron* 35:987–92.
10. Chen, P., Chen Y., 2012, "*Method of call-search for Markovian motion targets using UUV cooperation*," *Syst Eng Electron* 34:1630–4.
11. Sun, T., Chen, G., Yang, S., Wang, Y., Wang, Y., Han, T., Zhang, L., 2021, "*Design and optimization of a bio-inspired hull shape for AUV by surrogate model technology*," *Engineering Applications Of Computational Fluid Mechanics* 15, pp. 1057-1074.
12. Huang, T.T., Liu, H.L., Groves, N.C., 1998, "*Experiments of the DARPA (Defense Advanced Research Projects Agency) Suboff Program. No. DTRC/SHD-1298-02*," David Taylor Research Center Bethesda MD Ship Hydromechanics Dept.
13. Marshallsay, P.G., Eriksson, A.M., 2012, "*Use of Computational Fluid Dynamics as a Tool to Assess the Hydrodynamic Performance of a Submarine*," 18th Australasian Fluid Mechanics Conference, Launceston, Australia
14. Qu, Y., Wu, Q., Zhao, X., Huang, B., Fu, X., Wang, G., 2021, "Numerical investigation of flow structures around the DARPASUBOFF model," *Ocean Engineering* 239:109866.
15. Paz, J., D., M., Munoz, O., D., T., 2013, "*Multiobjective Optimization of a Submarine Hull Design*," *Ship Science & Technology - Vol. 7*, pp. 27-42, Cartagena, Colombia.
16. Gao, T., Wang, Y., Pang, Y., Cao, J., 2016, "*Hull shape optimization for autonomous underwater vehicles using CFD*," *Engineering Applications of Computational Fluid Mechanics*, 10:1, 599-607.

17. Divsalar, K., 2019, "*Improving the hydrodynamic performance of the SUBOFF bare hull model: a CFD approach*," The Chinese Society of Theoretical and Applied Mechanics and Springer-Verlag GmbH Germany.
18. Brennen, C., E., 2013, "*Cavitation and Bubble Dynamics*," Cambridge University Press.
19. Kitayama, N., Ueda, Y., Matsuzawa, T., 2017, "Experimental Investigation of Supercavitating Underwater Ballistic Projectile," 30th International Symposium on Ballistics.
20. Dzielski, J., E., 2011, "*Longitudinal stability of a supercavitating vehicle*," IEEE J. Oceanic Eng. 36 (4), 562–570.
21. Kim, M., J., Kim, S., H., Lee, K., C., Paik, B., G., Kim, M., C., 2021, "*Cavitator Design for Straight-Running Supercavitating TorpedoEs*," Appl. Sci., 11, 6247.
22. Janna, W., S., 2020, "*Introduction to Fluid Mechanics*," Sixth Edition, CRC Press.
23. Hinze, J., O., 1975, "*Turbulence*," New York, USA.: McGraw-Hill.
24. Bradshaw, P., 1971, "*A Introduction to Turbulence and Measurement*," Braunschweig, Germany.: Pergamon Press.
25. Samy, M., Mofreh, H., 2011, "*A comparative study of turbulence models performance for separating flow in a planer asymmetric diffuser*," Computers & Fluids 248-257.
26. Menter, F., R., 1992, "*Performance of Popular Turbulence Models for Attached and Separated Adverse Pressure Gradient Flows*," American Institute of Aeronautics and Astronautics Journal 30(8), 2066-2072.
27. Menter, F., R., 1993, "*Zonal Two Equation $k-\omega$ Turbulence Models for Aerodynamic Flows*," Orlando, Florida, USA.: American Institute of Aeronautics and Astronautics Report.
28. Layeb, A., 2021, "*The Tangent Search Algorithm for Solving Optimization Problems*," University of Constantine 2, NTIC Faculty, Department of Computer Science and Applications.
29. Talbi, E.G., 2002, "*A taxonomy of hybrid metaheuristics*," Journal of Heuristics, 8:541–564.
30. Layeb, A., 2013, "*A hybrid quantum-inspired harmony search algorithm for 0–1 optimization problems*," Journal of Computational and Applied Mathematics, 253: 14-25.
31. Torn, A., Zilinskas, A., 1989, "*Global Optimization*," Lecture Notes in Computer Science, Springer-Verlag Berlin Heidelberg.
32. Chong, E.K.P., Zak, S.H., 2001, "*An Introduction to Optimization*," Second Edition, John Wiley & Sons, New York.
33. Fernández, F. M., 2009, "*On some approximate methods for nonlinear models*," Applied Mathematics and Computation 215.1: 168-174.
34. Bozorg-Haddad, O., 2018, "*Advanced optimization by nature-inspired algorithms*," Springer Nature Singapore Pte Ltd.
35. Mason, R., Gunst, R., & Hess, J., 1989, "*Statistical Design and Analysis of Experiments*," John Wiley & Sons, New York.

36. Montgomery, D., 1984, "*Design and Analysis of Experiments*," John Wiley, New York.
37. Barr, R.S., Golden, B.L., Kelly, J.P., Resende, M.G.C., Stewart Jr., W.R., 1995, "*Designing and reporting on computational experiments with heuristic methods*," *Journal of Heuristics* 1, 9-32.
38. Manny, U., Telford, J.K., 2009, "*Optimization by Design of Experiment Techniques*," Johns Hopkins University Applied Physics Laboratory, Maryland.
39. Fisher, R. A., 1925, "*Statistical methods for research worker*," Edinburgh: Oliver and Boyd.
40. Box, G. E. P., Wilson, K. B., 1951, "*Experimental attainment of optimum conditions*," *Journal of the Royal Statistical Society*, 13, 1–45.
41. Taguchi, G., & Wu, Y., 1980, "*Introduction to off-line quality control*," Nagoya: Central Japan Quality Control Association.
42. Cavazzuti, M., 2013, "*Optimization Methods: From Theory to Design Scientific and Technological Aspects in Mechanics*," Springer, London.
43. Sobol, I.M., 1967, "*Distribution of points in a cube and approximate evaluation of integrals*," *U.S.S.R Comput. Maths. Math. Phys.* 7: 86–112.
44. Bingxiang, L., Qin, C., Daxiong, L., Shenghao, W., Xingyou, Y., 2017, "*Computationally expensive aerodynamic design optimization framework with adaptive search strategies and data fusion*," 7th European Conference for Aeronautics and Aerospace Sciences (Eucass), France.
45. Mordecai, A., 2003, "*Nonlinear programming: analysis and methods*," Courier Corporation.
46. Fuchang, G., Han, L., 2012, "*Implementing the Nelder-Mead simplex algorithm with adaptive parameters*," *Computational Optimization and Applications* 51.1: 259-277.
47. Russell, G., 1996, "*PALO: A probabilistic hill-climbing algorithm*," *Artificial Intelligence* 84.1-2: 177-208.
48. Laarhoven, V., Peter, J.M., Aarts, E.H, 1987, "*Simulated annealing: Theory and applications*," Springer, Dordrecht, 1987, 7-15.
49. Virginia, T., 1997, "*On the convergence of pattern search algorithms*," *SIAM Journal on Optimization* 7.1: 1:25.
50. Karaboga, D., Okdem, S., 2004, "*A simple and global optimization algorithm for engineering problems: differential evolution algorithm*," *Turkish Journal of Electrical Engineering & Computer Sciences* 12.1: 53-60.
51. Dorigo, M., Birattari, M, Stutzle, T., 2006, "*Ant colony optimization*," *IEEE computational intelligence magazine* 1.4: 28-39.
52. Sivanandam, S. N., and S. N. Deepa, 2008, "*Genetic algorithms: Introduction to genetic algorithms*," Springer, Berlin, Heidelberg, 15-37.
53. Seyedali, M., 2016, "*SCA: a sine cosine algorithm for solving optimization problems*," *Knowledge-based systems* 96: 120-133.
54. Zhao, J., 2019, "*Spherical search optimizer: A simple yet efficient meta-heuristic approach*," *Neural Computing and Applications*: 1-32.

55. Laith, A., 2021, "*The arithmetic optimization algorithm*," Computer methods in applied mechanics and engineering 376: 113609.
56. Salimi, H., 2015, "*Stochastic fractal search: a powerful metaheuristic algorithm*," Knowledge-Based Systems 75: 1-18.
57. Pachung, P., Bansal, J.C., 2022, "*An improved tangent search algorithm*," MethodsX 9: 101839.
58. Groves, N.C., Huang, T.T., Chang, M.S., 1989, "*Geometric characteristics of DARPA (Defense Advanced Research Projects Agency) SUBOFF models (DTRC model numbers 5470 and 5471)*," David Taylor Research Center Bethesda MD Ship Hydromechanics Dept.
59. International Towing Tank Conference, 2011, "*Practical Guidelines for Ship CFD Applications*"
60. Chisholm, C., Nugoroho, B., Chin, R.C., 2020, "*Hydrodynamic simulation of submarine far field flow*," 22nd Australian Fluid Mechanics Conference.
61. Gao, T., Wang, Y., Pang, Y., Chen, Q., Tang, Y., 2018, "*A time-efficient CFD approach for hydrodynamic coefficient determination and model simplification of a submarine*," Ocean Engineering 154, pp. 16-26.
62. Dantas, J.L.D., de Barros, E.A., 2013, "*Numerical analysis of control surface effects on AUV manoeuvrability*," Applied Ocean Research 42, pp. 168-181.
63. Xiaocui, W., Yiwei, W., Chenguang, H., Zhiqiang, H., Ruiwen, Y., 2015, "*An effective CFD approach for marine-vehicle manoeuvring simulation based on the hybrid reference frames method*," Ocean Engineering 109, pp. 83-92.
64. Shojaeefard, M.H., Khorampanahi, A., Mirzaei, M., 2018, "*RANS study of Strouhal number effects on the stability derivatives of an autonomous underwater vehicle*," J. Braz. Soc. Mech. Sci. 40, pp. 124-137.
65. Lintermann, A., 2020, "*Computational Meshing for CFD Simulations*", *Clinical and Biomedical Engineering in the Human Nose*, pp. 85-115.
66. Zore, K., Parkhi, G., Sasanapuri, B., Varghese, A., 2019, "*ANSYS Mosaic Poly-Hexcore Mesh for High-Lift Aircraft Configuration*," 21st Annual CFD Symposium.
67. Clarke, G., Vun, S., Giacobello, M. and Reddy, R., 2010, "*Estimation of ARH Tiger Fuselage Aerodynamic Characteristics Using Computational Fluid Dynamics Tools*," DSTO-TN-0965.
68. Tapia, X.P., 2009, "*Modelling of wind flow over complex terrain using OpenFOAM*", Masters Thesis, University of Gävle, Sweden.
69. Schubert, M., 2009, "*Computational Fluid Dynamics Applications for Nitrate removal in an Upper Mississippi River Backwater*," Master of Science Thesis Civil and Environmental Graduate College, University of Iowa.
70. Joubert, P.N., 2004, "*Some Aspects of Submarine Design Part 1 – Hydrodynamics*," Defence Science and Technology Organisation Technical Report DSTO-TR-1622.
71. Joubert, P.N., 2004, "*Some Aspects of Submarine Design Part 2– Shape of a Submarine 2026*," Defence Science and Technology Organisation Technical Report DSTO-TR-1920.
72. Overpelt, B., Nienhuis, B., Anderson, B., 2015, "*Free running manoeuvring model tests on a modern generic SSK class submarine (BB2)*," Pacific International Maritime Conference, Sydney, Australia.

73. Yazici, B.U., 2020, "*Hydro-Acoustic and Hydrodynamic Optimization of DarpaSuboff Submarine Bow Form Using Genetic Algorithm*", Istanbul Technical University.
74. Budak, G., 2015, "*Darpa Suboff Denizaltı Modeli İle Bu Modelden Yeni Türetilen Formların Hesaplamalı Akışkanlar Dinamiği (Had) İle Sayısal Direnç Hesabı*", Master of Science Thesis, Istanbul Technical University Department of Marine and Marine Technology Engineering .
75. Lackenby, H., 1950, "*On The Systematic Variation of Ship Forms,*" Transactions of The Institute of Naval Architects, Vol. 92, pp 289-316.
76. Nowacki, H., Creutz, C., Munchmeyer, F. C., 1977, "*Ship Lines Creation by Computer - Objectives, Methods and Results,*" Symposium on Computer-Aided Hull Surface Definition, Annapolis, MD, USA.
77. Kracht, A.M, 1978, "*Design of Bulbous Bows,*" SNAME, Vol.86, pp 197-217.
78. Kracht, A.M., Jacobsen, A., 1992, "*D-series systematic experiments with models of fast twin-screw displacement ships at Transactions,*" Society of Naval Architects and Marine Engineers, Vol. 100, pp 199-222.
79. Harries, S., Abt, C. 1998, "*Parametric Curve Design Applying Fairness Criteria,*" International Workshop on creating fair and shape-preserving curves and surfaces, Berlin (Potsdam, Teubner): Network Fairshape.
80. Abt, C., Harries, S. 2007, "*Hull Variation and Improvement using the Generalized Lackenby Method of the FRIENDSHIP-Framework,*" The Naval Architect, September.
81. K.J. Rawson, E.C. Tupper, 2001, "*Basic Ship Theory (Fifth Edition)*", Butterworth-Heinemann, Oxford, United Kingdom, pp 7-51.
82. Thune, S., 2015, "*Simulation of Submarine Manoeuvring,*" Royal Institute of Technology, Master of Science Thesis, Sweden.
83. Biran, A., 2012, "*Geometric Properties of Areas and Volumes,*" Ship Stability for Masters and Mates (Seventh Edition), Butterworth-Heinemann, Oxford, United Kingdom, pp 229-233.
84. Alhammadi, H.Y., Romagnoli, J.A, 2004, "*The Integration of Process Design and Control,*" Nonconventional and Vernacular Construction Materials (Second Edition), Woodhead Publishing Series in Civil and Structural Engineering, Woodhead Publishing, pp 63-80.
85. Moonesun, M., Mahdian, A., Korol, Y.,M., Dadkhah, M., Javadi, M.,M., Brazhko, A., 2016, "*Optimum L/D for Submarine Shape,*" Indian Journal of Geo-Marine Sciences, Vol.45(1), pp.38-43.